Feasibility study and design of AFM production wafer calibration method using Electrostatic Pull-in Instability

E. P. Molenaar

Report number : MNE 2013.012

Supervisor : prof.dr.ir. U. Staufer

Specialization : Micro and Nano Engineering

Date : April 8, 2013

Master of Science Thesis

Delft University of Technology

Precision and Microsystems Engineering

Feasibility study and design of AFM production wafer calibration method using Electrostatic Pull-in Instability

Master of Science Thesis

For the degree of Master of Science in Mechanical Engineering at Delft University of Technology

E. P. Molenaar

April 8, 2013

Faculty of Mechanical, Maritime and Materials Engineering (3mE) · Delft University of Technology

Delft University of Technology
Department of

The undersigned hereby certify that they have read and recommend to the Faculty of Mechanical, Maritime and Materials Engineering (3mE) for acceptance a thesis entitled

Feasibility study and design of AFM production wafer calibration method using Electrostatic Pull-in Instability

by

E. P. Molenaar

in partial fulfillment of the requirements for the degree of

Master of Science Mechanical Engineering

Dated: April 8, 2013

Supervisor(s): ______________________
prof.dr.ir. U. Staufer

Reader(s): ______________________
prof.dr.ir. A. van Keulen

____
dr.ir. M. Ghatkesar

____
ir. C. K. Yang

Abstract

Atomic Force Microscopy is one of the foremost tools used to image, measure and manipulate matter at the nanoscale. Information of the surface is gathered by a mechanical probe that "feels" the surface. The force acting on this probe is calculated by multiplying the deflection with the probe's stiffness. This stiffness is hard to estimate, as different material properties and measurement errors lead to large uncertainties in the determination of the stiffness. The size and fragility of the probes also make them difficult to handle. A new method is proposed to calibrate the probes while they are still connected to the wafer they were produced in.

By investigating the current techniques used to calculate the probe's stiffness the advantages and disadvantages of these techniques are identified. The biggest disadvantage being that the current calibration techniques are not able to define a stiffness for the values 20 N/m or more with an accuracy below 20%. Based on a physical phenomenon called the Electrostatic Pull-in Instability of the probe, a new calibration technique is introduced. This new calibration technique suffers less from the disadvantages common to the existing techniques but it requires a analytical model describing the problem. This analytical model has been developed and compared to results from experiments and finite element analyses.

The new analytical model shows an error of less then 5% when it is compared to the performed experiments and finite element analysis. Using this model to calculate the stiffness of calibrated probes showed a maximum error of 10% in the stiffness. Application of the model with commercial AFM probes shows an error of less then 15% in calculating the stiffness of compliant probes. For the probes with a stiffness higher than 10 N/m the error is rises to 16% but this can be attributed to the stiffness estimation done by the manufacturer.

From these results it can be concluded that the new technique can be used as a calibration method for the determination of the cantilever stiffness. Based on this technique a concept of an experimental set-up is proposed to investigate the use of the technique on the probes still attached to their wafers. This set-up will, if succesfull, be able to calibrate cantilever from all stiffness ranges without having to remove and handle each one of them.

Contents

List of Figures

List of Tables

Preface and Acknowledgments

This master thesis came to be after a discussion over a cup of hot chocolate with Eric Kievit. He told me about the new company he had founded and was looking into technologies that are able to calibrate AFM probes. A new technique had been developed at the Department of Precision and Microsystems Engineering by Prof.dr.ir. A. van Keulen and PhD students H. Sadeghian and C.K. Yang. This new technique looked promising and mr. Kievit was looking for Master students to do research in the further development of this technique. The new technique allowed for three distinct research objectives: 1 - An independent calibration system to be sold separately, 2 - integration of a calibration system into an AFM microscope and 3 - the development of a calibration system able to calibrate cantilevers while they are still attached to their production wafer. As the first assignment was already being developed by Laurens Pluimers, I choose to start work on the third option. To finish this assignment it turned out that I would need most of the course I had followed during my Bachelor studies and almost all of the subjects followed during my Masters study. Not all objectives set out at the start of this assignment have been completed and this work should not only be seen as a requirement for my graduation but should also be used to inform and provide students should they choose to follow up on my research.

During this graduation project I have come to rely on certain people which I wish to thank here:

First of all Prof.dr.ir. Urs Staufer has played a vital role in the completion of this study. During our weekly discussions sessions I could bring up any problem I was having with my project and I always left with new ideas to get around these problems. He kept me motivated during times when the project wasn't running as I wanted to and was always eager to know the results I got.

Next I want to thank Fred van Keulen and Eric Kievit for giving me the opportunity to work on this project. Working within a small start-up company run by a fellow student has been a unique experience which I will likely never experience again.

The scientific staff of the TU Delft and the PhD students of the PME department also have my thanks, especially Hugo Perez-Garza. I have never met anyone who is as driven and dedicated to his research but on the other hand is also willing and able to help with any problem. He was a great source of knowledge when I was designing my experimental set-up.

All of my fellow students have been enjoyable to work with. Especially Laurens Pluimers, since we could work out the problems we were both having with this subject and could keep each other motivated when the results were not what we were hoping for. And as my "boss", Eric Kievit has been a great source of motivation. During our daily lunches, coffee breaks and so-called monthly get-togethers we had good discussions about our different projects and he helped me a great deal in steering my research in the right direction. Last but not least I would like to thank my girlfriend Sharon, my family and my friends for their support and understanding during this project. They have been a great driving force to complete this work even if it meant that they had to read this thesis over and over again.

"No amount of experimentation can ever prove me right; a single experiment can prove me wrong."

— *Albert Einstein*

Chapter 1

Introduction

In 1986 the Nobel Prize for Physics was awarded to Gerd, Binnig and Heinrich Rohrer for their design of the Scanning Tunneling Microscope (also known as STM). This microscope, designed in the early 1980's, has a lateral resolution of around 0.1 nm and a depth resolution of 0.01 nm, which is more than 1000 times better than the resolution limit of optical diffraction microscopy. Further development by Binnig, Quate and Gerber led to the invention of the Atomic Force microscope (or AFM) in 1986. The AFM is one of the foremost tools for imaging, measuring, and manipulating matter at the nanoscale[3].

1-1 Basic principles

As the name suggests, the AFM is able to measure the interaction of atomic forces. When atoms are brought into each others vicinity, there can either exist van-der-Waals forces attracting the atom to each other, or repulsive force between electrons if the atoms are brought too close. Depending on the operational mode of the AFM either of these forces is measured. The AFM consists of a cantilever beam with at its end a sharp tip with a radius of several nanometers. This cantilever beam is most often manufactured out of silicon or silicon nitride. The tip is dragged along the surface that is to be measured. Any roughness or change of height of the surface will lead to the bending of the cantilever. The deflection caused by this bending is measured by reflecting a laser beam off of the reflective coating applied on the top of the cantilever surface. The movement of the laser spot on a photo diode, caused by the bending of the cantilever, can then be translated into the height change of the cantilever and thus the change of the topological profile of the surface. In Figure 1-1a a close-up can be seen of the cantilever attached to the AFM chip. On the right of this beam the tip is visible that is used to scan the surface. Figure 1-1b shows the a overview of the laserbeam's pathway during scanning. The resistance to this deflection is called the cantilevers' stiffness k, and it defines the force needed to deflect the beam a certain amount. With the deflection of the tip known, Hooke's law can be used to find the force that was subjected to the cantilever. Hooke's law states that force equals stiffness times deflection, so by using the stiffness of the cantilever

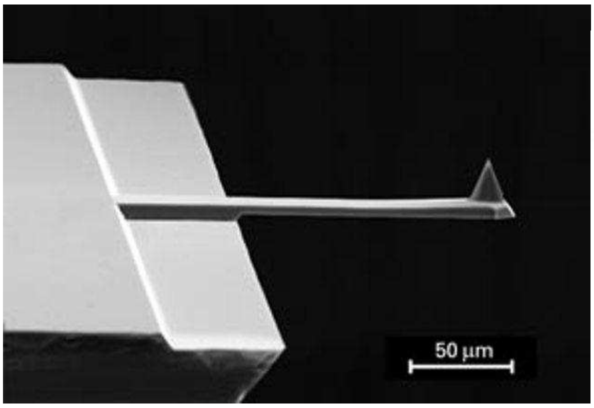

(a) Close up view of AFM cantilever with tip.

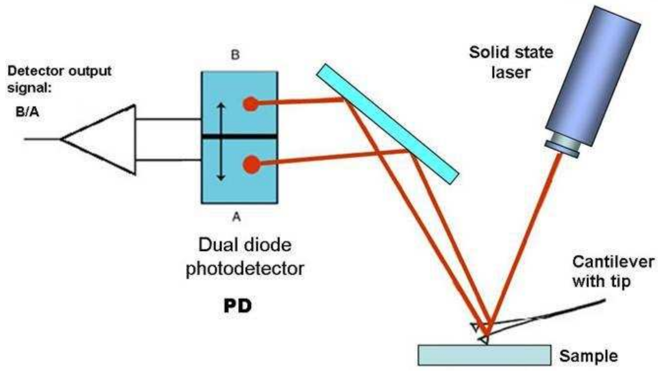

(b) Schematic view of working principle of AFM.

Figure 1-1: The Atomic Force Microscope scans the surface of an object by using a cantilever with a small tip attached to it. (a) A SEM image of the cantilever of the AFM probe. During scanning the AFM measures the deflection of this cantilever by interacting forces. (b) The deflection is measured by reflecting a laserbeam of the cantilever onto a photovoltaic detector. The change of position of the reflected beam is used to calculated the deflection of the cantilever.

and multiplying it with the deflection of the cantilever, the force acting on the tip can be calculated. Using the AFM, scientists face the problem of the inaccuracy of the cantilever's stiffness. Most AFM probe manufactures supply the probes with a nominal stiffness value with an inaccuracy of up to 30%.

1-1-1 Manufacturing AFM cantilevers

To understand the problems of stiffness determination, one must first look at the manufacturing process of the AFM chip and cantilever. The most used manufacturing technique is displayed in Figure 1-2 [1]. Starting with a silicon wafer, the top and bottom are covered with a layer of silicon dioxide (SiO_2), Figure 1-2a. By patterning the oxide on both sides with a resist patterned by photolithography, the areas that are to remain are protected. The silicon wafer is placed in a chemical solution which removes the silicon oxide at all the locations that are not protected by the resist shown, Figure 1-2b. This results in a structured piece of silicon. The resist is removed and the wafer is etched by a chemical solution called potassium hydroxide. Potassium hydroxide, or KOH, has the property that etches silicon at different rates depending on the orientation of the crystal. Etching a (100) silicon surface through a rectangular hole in the (SiO_2), creates a pit with flat sloping (111)-oriented sidewalls and a flat (100)-oriented bottom. The (111)-oriented sidewalls have an angle 54.7°. This etching is stopped when the oxide layer covering the tip falls away, Figure 1-2c. The front-side of the wafer is then covered by silicon nitride and a second KOH etch thins the thickness of the beam. This finishes the structure of the beam, Figure 1-2d. After this process the backside of the cantilever can be covered by a layer of aluminum to increase the reflectivity of the cantilever.

This manufacturing technique is capable of producing numerous AFM probes on one wafer. A four-inch wafer, Figure 1-3a is able to hold 388 AFM chips and a six-inch wafer, Figure

(a) Silicon wafer covered by silicon dioxide

(b) Result of etching silicon dioxide

(c) Creation of cantilever tip by KOH etching of the wafer

(d) Finished structure after thinning the rest of the cantilever

Figure 1-2: Producing an AFM cantilever requires different fabrication steps. (a) A silicon wafer is coated on both side with silicondioxide. This silicondioxide is covered with a resist, and this resist is patterned and developed. (b) The areas of silicondioxide no longer coated by the resist are etched away. The remaining traces of resist are removed. (c) The silicon wafer is submerged in a anisotropic etchant called KOH to further etch the silicon away. This process is stopped when the silicondioxide covering the tip falls away. (d) The topside is protected by resist material and the downside is again etch by KOH, thinning the cantilever.

1-3b will even hold more than 1000 chips. A close-up view of tweezers removing a AFM probe from the wafer can be seen in Figure 1-3c.

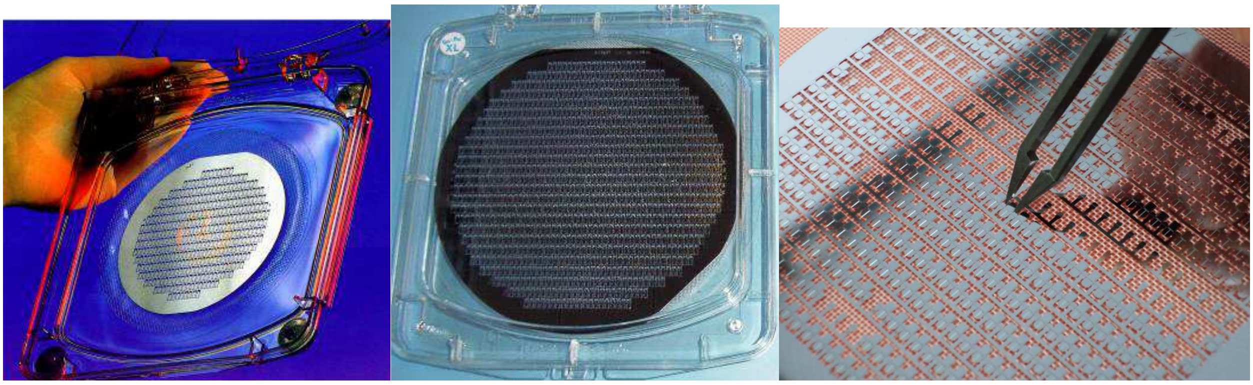

(a) 4-inch wafer **(b)** 6-inch wafer **(c)** Removal of AFM probe from wafer by use of tweezers

Figure 1-3: Different wafer sizes containing AFM probes. (a) A 4-inch wafer can contain up to 388 probes, which have been simultaneously produced. (b) A 6-inch wafer is capable of holding more than 1000 AFM probes. Due to the size of the AFM probes it is difficult to remove them. (c) Plastic tweezers are used to remove one of the AFM probes. Plastic is used to limit damage to the AFM probe during handling.

1-2 Problem

Due to the manufacturing techniques used, there are production inaccuracies in the cantilever's dimensions. The amount of material etched away by the etchant is given by the etch rate. The final dimensions are defined by the time the wafer is submerged, and careful monitoring of this time is essential. The cantilever's stiffness depends on its geometry, which necesitates to know the values of length, width and thickness. The cantilever's length and width can be measured using standard microscopy, white light or scanning electron microscopy. However, it's harder to measure is the cantilever's thickness. The aformentioned microscopy types view the object from above which makes it impossible to measure the side thickness. Careful manipulation of the AFM probe is needed to measure the beam's thickness. Even more difficult to measure is the layer thickness of the metal deposited on the backside of the cantilever. On most cantilever types an additional layer is deposited to increase its reflectivity. This added layer changes the combined Young's modulus and Poisson's ratio of the cantilever. So the inherent deficiencies of the manufacturing process, used to create the cantilevers, result in the absence of accurate knowledge of the cantilever's stiffness. Since this stiffness is needed to calculate the interacting forces encountered during scanning, a number of calibration techniques have been developed over the years. These calibration techniques make use of different physical phenomena. However, techniques which are fast do not give an accurate value of the stiffness and the most accurate calibration techniques are too time consuming. An additional problem is that each calibration technique is unable to calibrate more than one cantilever at a time. Due to the fact that the entire surface needs to be scanned by the small tip, the scanning speed needs to be high to make the scanning not too time consuming. Fast scanning means that the tip interacts more frequently with the surface and this interacting can cause vibrations in the beam. If the frequency is high enough the cantilever can start to oscillate in its eigenfrequency. This kind of oscillation should be avoided. The eigenfrequency is related to the stiffness of the cantilever beam, which means that a high stiffness leads to a high eigenfrequency. The need for these stiffer cantilevers is obvious but the current calibration techniques are not able to accurately calculate the stiffness of these cantilevers.

1-3 Objectives

The objective of this master thesis is to present a new calibration technique to determine the stiffness of AFM probes with an accuracy between 10-15%. This calibration method will be able to calibrate rectangular silicon cantilevers that are still attached to their production wafers within any stiffness range. To facilitate this calibration a concept for an experimental measurement set-up will be made.

1-4 Outline of thesis

The new calibration technique is based on the Electrostatic Pull-in Instability, or EPI, of cantilever beams. Initial research into this technique has been done by PhD's H. Sadeghian from the department of Precision and Microsystem Engineering and C.K. Yang from the department of Electronical Engineering, Mathematics and Computer Science at the TU Delft. The results of their study, [4], prove that the EPI method can be used in a laboratory environment on a custom built array of cantilevers. A continuation of this research by L. Pluimers (MSc), showed that AFM probes could be calibrated using EPI with the use of newly built calibration set-up [5]. By further extending the theories used in [4] and [5], the goal is to increase the accuracy of the model describing the behavior of the cantilever during calibration. This analytical model calculates the stiffness of the cantilever. With this improved model, a experimental set-up will be developed to use the EPI method to calculate the stiffness of cantilevers still attached to their wafers.

To understand the problems of stiffness determination it will first why it is necessary to know this stiffness. Chapter 2 will introduce the AFM probe and the way that the cantilever attached to this probe is subjected by forces. These forces cause the beam to deflect and the amount of deflection is given by its stiffness. To calculate this stiffness two models are presented that are used to calculate the stiffness and it is shown what their deficiencies are.

To develop the new experimental set-up it is first necessary to find the strengths and weaknesses of existing calibration techniques. In Chapter 3 a comparison between these techniques and the newly developed EPI technique will be made. The result of this comparison will indicate if the EPI technique is feasible as a calibration method. After introducing the EPI principle and explaining the physics behind the technique, it will be shown why the model needs to be improved.

In Chapter 4 the model describing the behavior of the cantilever will be introduced and it will be shown what research has been done into the improvement of this model. After comparison of the models with experimental data and results from a Finite Element Analysis, FEA, the most suitable model will be selected to be used in further experiments. The chosen model can perform well if the variables required to solve the model are measured accurately. The consequences of measurement errors will be discussed in Chapter 5. In this chapter an error budgeting analysis will be performed on the chosen model. This analysis will establish the maximum measurement tolerances allowed to calculate the stiffness with an acceptable accuracy. With the maximum measurement tolerances it is possible to implement rules on the design of the experimental set-up.

In Chapter 6 the most suitable measurement instruments will be chosen to satisfy these design rules. To establish the validity of the model a number of experiments will be performed on the set-up built for [5]. Chapter 6 also will give detailed information about the experimental procedures and the equipment to be used. The results of this experimentation will then be discussed in Chapter 7. With these design rules established, and with the results of the experiments, a number of design concepts will be presented that meet the specifications. Comparing the different design concepts will give the best design concept to be build. Using the best concept as a guideline, Chapter 8 will display the steps needed to manufacture the experimental set-up. The results of the experiments and the design of the set-up will be thoroughly discussed in Chapter 9 and recommendations will be given in Chapter 10.

Part I

Cantilever stiffness calculation

Chapter 2

Cantilevers and their stiffness

According to Merriam-Webster, the definition for a cantilever is: A projecting beam or member supported at only one end [6]. As this definition suggests, it is only possible to deflect one end of this kind of beam as the other end is supported. Loading of a cantilever beam can be done in several ways which will be described in this chapter. The resistance to this loading, also known as its stiffness, gives a relation between the force necessary to deflect the beam in any particular direction.

2-1 AFM probes

The cantilevers are attached to an AFM chip. It is possible that only one cantilever is attached or a whole array of cantilevers to increase the scanned area [7]. The chip makes it possible to handle the probe while it is being put into the AFM itself. These chips have the dimensions given Figure 2-1a. The standardization of the chips makes it possible to use the probes from any manufacturer in any AFM. Some AFM manufacturers have implemented an alignment feature in the chip-holders of the AFM. This alignment feature allows for replacement of the cantilever tip within 8 µm of the original position when exchanging probes [8]. The shape, size and material can vary between manufacturers and between purposes of the probe. Two of the most used shapes are the triangular and the rectangular shape. As the name suggests, the rectangular cantilever is a rectangle, but it's end can be of triangular shape. The triangular cantilever is a triangle with part of the material removed at its base, shown in Figure 2-1b. The manufacturers of these cantilevers claim higher stiffness in lateral load direction making them more robust, but a recent trend has researchers returning to the rectangular shape [9]. The material used to manufacture the cantilevers can be silicon or silicon nitride [1] either coated or uncoated with different materials, the choice of the best material decided by the application of use.

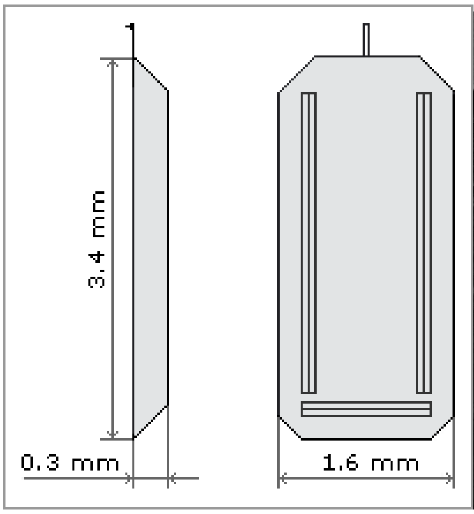

(a) The nominal dimensions of AFM chip carrying the cantilever.

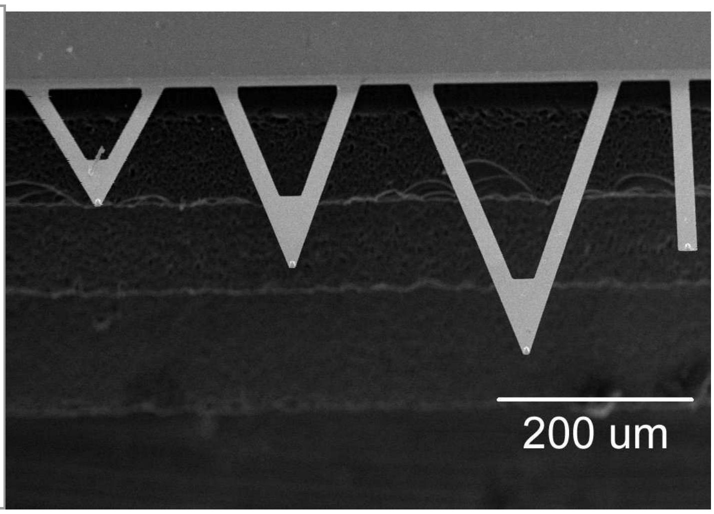

(b) An array of different sized and shaped cantilevers.

Figure 2-1: Schematic view AFM chip and SEM image of cantilever geometry. (a) A schematic overview of the AFM chip carrying the cantilever probe that is to be used. The alignment grooves can be seen on the underside of the chip. (b) An array of triangular cantilevers and rectangular cantilevers is shown which makes it possible to scan a surface with cantilevers of different stiffness values.

2-2 Cantilever loading

The AFM probes, which are cantilevers with a tip attached at the end, can be loaded in three different ways during scanning in the Atomic Force Microscope. These different loads cause the cantilever to deflect in different ways:

- **End loads -** A force [F] acting at the end of the cantilever beam causes a deflection of the beam.
- **End moment -** A moment [M] acting at the end of the cantilever beam causes a rotation along the x-axis.
- **Torque -** A torque [T] acting at the end of the cantilever beam causes a rotation along the y-axis.

Although these three loads can occur during the operation of the AFM, the focus of this thesis will only be on the cases where deflections are caused by forces acting at the end of the beam. The main deflection is caused by a force pushing or pulling at the scanning tip. These forces cause a deflection along the y-axis. As was mentioned in Section 1-1, using Hooke's law the deflection is used to calculate the stiffness k. The assumption used in this thesis is that the stresses inside the cantilever, caused by the deflection, remain in the linear-elastic region which will cause the stiffness to stay linear. Also assuming that the Young's modulus E stays constant, the displacement δ of a rectangular cantilever is given by

$$\delta = \frac{4FL^3}{Ewt^3} \tag{2-1}$$

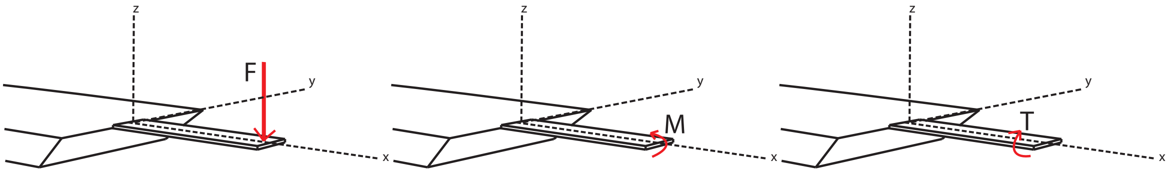

(a) A force acting on the cantilever tip.

(b) A moment acting on the cantilever tip.

(c) A torque acting on the cantilever tip.

Figure 2-2: Three different load types can affect the cantilever during scanning. (a) Forces acting at the end of the cantilever cause it to deflect in the y-direction. (b) A rotation around the y-axis is caused by a moment acting at the end of the cantilever. (c) Applying a torque at the end of a cantilever will cause a rotation around the x-axis.

where L, w, and t represent the length, width and thickness of the cantilever respectively. Using Hooke's law and rewriting Equation (2-1) gives the stiffness k of the cantilever as

$$k = \frac{F}{\delta} = \frac{Ewt^3}{4L^3}. \tag{2-2}$$

It can be clearly seen from Equation (2-2) that the stiffness depends on the material properties, through the Young's modulus, and the geometry of the cantilever. As is already mentioned in Section 1-2 that the cantilever can be coated with another material to improve the reflectiveness. This added layer will not only add to the height of the cantilever but it will also change the Young's modulus of the material [10]. Without information about the layer thickness it is not possible to give an accurate value for the new combined Young's modulus. The width and height in Equation (2-2) can be replaced with the moment of inertia of the beam which is given by

$$I = \frac{wt^3}{12}. \tag{2-3}$$

This moment of inertia can be calculated for any cross-section of the cantilever. Combining Equation (2-3) with Equation (2-2) leads to the following expression of the stiffness,

$$k = \frac{3EI}{L^3}. \tag{2-4}$$

The reason behind this combination is that the cross-section of the cantilever beam is no longer rectangular after the anistropic etch used during production. The sides of the cantilever are angled at 54.7° with respect to the ground plane, so Equation (2-2) no longer applies [11]. But the moment of inertia can be calculated for any cross-section, making it easier to use Equation (2-4).

2-3 Beam versus plate

Equation (2-4) is part of the Euler-Bernoulli beam theory which is a simplification of the linear theory of elasticity [12]. Due to the dimensions of the cantilever it needs to be considered whether the stiffness can be calculated by the equation for a beam or for a plate. When a beam deflects due to application of a load, it causes stresses inside the beam. Looking at

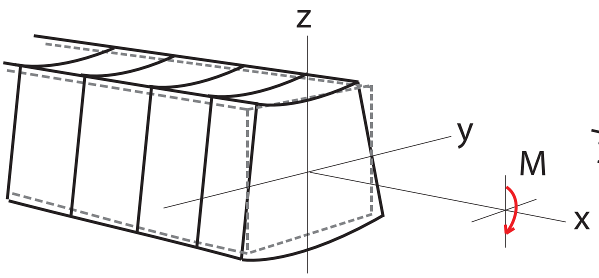

(a) Deformation of a beam

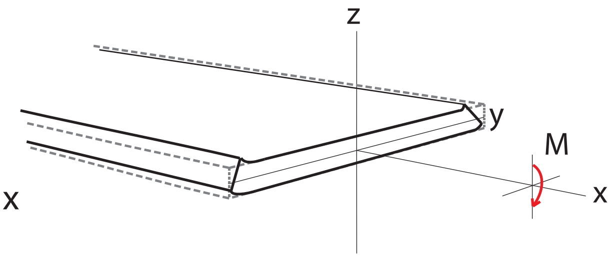

(b) Deformation of a plate

Figure 2-3: The result of a deflection applied to the end of a cantilever. In (a) it is exaggeratedly shown how a beam deformes due to this deflection. The grey dashed lines depict the beam in its rest state, the black lines the deformed state. The same is shown in (b) for a plate which is deflected by a force.

Figure 2-3a, it is shown that the positive stress above the center causes a contraction of the sides of the beam while the negative stresses underneath causes an expansion of the sides. The case of a plate bending shows a different result. The positive and negative stresses again cause a deformation, but it can only take place at the sides of the plate [12]. Due to this fact, the side of the plate angle up to compensate for the expansion of the top side and the compression of the lower side. This is shown in Figure 2-3b. This difference in deformation behaviour during bending between a plate and a beam is accounted for by introducing the materials Poisson ratio ν into Equation (2-4). This added term compensates for the deformation at the sides of the plate with

$$k = \frac{3EI}{(1-\nu^2)L^3} \tag{2-5}$$

and is part of the Kirchoff-Love plate theory. To establish if the cantilever needs to be considered as a beam or a plate, a rectangular cantilever is modeled in COMSOL Multiphysics. The Finite Element analysis calculates the deflection of the cantilever due to different magnitudes of forces applied at the free end of the cantilever. Results of this analysis are displayed in Table 2-1. From this analysis it can be determined that the behaviour of the cantilever is beter modelled by a plate, than by a beam. With accurate knowledge of the cantilever geometry

Cantilever with length 400 µm, width 40 µm, thickness 2 µm			
Force	calculated beam deflection [µm]	calculated plate deflection [µm]	FEA deflection [µm]
1 µN	5.29	4.93	4.93
2 µN	10.46	9.85	9.85
3 µN	15.69	14.78	14.78
4 µN	20.92	19.71	19.71
Mean error	6.1%	0	ref

Table 2-1: Results of FE analysis on the bending of an AFM probe cantilever.

and material properties, Equation (2-5) can be used to find the stiffness of that particular cantilever. But the added layer of reflection increasing material leads to a new combined Young's modulus and Poisson's ratio. This has been the reason for numerous studies into the evaluation of the cantilever stiffness through different methods.

Chapter 3

State of the art

As discussed in Chapter 2, it is difficult to define an accurate value for the stiffness of a cantilever if its exact geometry and material properties are unknown. This chapter will discuss the current calibration techniques that make it possible to determine the stiffness through other physical properties. After a comparison of these properties a newly proposed calibration technique will be introduced and the physics behind this technique will be explained.

3-1 Current calibration techniques

Finding the stiffness of a cantilever is commonly referred to as calibrating the cantilever. Presently there are numerous calibration techniques, based on different physical properties, used to estimate the stiffness. These techniques can be divided into three categories: dimensional, static and dynamic.

- **Dimensional -** The dimensional category is an analytical calculation of the spring constant based on the measurement of the cantilever dimensions combined with an estimation of the layer and material's elastic properties. Typical methods include: simple beam estimation and finite element analysis.
- **Static -** Determination of the spring constant based on the static force-displacement measurements. Typical methods include: deflection on reference structures such as reference cantilever or reference spring micro-structures, deflection by force balance or indent meters and deflection by electrostatic force.
- **Dynamic -** Determination of the spring constant based on the resonant response of the cantilever. Typical methods include: frequency scaling, thermal tune, Sader's method, and added mass.

3-1-1 Dimensional

Dimensional calibration methods use, among others, the equations developed in the previous Chapter to calculated the cantilever's stiffness. These dimensions are often measured with microscopes or supplied by the cantilever manufacturers.

Finite Element Model

The analytical beam model is a Finite Element Model (FEM) which calculates the bending stiffness of the beam according to the parameters that are put into a model. The accuracy of this method greatly depends on the accuracy of the values of length, width, height, Young's modulus and specific weight of the cantilever. If all these values are known, the FEM's output will be the stiffness of the cantilever. The greatest advantage of this method is that it is non-destructive, fast and doesn't require handling of the AFM probe. The measurements needed to get all relevant parameters do not interact with the cantilever, so no damage or contamination will occur. The main drawback of this method is that the parameters to be used, must be as accurate as possible for the model to give an accurate stiffness. Another drawback is that the model itself needs to represent the real cantilever as close as possible. This is quite hard to accomplish. The thin layer of added reflective material is hard to measure accurately making the model less accurate [13, 14].

Simple beam estimation

The simple beam estimation is the method described in Section 2-2. Calculation of the stiffness is done by filling in all the variables in Equation (2-2). It has the same deficiencies as the Finite Element Analysis, but it is much faster in getting a rough estimation of the cantilever's stiffness [9]. The same disadvantages as the Finite Element Model apply for this calibration technique.

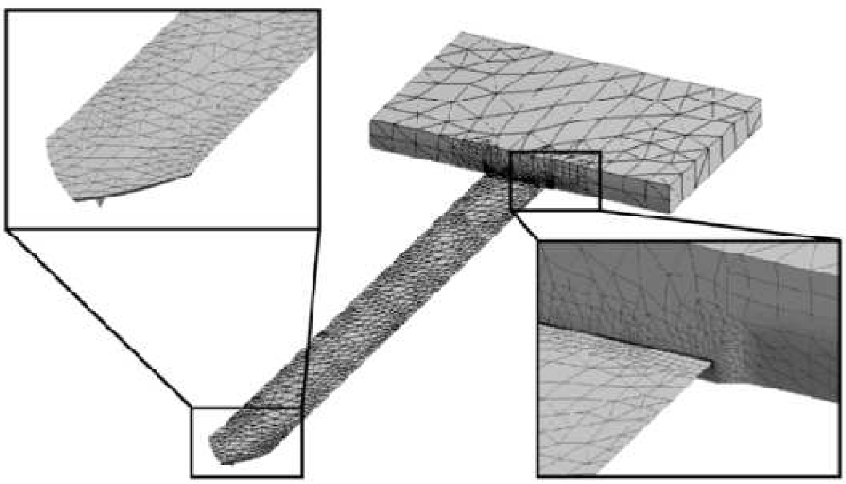

Figure 3-1: FEA model of rectangular cantilever with a triangular end.

3-1-2 Static

The static calibration depends on the static displacement of the cantilever by a reference force. With knowledge of the applied force it is possible to calculate the bending stiffness of the cantilever.

Reference structures

Reference structures are used of which the stiffness is known. These structures can take any shape or form as long as the stiffness of these structures can be precisely calculated. The most common of these structures are reference cantilevers and reference springs. The tip of the cantilever is placed at a specific point of the reference structure and the tip is moved downward. Relating the difference of deflection between the cantilever and the reference structure to the downward movement gives the stiffness of the cantilever [15, 16, 17]. The disadvantages of this technique are the possibility of breaking the cantilever and the uncertainty of the placement of the probe on the reference cantilever. If the probe is not placed at the right location the calculated stiffness will have an error.

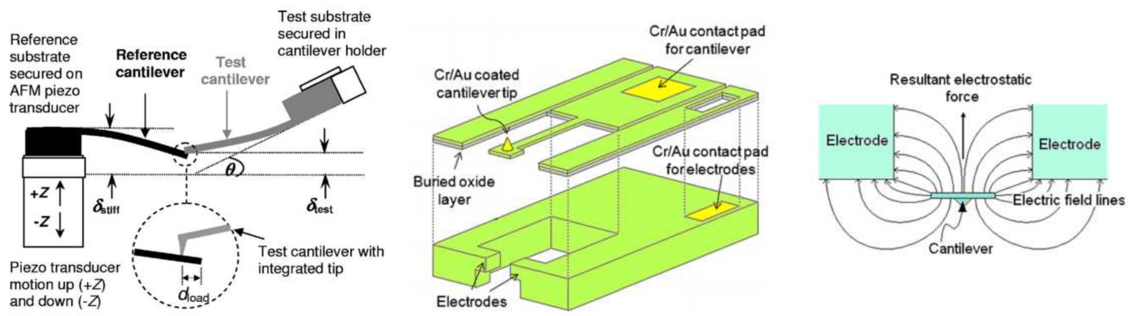

(a) Schematic view of a AFM probe being calibrated on a reference cantilever.

(b) Schematic overview of the structures used in electrostatic calibration.

(c) The electric field lines generating an upward force on the cantilever.

Figure 3-2: Images showing the working principal of the reference structure and electrostatic force. (a) A cantilever secured in a holder is pressed against a reference substrate and the resulting deflection is measured [15]. (b)Assembly to measure the stiffness of a cantilever placed on top of the structure [18]. (c) The vertically asymmetric electric filed between cantilever and electrodes results in an upwards force on the cantilever [18]

Electrostatic force

Electrostatic force calibration is performed by charging an electrode and the cantilever by a voltage potential. Due to the charge built up on the surfaces of electrode and cantilever an electrostatic force will attract the two object towards each other. The amount of voltage potential can be related to electrostatic force acting on the cantilever. Using Hooke's law again gives the value for the cantilever stiffness [18, 19]. The disadvantage of this method lies in the fact that the model describing the behavior needs to be accurate. The force acting on the cantilever is non-linear which increases the difficulty of solving this problem.

Force balance and load button

The force balance and load buttons use Hooke's law, to determine the force needed to deflect the cantilever. The load button is a small plate capable of detecting very low forces. By pressing the cantilever onto the load button until a deflection is seen, it can be established what the cantilever stiffness is. The force balance uses small structures that displace a preset weight by the pressure exerted by a cantilever pressing on a plate. This also leads to the stiffness of the cantilever [20, 21] The disadvantage of this technique is the angle necessary between the load button and cantilever. The application of force by the cantilever on the load button deforms the cantilever. This deformation changes the area of contact and changes the location the force is working on. This angle and the possibility of breaking the cantilever are its main disadvantages.

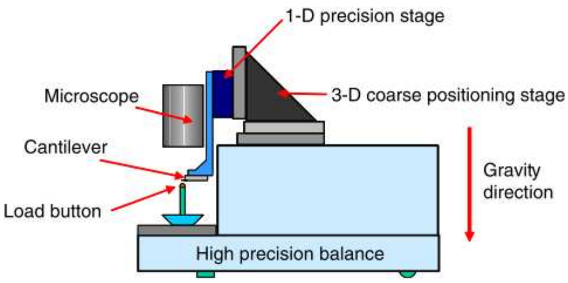

(a) Schematic view of the positioning stage placing the AFM probe on the load button.

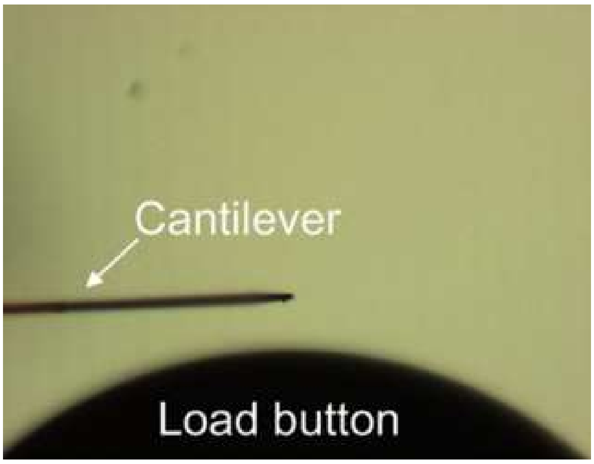

(b) Close-up view of a cantilever moved in proximity of a load button.

Figure 3-3: The working principle behind the load button. (a) A positioning stage is used to bring a cantilever towards a load button, while viewing it with a microscope. (b) A close-up view of the cantilever approaching the load button. When the cantilever makes contact and deforms due to a further downward displacement, a force is measured by the load button. The orientation of the cantilever with respect to the load button is very important. [20].

3-1-3 Dynamic

Dynamic testing of the cantilever stiffness is done by examining the characteristics of the cantilever when it is excited. The eigenfrequency or thermal excitation is measured since they can be related to the cantilever stiffness.

Cleveland

The resonance frequency of a cantilever is dependent on its mass and on its stiffness. If you measure the resonance frequency of the cantilever and know its mass using $k = mf^2$, where m and f are the mass and frequency in radians per second respectively, will give the value of the stiffness. The biggest disadvantage of this equation is the need for determining the mass of the cantilever. Since the cantilever is attached to a chip-holder, it is not possible to measure the weight on an finely calibrated scale. A solution to this problem is proposed by Cleveland et al. [22]. By placing a tungsten sphere near the tip of the cantilever, the total mass of the cantilever will change. By measuring the radius of the ball and using its bulk weight gives the added weight. This added weight will lower the resonance frequency. The change in weight and the change in frequency can now be used to solve for the stiffness. Disadvantages of this technique are the approximation of the added mass and the possibility of breaking the cantilever. The sphere attached to the cantilever is assumed to be perfectly spherical, but in reality this isn't the case. The mass is only an approximation of the real situation. The placement of the added mass can also damaged the cantilever.

Sader

Using the dimensions of the cantilever and measuring the eigenfrequency and quality factor of the fluid in which the cantilever is placed, most often air, the Sader method determines the stiffness of the cantilever with the following equation,

$$k = 0.1906 \rho_f b^2 L Q_f \Gamma_i(\omega_f) {\omega_f}^2, \tag{3-1}$$

where rho_f, b, L, Q_f, Γ_i and ω_f are the density of the fluid, cantilever width, length, quality factor in the fluid, the imaginary components of the hydrodynamic function Γ and the fundamental mode resonance frequency respectively. This equation is only valid for quality factors » 1, which is the case with cantilevers suspended in air [23]. The hydrodynamical expression $\Gamma_i(\omega)$ only depends on the Reynolds number:

$$\mathrm{Re} = \frac{\rho_f \omega b^2}{4\eta}, \tag{3-2}$$

where η is the viscosity of the fluid. The resonance frequency is calculated by measuring the thermal noise spectrum, which is transformed with Fast Fourier Transformation.

Thermal tune

One method to arrive at a more accurate estimate of the stiffness involves measuring the cantilever's mechanical response to thermal noise. This is the cantilever's motion in response to thermal agitation, including the Brownian motion of the molecules of the surrounding fluid. This fluid is usually air or water. This method offers a combination of speed and ease-of-use, and is widely accepted and adopted by AFM users worldwide [24]. The thermal tune method measures the cantilever's fluctuations as a function of time. From the time-domain measurement, it extracts the frequency spectrum of the cantilever's mechanical response (proportional to the power spectral density, PSD). By fitting the frequency spectrum to a Lorentzian line shape, Figure 3-4b, the software arrives at an estimate of the cantilever's stiffness. The method assumes the cantilever has a single degree of freedom, and makes use of the energy equipartition theorem. This theorem relates the temperature to the cantilever's average fluctuation energy, which is found through integrating the Lorentzian fit [25].

Principal method	**Dimensional**		**Dynamical**			**Static**		
Approach	Beam estimation	FEM	Cleveland	Sader	Thermal tune	Reference structures	Load button	Electrostatic actuation
Uncertainty of method	25%	10%	15-25%	5-10%	20 %	10-30%	0.4%	15-25 %
Main source of uncertainty	Equation, thickness, Young's modulus	Thickness, Young's modulus	Added mass	Knowledge of Reynolds No.	Interference other noise source	Stiffness of reference	Force balance calibration	Equation
Potential damage tip	N.A.	N.A.	High	Low	Low	Medium	Medium	Low
User friendliness	High	High	Poor	Medium	High	Medium	Medium	Medium
Advantages	Fast	Fast	Independent of shape	No modification, can be used in any environment	Independent of material properties and shape	Not dependent on cantilever geometry or material	Accuracy. Measures stiffness directly	Ease of use
Disadvantages	Highly simplified model, accurate knowledge of material properties needed	Computation time, accurate model properties needed	Accurate placement mass, calibrated mass spheres needed, destructive	Only rectangular cantilevers, tip and poistion of mass	Only soft cantilever, temperature data T needed	$k_{ref} \sim k_{test}$, accurate probe positioning	Calibration balance, expensive equipment, $k_{test} > 1N/m$	Equation deficiencies

Table 3-1: Summary of different kinds of calibration methods [2]

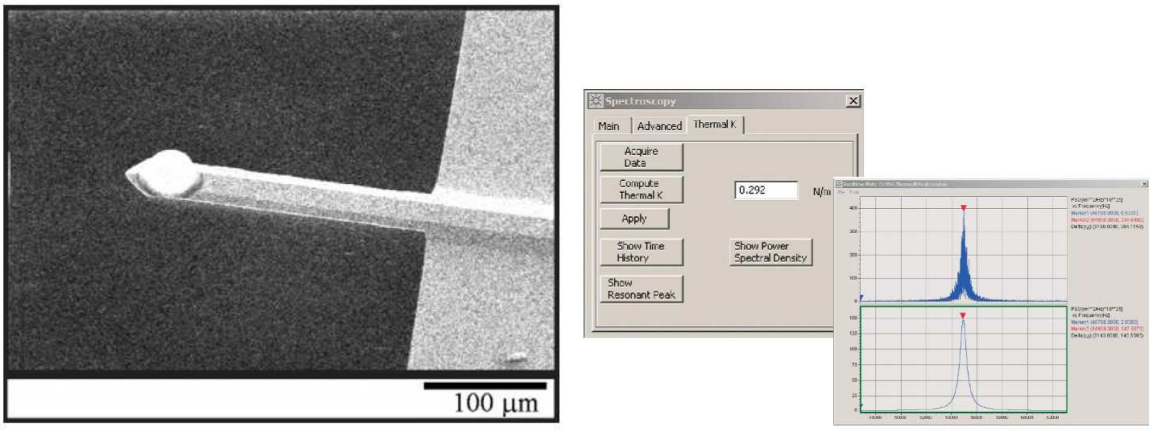

(a) Tungsten ball placed at the end of a AFM probe.

(b) The power spectral density plot of the deflections caused by thermal excitations.

Figure 3-4: Images displaying the techniques used with dynamic calibration. (a) Taking a cantilever and placing a tungsten ball with a known mass will change the eigenfrequency of the cantilever. With the change of frequency and the added mass known, the stiffness can be determined. (b) The power spectral density plot of fluctuations in the output of the cantilever deflection detector. From this plot the stiffness can be calculated [26].

3-2 Electrostatic Pull-in Instability (EPI)

Since all the current calibration techniques have shortcomings a new calibration method is suggested. This calibration method is based on the phenomenon called Electrostatic Pull-in Instability, from now on referred to as EPI. This chapter will first explain the physics behind EPI with the use of an example. Thereafter it will be explained how this phenomenon can be used to evaluate the stiffness of a cantilever.

3-2-1 Physics behind EPI

Coulomb's law states that the magnitude of the electrostatic force of interaction between two point charges is directly proportional to the scalar multiplication of the magnitudes of charges and inversely proportional to the square of the distances between them. This force is attractive when the product of the two charges is negative and repulsive when this product is positive. When two oppositely charged plates are brought into vicinity of each other, there will be a force acting between these plates. To calculate this electrostatic force one needs to multiply this charge with the electric field. The charges on one plate don't create forces upon that plate so only half of the force should be used

$$F_{es} = \frac{1}{2}\sigma E \tag{3-3}$$

The electric field is given by $E = -\frac{V}{g}$, the change of electric potential along the gap between plates. Considering Gauss' law $E = -\frac{\sigma}{\epsilon}$ and combining this with the expression for the electric field in Equation (3-3) gives the alternate expression for the electrostatic force:

$$F_{es} = -\frac{1}{2}\epsilon\frac{V^2}{d^2} \tag{3-4}$$

Consider the following lumped model shown in Figure 3-5 with one degree of freedom. Two plates, one attached by an ideal spring and one fixed, are brought to a distance d of each other. Between these two plates a bias voltage is applied. Assuming that the plates are rigid, the dynamic equation of this set-up can be established. The two forces acting on these plates are the previously mentioned electrostatic force and the spring force. The equation of the force applied by the spring is

$$F_{spring} = k(g - g_0), \tag{3-5}$$

where g and g_0 are the distance and the original distance between the plates.

As shown in Equation (3-4), an increase in the applied voltage will cause an increase in the electrostatic force. This increase in force is balanced by the elongation of the spring until the force exerted by the spring is again equal to the electrostatic force. But since the force, exerted by the spring, grows linearly with distance and the electrostatic force grows with the inverse of the distance squared, the restoring force of the spring will, at some point, not be sufficient to keep the plates apart. Considering the static part of Newton's equation,

$$F_{spring} + F_{es} = 0 = k(g - g_0) - \frac{1}{2}\epsilon\frac{V^2}{g^2} = 0 \tag{3-6}$$

This can be rewritten to express the stiffness of the spring as a function of the applied voltage and the distance between the plates.

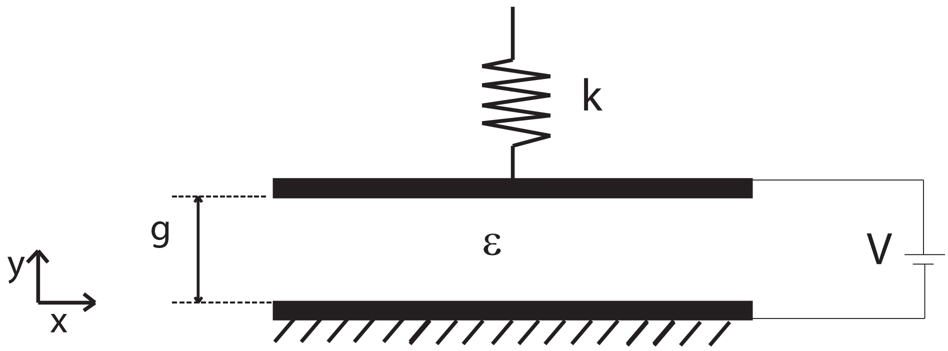

Figure 3-5: Two charged plates

At a certain bias voltage the restorative force of the spring will not be able to counteract the electrostatic force generated between the plates. This voltages is called the pull-in voltage (V_{pi}). If Equation (3-4) is rewritten to solve for k one gets:

$$k = \frac{27 \cdot \varepsilon \cdot {V_{pi}}^2}{8 \cdot {g_0}^3}. \tag{3-7}$$

The stiffness of the spring in this experiment is a function of the pull-in voltage and the original distance between the plates g_0.

3-2-2 Electrostatic Pull-In used as a calibration method

As shown in the previous Section, the pull-in voltage is distinctive for the system of parallel plates. This voltage depends in this case on the gap between plates and the spring constant of the suspended spring. This is only a one-dimensional example and the cantilever isn't. The equation however can be changed for a three dimensional situation by taking into account the area of the cantilever. By using Equation (3-7) and multiplying it with the area of the cantilever one gets

$$k = \frac{27 \cdot \varepsilon_0 \cdot {V_{in}}^2 \cdot b \cdot L}{8 \cdot g^3}, \tag{3-8}$$

where L and b are the length and width of the cantilever respectively.

It can be seen from Equation (3-8) that the stiffness only depends on the dimensions of the cantilever and the gap underneath it. By using the pull-in phenomenon the mass and stiffness of the cantilever have been decoupled, that is to say that the mass of the cantilever no longer has an influence on the calculation of the stiffness. Contamination of the cantilever will not have an influence on the calculated stiffness values, which does impact the other calibration methods that require its mass. Although the dimensions of the cantilever are easily measured, the gap between the cantilever and electrode is harder to evaluate. A top view of the cantilever will only permit a distance measurement form the top plane of the cantilever to the electrode. The thickness of the cantilever is thus needed again to measure the gap. Sadeghian et al. [4] suggests using a technique which they call the differential gap approach. The differential gap approach is explained as follows:

- The first measurement of the pull-in voltage V_{pi1} is performed with an unknown gap.
- The gap is increased with an amount of Δg.
- The second measurement of the pull-in voltage V_{pi2} is performed with an unknown gap + Δg.
- Use the values of V_{pi1}, V_{pi2} and Δg to calculate the stiffness.

To use the differential gap approach Equation (3-8) needs to be re-written to

$$k = \frac{27 \cdot \varepsilon_0 \cdot b \cdot L}{8} \cdot \frac{\left({V_{pi2}}^{\frac{2}{3}} - {V_{pi1}}^{\frac{2}{3}}\right)^3}{\Delta g^3}. \tag{3-9}$$

Using Equation (3-9) it can be seen that two pull-in measurements and the change of gap are sufficient to extract the stiffness. This eliminates the need to do an initial measurement of the gap between cantilever and electrode. The absolute measurement is replaced by the relative measurement of the gap increments.

3-3 From lumped model to cantilever

The cantilevers used in AFM microscopes can't be seen as a solid plate suspended by a spring. Since one end is fixed, only the end of the beam is able to move towards the electrode. This movement causes bending of the beam. As the beam bends, the electrostatic force increases fastest at the point where the beam is closest to the electrode. Instead of calculating the stiffness of a suspended spring, the bending stiffness of the beam needs to be determined. Hence, Equation (3-9) can not be used in its current form. By using potential energy equation an equilibrium equation can be found. The potential energy stored by the electric charge on the plates is given by

$$U = 1/2 \cdot C \cdot V^2 \tag{3-10}$$

Taking the derivative of this equation with respect to the vertical coordinate 'y'

$$F = \frac{\partial U}{\partial y} = \frac{1}{2} \cdot \left(\frac{\varepsilon \cdot A}{g} \right) \frac{\partial}{\partial y} \cdot V^2 = -\frac{1}{2} \cdot \varepsilon \cdot A \cdot \frac{V^2}{g^2}, \tag{3-11}$$

gives the total electrostatic force working between the cantilever and the electrode. The electrostatic force distribution over the length of the plate can be found by taking the derivative with respect to the horizontal coordinate x,

$$\frac{\partial F}{\partial x} = \left(-\frac{1}{2} \varepsilon b x \frac{V^2}{g^2} \right) \frac{\partial}{\partial x} = -\frac{1}{2} \varepsilon b \frac{V^2}{g^2}. \tag{3-12}$$

The orientation of the coordinates x and y are given in Figure 3-5. The gap between cantilever and electrode g is equal to the initial gap g_0 minus the deflection of the cantilever. Thus the electrostatic force is a function of the displacement shape. If the deflection function of the cantilever in the y-direction is called 'g(x)' the distributed force results in

$$q(x) = \frac{\partial F}{\partial x} = -\frac{1}{2} \varepsilon b \frac{V^2}{\left(g_0 - g\left(x\right)\right)^2} \tag{3-13}$$

The force exerted by the bending of the beam can be found by using the Euler-Bernoulli beam equation and combined with Equation (3-13) gives the equation for the general governing nonlinear differential equation of the pull-in behavior as stated in [27],

$$EI \frac{\partial^4 v}{\partial x^4} = q\left(x\right). \tag{3-14}$$

Substituting variables and a superscript notation indicates the order of derivation with respect to 'x'

$$\begin{aligned} w\left(x\right) &= g_0 - g\left(x\right) \\ w^{(4)} &= -g^{(4)} \end{aligned} \tag{3-15}$$

Setting parameter 'c' to hold all the constants and voltage V,

$$c = -\frac{1}{2} \cdot \frac{\varepsilon \cdot b \cdot V^2}{E \cdot I}. \tag{3-16}$$

After rewriting the 4^{th} order non-linear differential equation the notation of the problem simplifies to

$$w^{(4)} = -\frac{c}{w^2} \tag{3-17}$$

The resulting equation is a fourth order differential equation which has no exact solution.

Chapter 4

Modeling the cantilever beam

Although it is possible to solve Equation (3-17) by the Generalized Differential Quadrature Method [27], it can only be used for straight cantilevers. The first problem that is encountered is the fact that the cantilever beams can become bent during the fabrication process. Since the reflectivity-increasing metals and silicon have different thermal expansion coefficients, cooling down the probe to room temperature after etching will cause the two materials to contract at different rates. The residual stresses, caused by the difference of contraction rate, result in out-of-plane bending of the cantilever. This out-of-plane bending creates a curvature along the length of the cantilever. Another physical phenomenon that is present with electrostatic actuation is fringing. The fringing will increase the force acting on the cantilever which, if neglected, would result in a lower stiffness. With these side effects it has become clear that the fourth order differential, mentioned in the previous chapter, is not sufficient to describe the behavior of the cantilever. This chapter will introduce models that have been developed to define the behavior between electrode and cantilever. A brief overview of these models will be given and their results will be compared with a Finite Element Analysis performed in COMSOL Multiphysics. The model that shows the best comparison with experimental values and the FE-analysis is chosen and more details about this model will be given. The orientation of the x- and y-coordinates given in this Chapter is taken as shown in Figure 4-1.

4-1 Modeling Electrostatic Pull-in

To model the behavior of the cantilever acted on by electrostatic forces, it needs to be decided if the inclusion of fringing fields and curvature are needed. For some ratios between the gap and width of the cantilever, the fringing can be neglected according to [28, 29] but for completeness it still needs to be considered. This is also the case for the curvature of the cantilever, although some sources neglect the change of gap due to the curvature [30, 31], the electrostatic force grows with the inverse of the gap squared. This will result in a higher force on the cantilever tip when it curls towards the electrode.

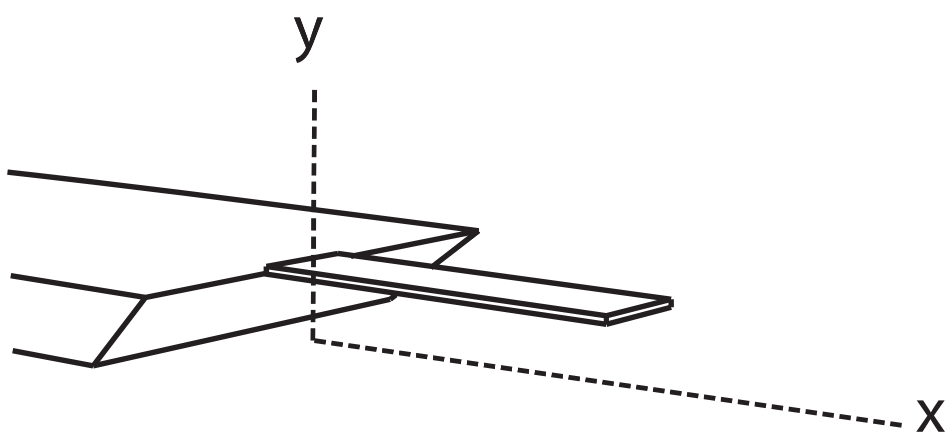

Figure 4-1: The orientation of x- and y-coordinates

Fringing

Using electrostatic actuation has some side-effects when it comes to modeling its behavior. Until now it has been assumed that the electric field between the cantilever and electrode runs in straight lines. This doesn't happens in reality where the field lines don't necessarily run in straight lines but can be curved. This happen especially with fringing fields. Since the whole surface of the cantilever becomes charged, the sides and front of the cantilever will added to the area that is generating an electrostatic force as is shown in Figure 4-2a. This Figure shows that the field lines between the electrode and cantilever are straight. But since a charge also builds up on the sides of the cantilever, field lines also run from the sides and tip towards the electrode. These field lines will increase the force exerted between the cantilever and electrode [32].

Influence of curvature on the gap

The cantilever can curl upwards or downwards along its length axis due to residual stresses. This curling thus in- or decreases the gap along the length of the cantilever. To define the increase of the gap as a function of x, geometry as shown in Figure 4-2b needs to be studied. Based on the geometry as shown, [33] states that

$$\begin{aligned} y(L) &= \rho - h \\ &= \rho - \rho \cdot \cos\theta \\ &= \rho - \rho \cdot \cos\left(\tfrac{L}{\rho}\right) \\ &= \rho\left(1 - \cos\left(\tfrac{L}{\rho}\right)\right) \end{aligned} \tag{4-1}$$

For small angles one can assume that the increment in x is equal to the increment along L, and one gets

$$y(x) = \rho\left(1 - \cos\left(\frac{x}{\rho}\right)\right) \tag{4-2}$$

If the AFM chip is placed in such a way that the plane of the chip is not perpendicular to the plane of the electrode, another variable needs to be taken into account. Setting the plane

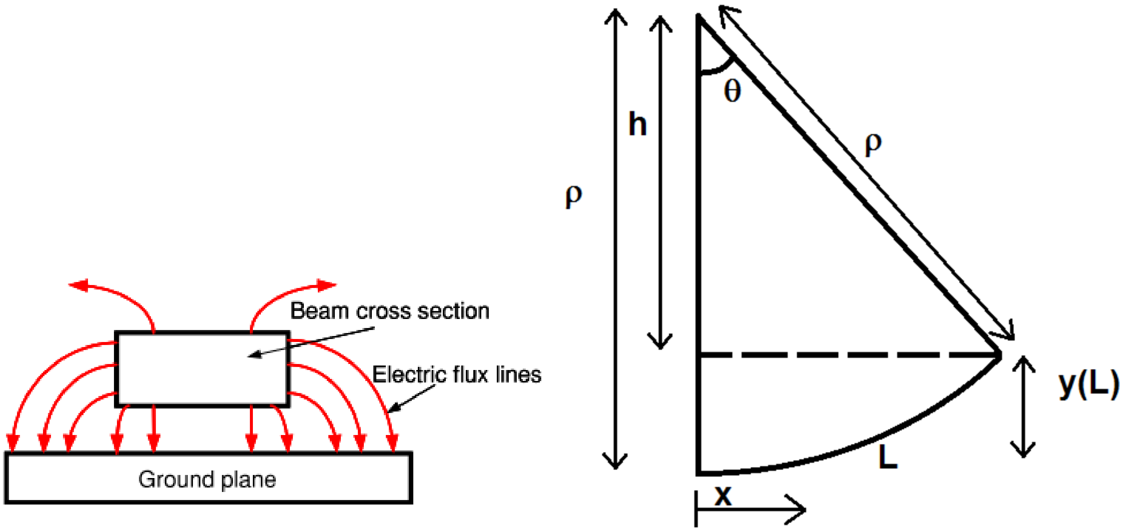

(a) Fringing fields between a beam and an electrode.

(b) Deriving a parameter for the curvature from the geometry.

Figure 4-2: To make the model describing the cantilever behavior during electrostatic actuation more accurate the following effects need to be included (a) Due to fringing fields the area which is charged is larger than just the surface facing the electrode. (b) Manufacturing the AFM probes leaves residual stresses inside the cantilever causing it to bend. To describe this bending a variable is needed.

of the AFM chip as the reference plane, the gradient of the electrode plane determines the change of the gap along the length of the electrode. The gradient *alpha* is given by

$$gradient \cdot x = \frac{change\,in\,height}{change\,in\,length} \cdot x = \alpha \cdot x. \tag{4-3}$$

Combining Equation (4-2) and Equation (4-3) with the initial gap g_0 now defines the gap between the cantilever and the electrode as

$$G = g_0 + \rho\left(1 - \cos\frac{x}{\rho}\right) + \alpha \cdot x, \tag{4-4}$$

for every x along the length of the cantilever.

4-1-1 Potential energy equation

The basis of all the models is the solution of the energy equation. Instead of using the forces acting between cantilever and electrode, the mechanical bending strain energy and the electric potential energy stored in the beam is used. The mechanical bending strain energy is given by U_m,

$$U_m = \int_0^L \frac{E \cdot I}{2}\left(\frac{d^2 w}{dx^2}\right)^2 dx, \tag{4-5}$$

where E, I, L and w represent the Young's modulus, the cross-sectional area moment of inertia, the length and the deflection as a function of the positions x respectively. The electrical potential energy is given by U_e,

$$U_e = -\int_0^L \frac{\varepsilon_r \cdot \varepsilon_0 \cdot b \cdot V^2}{2(G-w)} dx, \tag{4-6}$$

where b, G, V, ε_r and ε_0 represent the beam width, the initial gap between the beam and the electrode, the applied bias voltage the permittivity of free space and the dielectric constant of the dielectric medium between the beam and the ground, respectively. Combining Equation (4-5) and Equation (4-6) gives the equation for the total potential energy,

$$U = U_m + U_e = \int_0^L \frac{E \cdot I}{2} \left(\frac{d^2 w}{dx^2}\right)^2 dx - \int_0^L \frac{\varepsilon_r \cdot \varepsilon_0 \cdot b \cdot V^2}{2(G-w)} dx \tag{4-7}$$

The electrostaticly actuated cantilever beam has a difficult solution since the system behaves non-linearly with the nonlinear electrostatic force coupled with the structural deflection. The approximate analytical solution, also known as the assumed mode method, is often used to solve such a problem[34]. This method expresses the deflection function $w(x)$ of the beam as

$$w(x) = \eta \cdot \phi(x), \tag{4-8}$$

where $\phi(x)$ is the assumed shape function satisfying the boundary conditions and the coefficient η is the associated modal participation factor. These boundary conditions state that for a cantilever beam, the deflection and rotation angle are both zero at the fixed end, and the moment and transverse shear force are both zero at the free end [35]. In other words,

$$\begin{aligned} w\,(0) &= w'\,(0) = 0 \\ w''(L) &= w'''\,(0) = 0 \end{aligned} \tag{4-9}$$

With Equation (4-8) the system can be solved. The system is in equilibrium when the first-order derivative of the total potential energy U with respect to η is equal to zero,

$$\frac{dU}{d\eta} = EI\eta \int_0^L \left(\phi''\right)^2 dx - \frac{\varepsilon_r \varepsilon_0 b V^2}{2} \int_0^L \frac{\phi}{(G-\eta\phi)^2} dx = 0. \tag{4-10}$$

Whether this equilibrium is stable or unstable can be determined by taking the second-order derivative of the total potential energy with respect to η.

$$\frac{d^2 U}{d\eta^2} = EI \int_0^L \left(\phi''\right)^2 dx - \varepsilon_r \varepsilon_0 b V^2 \int_0^L \frac{\phi^2}{(G-\eta\phi)^3} dx = 0. \tag{4-11}$$

Equations (4-8),(4-10) and (4-11) can now be used to find the Pull-in voltage. The approach to find the pull-in voltage can still be performed in different ways. Literature [36, 33] assumes the deflection function $w(x)$ of the cantilever beam as a square function of position x in their analytical model. Other models [37, 38, 5], assume a polynomial function since there is no exact solution.

4-1-2 Comparison of models

Detailed descriptions about models developed to solve the electrostatic pull-in voltage can be found in [39, 40, 36, 41, 5]. A table of models with the best results is given in Table 4-1, which compares the calculated pull-in voltages for different lengths of cantilevers to measurements made in [42]. These measurements were made on specially-made test structures where the geometry of the cantilevers and the gap were closely monitored. The details of these variables are given in Table 4-1.

Variables	Values
Young's modulus, E (GPa)	153
Permittivity of free space, ε_0(F m^{-1})	$8.85.10^{-12}$
Dielectric constant between beam and ground ε_r	1.2046
Beam length, L (µm)	100-500
Beam width, b (µm)	40
Beam thickness, h (µm)	2.1
Radius of curvature, ρ (µm)	40000
Gap, g_0 (µm)	2.4

Table 4-1: Material and geometrical parameters.

From Table 4-2 it can be concluded that the full-order model and fourth-order model have the lowest mean error compared with the experimental data from [42]. The values of the models which take fringing into account indicate that including fringing with the calculations leads to pull-in voltages that are too low. These results show that the pull-in voltage can be neglected.

4-1-3 Finite Element Model made in COMSOL

COMSOL Multiphysics was used to calculate the pull-in voltage of a beam without curvature. It's model library contains an example of an electrostaticly actuated cantilever. This model was modified to be comparable with the results from the earlier comparison. The gap between cantilever and electrode was set at 2.1 µm, the width to 40 µm, and it's length varied between 100-500 µm. The material properties were kept equal to those shown in Table 4-1. Figures 4-3a and 4-3b show the results of one of the performed calculations. It is shows that the electric field lines do not only travel between the lower surface of the cantilever, but also emanate from its top, sides and front. The result of these additional field lines is an added attractive force, which lowers the pull-in voltage. These calculation were performed to investigate if the effect of fringing can be neglected as is proposed in [41].

A comparison of the results of the COMSOL calculation with the results of the different models has been made in Table 4-3. Comparing the mean errors of the different models shows that both the Full-order model and Fourth-order model, both without taking fringing into effect, show the least deviation from the calculated values done in COMSOL.

Length [µm]	Full-order	Fourth-order	Third-order	Wei's model	Full-order with fringing	Fourth-order with fringing	Uniform load deflection	Square law	Gupta's measured data[42]
100	75.51	78.74	85.62	81.09	69.45	68.93	84.1	95.2	72.07
125	49.67	51.82	56.35	66.72	47.35	46.00	54.91	64.1	48.60
150	35.65	37.21	40.46	48.18	34.10	33.34	38.43	45.42	35.82
175	27.25	28.40	30.87	36.74	26.74	25.61	32.14	35.12	27.89
200	21.76	22.68	24.65	29.48	20.84	20.56	25.00	28.95	22.55
225	18.01	18.76	20.39	24.30	17.95	16.95	22.94	24.06	18.79
250	15.30	15.96	17.34	20.79	15.01	14.56	18.58	20.84	15.95
300	11.82	12.31	13.38	16.12	12.06	11.27	14.28	15.64	12.61
400	8.36	8.70	9.45	11.69	8.56	8.00	10.29	11.76	9.10
500	6.77	7.05	7.65	9.69	7.02	6.49	8.18	10.48	7.27
Mean error	4.27%	3.21 %	10.02%	29.61%	4.68%	8.56%	14.05%	30.12%	ref

Table 4-2: Pull-in voltage of different analytical model describing the pull-in behavior. The measurements performed by Gupta are given as a reference.

Length [µm]	Full-order with fringing	Fourth-order with fringing	Full-order	Fourth-order	COMSOL solution
100	65.50 (12.1%)	71.37 (4.20%)	74.39 (0.14%)	74.76 (0.34%)	74.52
125	42.52 (10.85%)	45.55 (4.51%)	47.61 (0.19%)	47.85 (0.30%)	47.71
150	29.82 (9.90%)	31.57 (4.62%)	33.06 (0.11%)	33.22 (0.35%)	33.11
175	22.06 (9.19%)	23.16 (4.70%)	24.29 (0.03%)	24.41 (0.45%)	24.34
200	16.98 (8.82%)	17.71 (4.79%)	18.59 (0.05%)	18.68 (0.48%)	18.63
225	13.47 (8.52%)	13.98 (4.91%)	14.69 (0.07%)	14.76 (0.45%)	14.72
250	10.95 (7.95%)	11.31 (4.92%)	11.90 (0.01%)	11.96 (0.51%)	11.9
275	9.08 (7.36%)	9.34 (4.66%)	9.83 (0.38%)	9.88 (0.87%)	9.8
300	7.64 (7.26%)	7.85 (4.77%)	8.26 (0.24%)	8.31 (0.80%)	8.24
400	4.33 (7.01%)	4.41 (5.35%)	4.65 (0.15%)	4.67 (0.35%)	4.65
500	2.78 (6.33%)	2.82 (5.14%)	2.97 (0.17%)	2.99 (0.68%)	2.97
Mean error	8.64%	4.78%	0.14%	0.5%	ref

Table 4-3: Comparison between pull-in voltages of different numerical models and COMSOL solution.

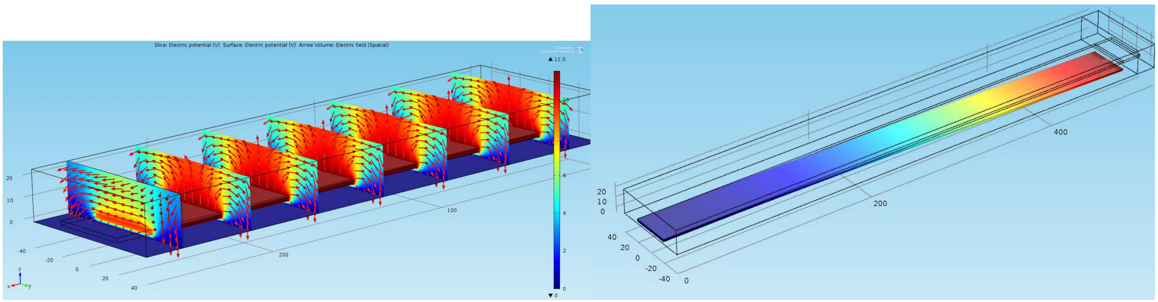

(a) Electric Potential **(b)** Deflection of 500 µm beam due to 2.8V

Figure 4-3: Results of calculations of the pull-in voltage performed with COMSOL Multiphysics. (a) The electric field lines emanate from every charged surface of the cantilever. (b) The deflection of the cantilever towards the electrode due to 2.8V bias voltage.

4-1-4 Conclusion of the comparison of models

Two comparisons have been made in this section. The first one, comparing analytical models and experimental data showed that the full-order model and the fourth-order model (without fringing) both approximated the experimental data with a mean error below 4.5%. The second one comparing the same models with a finite element model showed that both the full-order as the fourth-order model approximate the calculated values with a mean error below 0.5%. Although the model in COMSOL takes fringing into account, the resulting added attractive force isn't as high as the one used in the other models where fringing is taken into account. From this comparison it can also be concluded that fringing effects can be neglected, and that the full-order model resembles the experimental and calculated data the best. The largest side effect of the full-order model is the calculation of the associated modal participation factor η. This factor changes for any variation of the gap between cantilever and electrode and to solve for this variable, numerical methods are needed since it is difficult to solve it analytically [41]. The model that is going to be used will thus be the Fourth-order model proposed in [41]. A detailed description of this model will be given in the next section.

4-2 Analytical model described

Instead of solving the full-order model numerically, the term $\frac{1}{G-w}$ in Equation (4-6) is expanded about the initial equilibrium position, i.e. $w = 0$, as

$$\frac{1}{G-w} = \frac{1}{G} + \frac{w}{G^2} + \frac{w^2}{G^3} + \frac{w^3}{G^4} + \frac{w^4}{G^5} + \Delta, \tag{4-12}$$

where Δ represents the remaining higher order terms and G is given in Equation (4-4). This Taylor expansion introduces an error into the model. The pull-in phenomena occurs at roughly half the height of the gap [43], which makes $w = 0.5G$. Comparing the result of $\frac{1}{G-w}$ against its Taylor series expansion, shown in Figure 4-4, gives a mean error of 4.5% with gaps smaller than 20 µm.

Substituting Equation (4-12) into Equation (4-7) and solving for V gives the solution for the

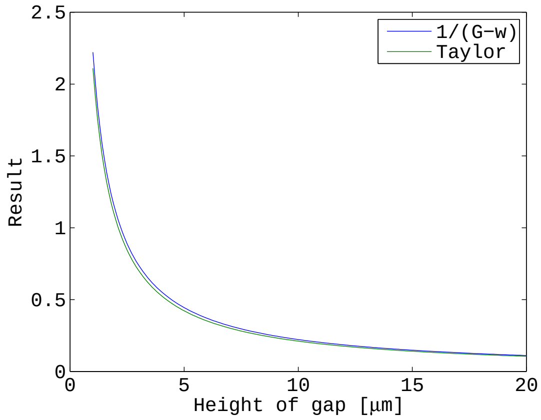

Figure 4-4: Result of $\frac{1}{G-w}$ compared to its Taylor series expansion for gaps smaller than $20\,\mu\mathrm{m}$. The two lines closely resemble each other, where the Taylor series has a mean error of 4.5%.

pull-in voltage V_{pi} as

$$V_{in} = \left(\frac{EI}{\varepsilon_0 \varepsilon_r b} \cdot \frac{\int_0^L (\phi'')^2 dx}{\int_0^L \frac{\phi^2}{G^3} dx + C1 \int_0^L \frac{\phi^3}{G^4} dx + C2 \int_0^L \frac{\phi^4}{G^5}} \right)^{1/2} \tag{4-13}$$

where ϕ is the first natural mode of the cantilever beam. This mode is given by [34] as

$$\phi(x) = (\cosh \lambda x - \cos \lambda x) - \sigma(\sinh \lambda x - \sin \lambda x), \tag{4-14}$$

where

$$\sigma = \frac{\sinh(\lambda L) - \sin(\lambda L)}{\cosh(\lambda L) + \cos(\lambda L)}, \tag{4-15}$$

and the coefficient λ satisfies the following equation,

$$\cos(\lambda L)\cosh(\lambda L) + 1 = 0. \tag{4-16}$$

The constants C1 and C2 depend on the geometry of the cantilever. The values for these constants and a more detailed example of the derivation of Equation (4-13) can be found in Appendix A. With Equation (4-13), the pull-in voltage has become a function of the initial gap g_0 and the curvature ρ. The other variables are all given by the geometry and material of the cantilever. For ease of discussion the term

$$\int_0^L \frac{\phi^2}{G^3} dx + C1 \int_0^L \frac{\phi^3}{G^4} dx + C2 \int_0^L \frac{\phi^4}{G^5} \tag{4-17}$$

will now be referred to as: $f(g_0, \rho)$. As the length of the cantilever doesn't change during experimentation, the value of this term only depends on the variables for the initial gap g_0 and the curvature ρ.

4-2-1 Different tip

The derivation of Equation (4-13) assumes a constant width along the length of the cantilever. Although the focus of this thesis is on rectangular cantilevers, it may be the case that these cantilevers have a triangular ending. To get an indication of the size of this triangle refer to Figures 4-5a and 4-5b. The tip moves faster towards the electrode compared to the rest of the cantilever, hence the electrostatic force acting on this area is larger. As the triangular end has a smaller surface area, Equation (4-13) needs to be adapted for this type of cantilever. Assuming that the cantilever has a uniform width from the base of the cantilever until L1 (Figure 4-6a), the electrostatic force acting on this part is equal to the force acting on a rectangular cantilever with length L1. The added electrostatic force acting on the triangle needs to be calculated differently. The electrostatic force along L2 is non-linear and dependent on the gap. Dividing the triangle into smaller rectangles will give an approximation of the total electrostatic force acting on this surface area,(Figure 4-6b). The elements with width $b(i) = b - \frac{i \cdot b}{m}$ and the length $\frac{h}{m} \cdot L2$ with $i^t h$ number of the m elements are now considered as separate cantilevers. The electrostatic force acting on this triangle is given by

$$F_{tri} = \sum_{i=1}^{m} b(i) \left(\int_{L1+(i-1)h}^{L1+ih} \frac{\phi^2}{G^3} dx + C1(i) \int_{L1+(i-1)h}^{L1+ih} \frac{\phi^3}{G^4} dx + C2(i) \int_{L1+(i-1)h}^{L1+ih} \frac{\phi^4}{G^5} dx \right). \tag{4-18}$$

Defining the electrostatic force on the first part of the cantilever as

$$F_{rect} = b \left(\int_0^{L1} \frac{\phi^2}{G^3} dx + \int_0^{L1} C1 \frac{\phi^3}{G^4} dx + \int_{L0}^{L1} C2 \frac{\phi^4}{G^5} dx \right), \tag{4-19}$$

the equation to calculate the pull-in voltage becomes

$$V_{in} = \left(\frac{EI}{\varepsilon_0 \varepsilon_r} \cdot \frac{\int_0^L (\phi'')^2 dx}{F_{rect} + F_{tri}} \right)^{1/2}. \tag{4-20}$$

Taking a large number for the m segments will give a better approximation of the real situation.

4-3 Cantilever stiffness

The main focus until now has been on finding a model that closely describes the behavior of an electrostaticly actuated cantilever. With the Fourth-order model, one can find the stiffness of a cantilever when Equation (4-13) is rewritten into

$$EI = \left({V_{in}}^2 \varepsilon_0 \varepsilon_r b \right) \cdot \frac{f(g_0, \rho)}{\int_0^L (\phi'')^2 dx.} \tag{4-21}$$

With the value for EI, by either using Equation (2-4) or Equation (2-5) depends on the fact whether the value for the Poisson's ratio is known. Since the Poisson's ratio is unknown for most cantilevers [44], the use of Equation (2-4) is necessary. Combining Equation (2-4) with

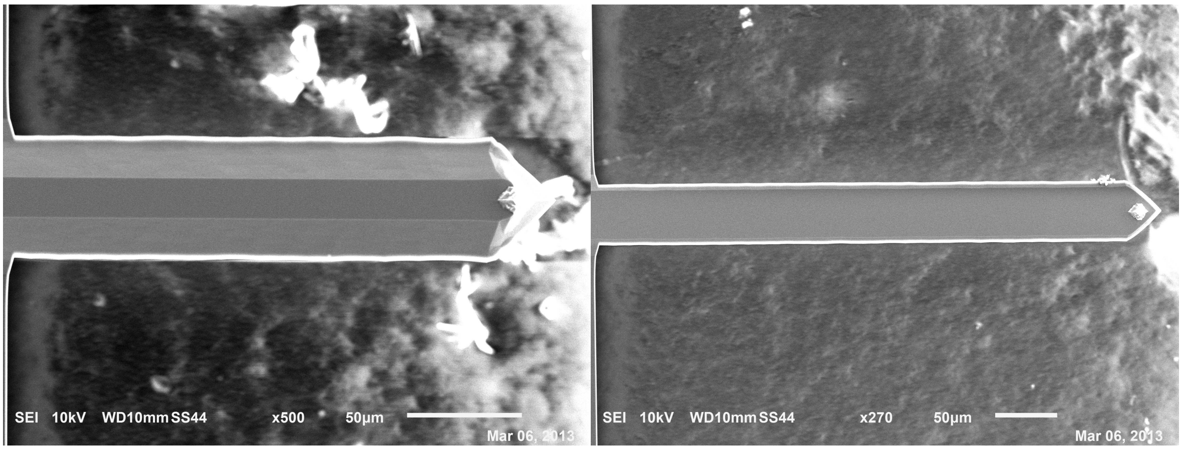

(a) Stiff cantilever k≈30 N/m. **(b)** Compliant cantilever k≈0.17 N/m.

Figure 4-5: SEM images of cantilevers with a triangular tip. (a) A Nanoworld NCLR-10 cantilever with a triangular tip used for tapping mode operation. Note the position of the scanning tip w.r.t. cantilever end. (b) A Nanoworld CONTR-10 cantilever used for contact mode.

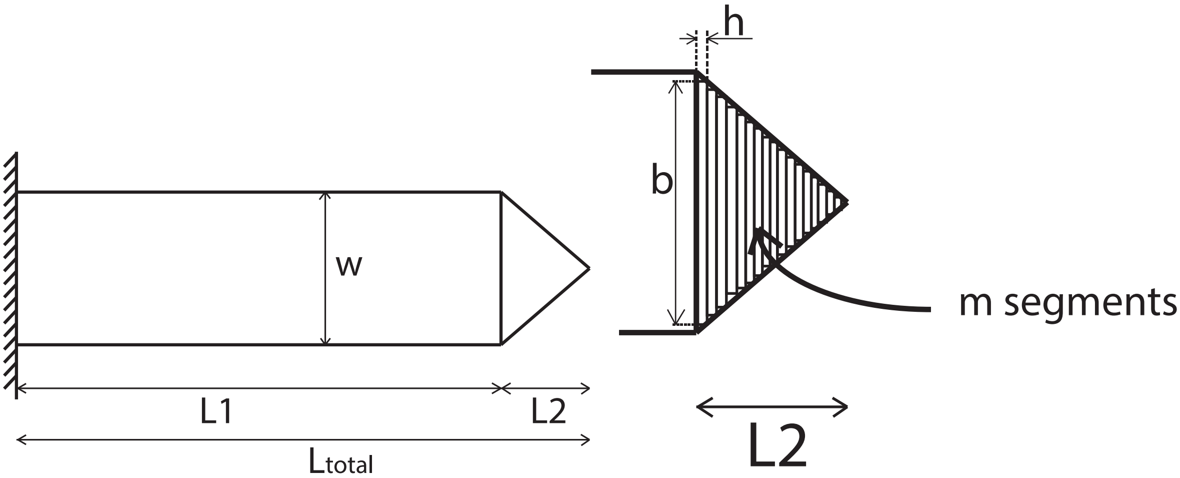

(a) Schematic view of cantilever. **(b)** Close-up of triangular tip.

Figure 4-6: Dimensions used to calculated the additional force acting on the tip of a rectangular cantilever with a triangular tip. (a) The length divided into a rectangular region on the left and a triangular area on the right. (b) The triangular area is divided into small rectangles to ease calculation.

Equation (4-21) will lead to the equation for the cantilever stiffness,

$$k = \frac{3{V_{in}}^2 \varepsilon_0 \varepsilon_r b}{L^3 \int_0^L (\phi'')^2 dx} \cdot f(g_0, \rho). \tag{4-22}$$

It should be mentioned that the AFM probe manufacturers define the spring constant with respect to the tip attached at the end of the cantilever, since forces interact at this location with the cantilever. The tip is not necessarily placed at the very end of the cantilever but can have an offset with the free end, Figure 4-7. To account for this, one needs to distinguish between the lengths used in the calculation of the stiffness. The length L used in Equation (4-21) is the length along which a electrostatic force is working. As the location of the tip has no influence on the area over which the electrostatic force does work, this equation doesn't need to be changed. The length to the third power in Equation (2-4) determines the stiffness of the cantilever when a force is working at that position. This length will now be considered the length between the base of the cantilever and the tip fixed at a certain location on the cantilever, L_{tip}. This changes Equation (4-22) into

$$k = \frac{3{V_{in}}^2 \varepsilon_0 \varepsilon_r b}{L_{tip}^3 \int_0^L (\phi'')^2 dx} \cdot f(g_0, \rho). \tag{4-23}$$

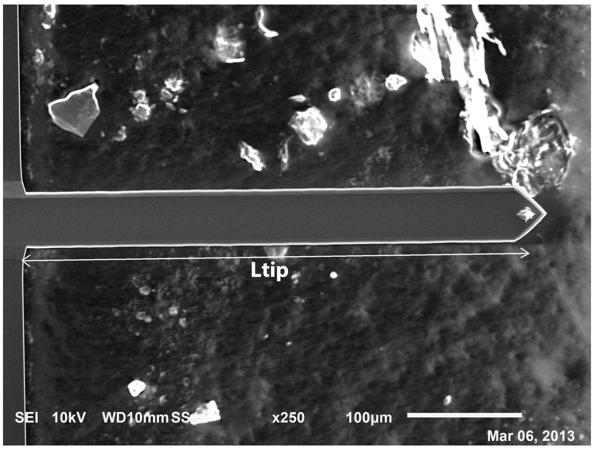

Figure 4-7: The value for the distance from the cantilever base to the location of the scanning tip. This length will be denoted by L_{tip}.

4-3-1 Differential gap approach

In Section 3-2-2 the differential gap approach was introduced. The same difficulty of needing knowledge about the gap between electrode and cantilever is present in the current model. The differential gap approach can also be used with the Fourth-order model. The procedure to calculate is as follows:

- Measure the width (b), length (L), length to the tip (L_{tip}) and curvature (ρ) of the cantilever.

- Place the cantilever over an electrode at a certain unknown gap g_1 and measure pull-in voltage (V_{pi1}).
- Increase gap by known amount Δgap and measure pull-in voltage (V_{pi2}).

Assuming the fact that the curvature of the beam remains the same after each pull-in measurement, Equation (4-13) becomes for the two experiments:

$$V_{pi1}{}^2 = c \cdot \frac{1}{f(g_0, \rho)} \tag{4-24}$$

$$V_{pi2}{}^2 = c \cdot \frac{1}{f(g_0 + \Delta g, \rho)}, \tag{4-25}$$

where $c = constant = \frac{E \cdot I}{\varepsilon_0 \cdot \varepsilon_r \cdot b} \cdot \int_0^L (\phi'')^2 dx$. Dividing Equation (4-24) by Equation (4-25) leads to

$$\frac{V_{pi1}{}^2}{V_{pi2}{}^2} = \frac{f(g_0 + \Delta g, \rho)}{f(g_0, \rho)}, \tag{4-26}$$

which can be solved iteratively for the gap (g_0). With the value for the initial gap (g_0) and the first pull-in voltage (V_{pi1}) known, the value for the stiffness k can be found by filling them into Equation (4-23). By introducing another measurement step in the differential gap approach it is no longer necessary to measure the curvature of the cantilever. This third measurement gives the values for the third pull-in voltage (V_{pi3}) and the second gap increment which for ease of use is given as

$$2\Delta g.$$

The three measurements will give the following results:

$$V_{pi1}{}^2 = c \cdot \frac{1}{f(g_0, \rho)} \tag{4-27}$$

$$V_{pi2}{}^2 = c \cdot \frac{1}{f(g_0 + \Delta g, \rho)} \tag{4-28}$$

$$V_{pi3}{}^2 = c \cdot \frac{1}{f(g_0 + 2 \cdot \Delta g, \rho)} \tag{4-29}$$

Subtracting Equation (4-28) from Equation (4-27) and dividing this by Equation (4-29) gives

$$\frac{V_{pi1}{}^2 - V_{pi2}{}^2}{V_{pi3}{}^2} = f(g_0 + 2 \cdot \Delta g, \rho) \left(\frac{1}{f(g_0, \rho)} - \frac{1}{f(g_0 + \Delta g, \rho)} \right) \tag{4-30}$$

which can again be solved iteratively for g_0 and ρ.

Conclusion Part 1 - Cantilever stiffness calculation

This part of the thesis has dealt with the present calibration techniques used to estimate the stiffness of an AFM probe. The AFM probes use a cantilever beam to scan the surface of an object. To get an accurate result of from the AFM an accurate value of the cantilever's stiffness is needed. Since the production techniques used to manufacture the AFM probes have deficiencies when it comes to replicating dimensions it is necessary to calibrate the canitlever's after manufacturing. The current calibration techniques have a number of disadvantages and a new technique is introduced that doesn't suffer from these disadvantages. The most important being the inability to calibrate stiff cantilevers. This new calibration technique called the Electrostatic Pull-in Instability method establishes a voltage specific to the geometry of the cantilever and a gap between the cantilever and an electrode. This voltage can then be used to calculated the stiffness. Models describing the behavior between cantilever and electrode have been studied, and it has been shown that there are difficulties in solving this non-linear problem. Using a model that simplifies this non-linear problem has been developed and compared with the results of experiments done in this field. The comparison showed an mean error lower than 5% between the model and the experiments. Using a Finite Element Analysis to model the behavior showed a mean error lower then 0.5%. These error values suggest that the model can be used to calculate the cantilever's stiffness within the objective given in the introduction (=accuracy between 10-15%).

Part II

Experimentation and conceptual design

Chapter 5

Error budgeting

With a model describing the behaviour of an electrostaticly actuated cantilever one can now calculate the stiffness of this cantilever. The physical world always introduces errors into any measurement making it necessary to evaluate the impact of these errors on the calculation. The experimental set-up used in [5] will be studied to find the value of the uncertainty due to measurement inaccuracies of that set-up. In order to develop a calibration technique that is suitable to calibrate cantilever stiffness, knowledge about deviations resulting from error sources is needed. This chapter will first display the errors resulting from incorrect measurement data. The combined effect of these measurement errors will eventually give the stiffness with a certain uncertainty. This will determine the accuracy of the calibration technique. The accuracy of the technique depends on the accuracy of the measurement systems being used, so an analysis of the minimum accuracy is made. After this analysis it needs to be determined if how well the real world is described by the model. A number of cantilevers is calibrated using the aforementioned model to investigate the error between the reference values and the calculated values. If this error stays between the values given in the objective of this thesis it will be used as a guideline to design a concept of an experimental set-up. This set-up will be able to calibrate cantilevers subjected to the conditions and limitations of cantilevers attached to their production wafer.

5-1 Sensitivity analysis

As can be seen from the comparison carried out in Section 4-1-4, the Fourth-order model has a mean error of 3.21% compared to the measurement data from [42] and a mean error of 0.3% compared to the analysis performed in COMSOL. Though the mean error is low, it can become higher when measurement errors are introduced into the equation. The cantilever stiffness is defined by the following variables:

- **Pull-in Voltage** [V_{pi}] **-** the voltage at which the elastic bending force becomes lower than the electrostatic force.

- **Width** $[b]$ **-** the width of the cantilever.
- **Length** $[L]$ **-** the total length of the cantilever, measured from the fixed base to the end of the cantilever.
- **Length to the tip** $[L_{tip}]$ **-** the distance from the base of the cantilever to the point of the scanning tip.
- **Gap** $[g_0]$ **-** the initial gap between the fixed base and the electrode.
- **Radius** $[\rho]$ **-** the radius of curvature of the cantilever.
- **Electrode orientation** $[\alpha]$ **-** the rate of change of distance between cantilever and electrode.
- **Electrode offset** $[o]$ **-** the distance between the front edge of the electrode and the fixed base of the electrode.

Measurement errors introduced to each of these variables will have an effect on the stiffness. Suppose that x,...,w are measured with uncertainties δx,...,δw and the measured values are used to compute

$$q = \frac{x \times ... \times z}{u \times ... \times w}. \tag{5-1}$$

If the uncertainties in x,...,w are independent and random, then the fractional uncertainty in q is the sum in quadrature of the original fractional uncertainties,

$$\frac{\delta q}{|q|} = \sqrt{\left(\frac{\delta x}{x}\right)^2 + ... + \left(\frac{\delta w}{w}\right)^2}. \tag{5-2}$$

In any case, it will never be larger than their ordinary sum,

$$\frac{\delta q}{|q|} \leq \frac{\delta x}{|x|} + ... + \frac{\delta w}{|w|}. \tag{5-3}$$

If q is a power,

$$q = x^n,$$

then

$$\frac{\delta q}{|q|} = |n| \frac{\delta x}{|x|}. \tag{5-4}$$

For Equation (4-23) this means that the uncertainty in k is equal to

$$\frac{\delta k}{|k|} = 2\frac{\delta V_{in}}{|V_{in}|} + \frac{\delta b}{|b|} + 3\frac{\delta L_{tip}}{|Ltip|} + errors\, due\, to\, dependent\, variables[45]. \tag{5-5}$$

From this equation it can be seen that only three of the eight variables have a independent relation between measurement error and stiffness error. The other five variables all influence the outcome of the equation. To identify the maximum uncertainty of the stiffness resulting from their measurement errors, the impact of each individual variable is measured and then the combined effect is studied to find the maximum measurement error.

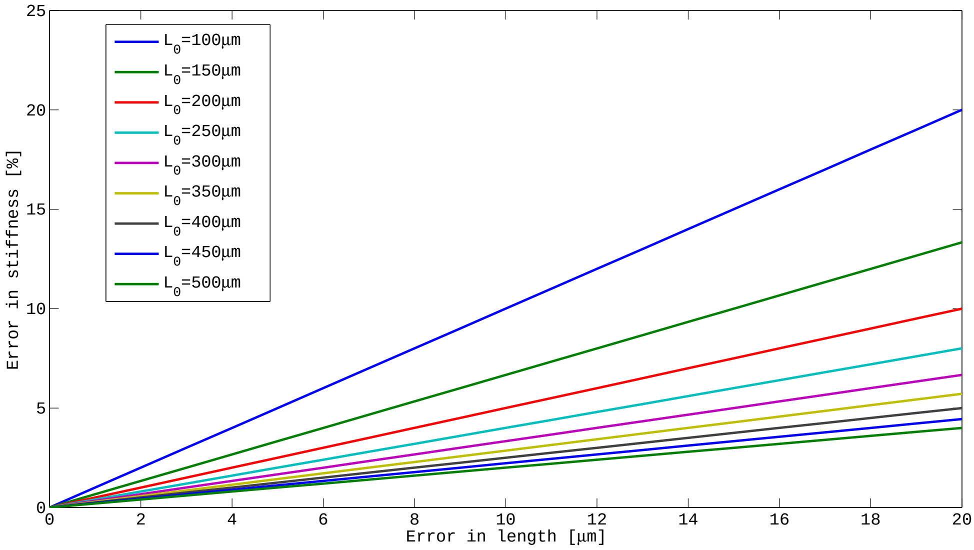

Figure 5-1: Change of calculated stiffness due to measurement error of the length of the cantilever.

5-1-1 Cantilever geometry

The first three variables are related to the geometry of the cantilever. The length, gap and curvature are defined by the production process of the AFM chip.

Length

Figure 5-1 represents the effect of a measurement error of several microns with respect to the calculated stiffness. It shows that measurement errors made on short cantilevers result in a much higher calculated stiffness than long cantilevers. The relation between measurement error given in µm is linear with the error in stiffness.

Gap

As shown in Equation (3-7), the stiffness scales with the inverse of gap to the third power. Any error introduced when measuring the gap will have a large effect on the calculated stiffness. Figure 5-2 shows that by underestimating the gap by 10%, the calculated stiffness will be nearly 40% too high. Since the differential approach is used, the measurement of the relative gap difference is needed instead. The relative gap difference is in the order of microns, making it necessary to have an accuracy below the micron range to prevent the calculated stiffness error becoming too high.

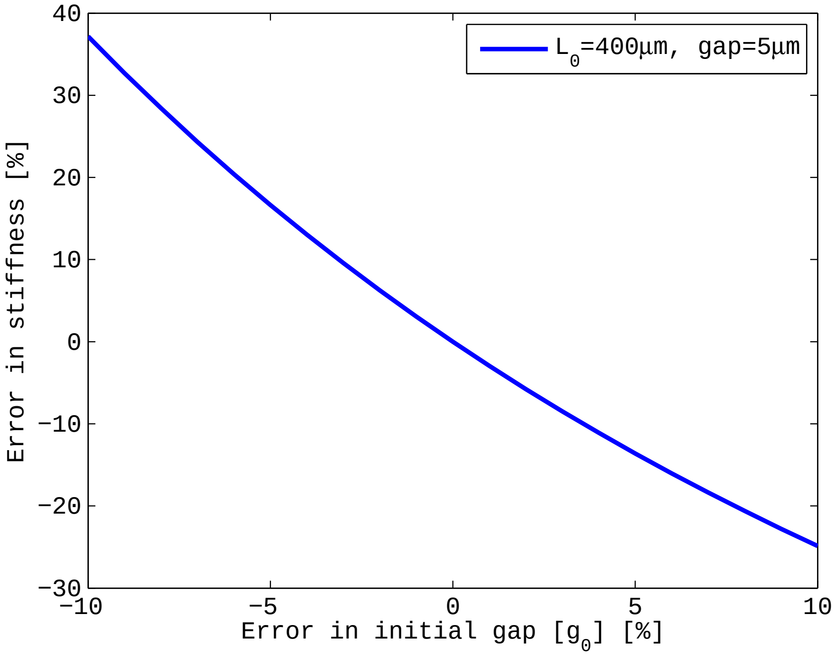

Figure 5-2: Error in cantilever stiffness due to measurement error of the gap.

Curvature

With a value for ρ it is possible to describe the in- or decrease of the gap along x. Figure 5-3 shows the result of measurement errors of the curvature of the cantilever. It is clear that for a longer length of the cantilever the measurement error has a larger influence on the calculated stiffness. A longer cantilever, bent at the same curvature as a short one, will have a greater tip deflection. A measurement error in the curvature has a greater impact on long cantilevers than on short ones.

5-1-2 Electrode

By placing an electrode underneath the cantilever instead of under the AFM chip holding the cantilever, the gap between electrode and cantilever can be reduced. This reduction of the gap will result in a lower pull-in voltage, thus eliminating the need for high voltage power sources. The placement of the electrode under the cantilever can induce an additional error into the stiffness equation. The gradient of the electrode with respect to the plane of the chip will either increase or decrease the gap along the cantilever's length. This effect can be seen in Figure 5-4. However it is not possible to place the electrode in such a way that the cantilever covers the whole electrode. Otherwise the chip holding the cantilever will come into contact with the electrode. By making contact a current will start flowing between the electrode and cantilever and no charge would build up. To prevent this from happening, the electrode needs to be placed at a distance from the AFM chip. The resulting gap is defined by the offset in µm, and takes into account the decreased area that is facing the cantilever.

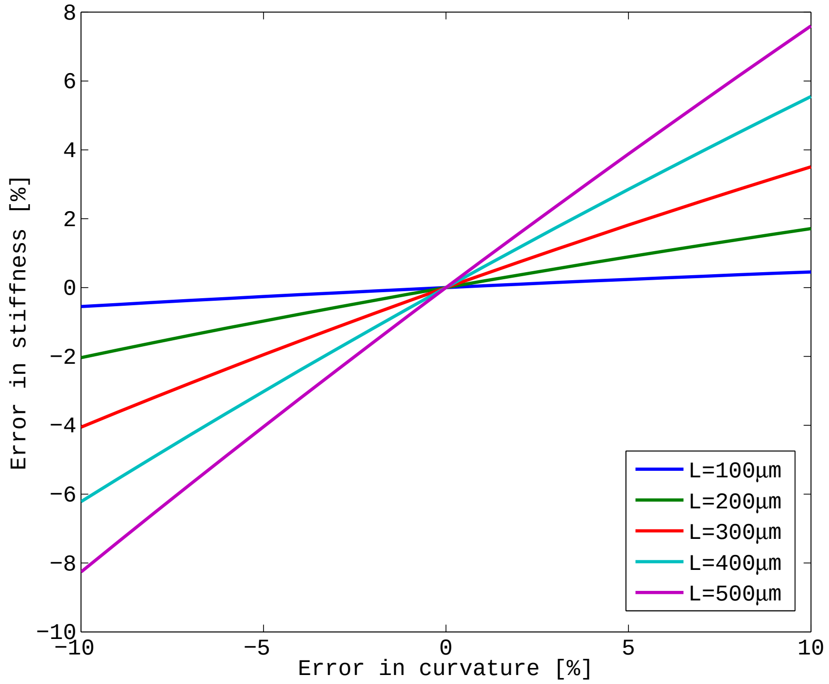

Figure 5-3: Error in cantilever stiffness due to measurement error of curvature.

Electrode orientation

To give a variable for the cantilevers orientation, one looks at the cantilever's gradient with respect to the AFM chip. Setting the chip as a reference the gradient will both tell if the electrode is positioned at an upward or downward angle and what the rate of change is. From Figure 5-5 it can be concluded that measurement errors of the rate of change will lead to high errors in calculated stiffness. Underestimating the rate of change by 10% will give a calculated error close to 35 %. Although not as high, an overestimation of 10% will lead to a calculation error of more than 20%.

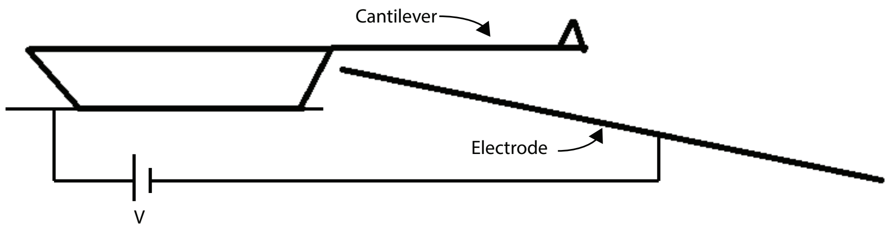

Figure 5-4: Example of electrode orientation compared to cantilever.

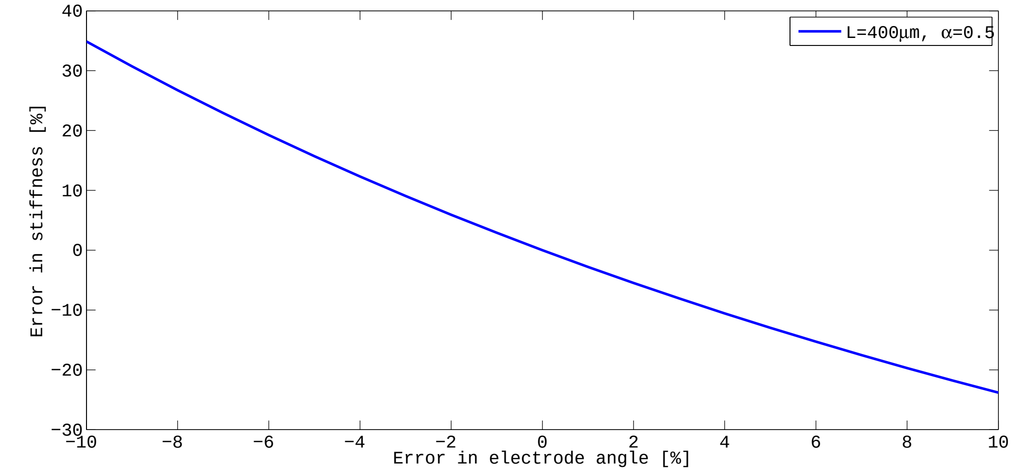

Figure 5-5: Error in cantilever stiffness due to measurement error of orientation.

Electrode offset

The resulting change in calculated stiffness due to the offset between base and electrode is shown in Figure 5-6. It can be seen that for the short cantilever of 100 μm the stiffness becomes increasingly smaller with an increase of the offset. If the offset is kept smaller than 15 µm for any length of cantilever the calculated stiffness will be no more than 0.2%. This lack of impact on the stiffness can be attributed to the fact that the electrostatic force acting near the base of the cantilever has the smallest lever to work with. The influence of this force will have an insignificant impact on the deflection of the cantilever.

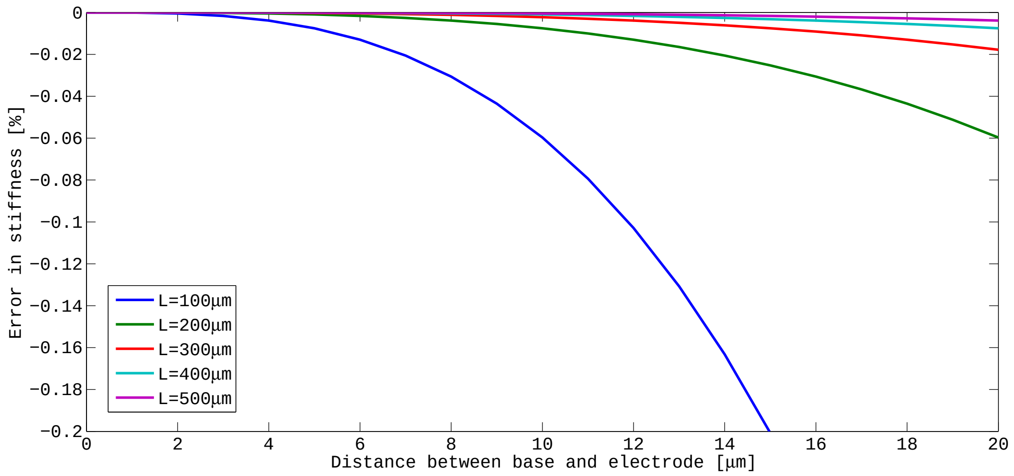

Figure 5-6: Error in calculated stiffness due offset between base and electrode.

5-1-3 Result of dependent errors

From the results presented in this section it can be concluded that:

- Measurement errors in estimating the values for the gap and electrode angle have a large impact on the calculated stiffness. The error of the stiffness will be higher than 20% for measurement errors of 10% or more.
- Errors made in measuring the length and curvature of 10% will introduce a stiffness error of smaller then 10%. Although these errors are smaller than those of item 1, they still are too large to neglect.
- The offset between the electrode and AFM chip can be neglected for values lower then 10 µm. With an offset of 10 µm, the resulting stiffness will become only 0.07% lower than the true value.

These variables are all dependent variables making it impossible to use Equation (5-2). Reference [45] doesn't offer any solutions to this problem. Instead the worst-case scenario is used to find the combined resulting error caused by the percentile errors in the measurements of the dependent variables. Using these errors together with Equation (5-3) will give an upper limit to the size of the error in the calculation of the stiffness. Figure 5-7 shows the result of having the same percentile error on all the variables. It appears that it is better to overestimate the measured values than underestimating them since the calculated stiffness shows a higher error in that case.

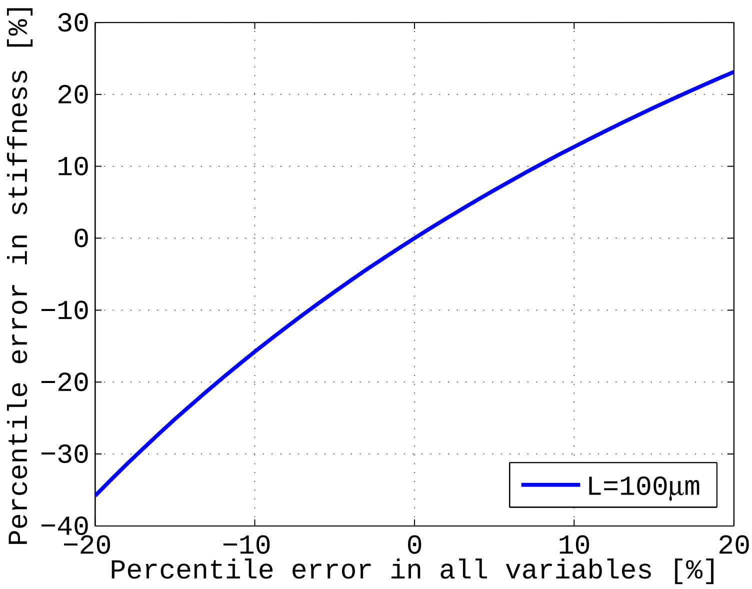

Figure 5-7: Combined calculated error of the stiffness due to measurement errors in the dependent variables.

Chapter 6

Experimental set-up and experimentation

6-1 Experimental set-up

To verify that the Fourth-order model is the best approximation of the cantilever stiffness, a number of experiments have been performed on reference cantilevers. These reference cantilevers are calibrated with techniques that guarantee an inaccuracy below 5%. The equipment used for these experiments is a set-up built for [5].

6-1-1 Set-up

The basis of the experimental set-up are two stages, one x-y stage and one piezo actuator allowing movement in the z-direction. The x-y stage is used to bring a AFM chip holder towards the electrode. This chip holder is a recess milled in a piece of aluminum into which the AFM chip is placed. The AFM chip is then held into place by a leaf spring which also serves as a connection to the positive voltage terminal. A small platfrom with a recess for the electrode is bolted on the piezo actuator stage. The electrode is clamped onto the piezo actuator by a similar leaf spring which is now connected to the negative voltage terminal.

The pull-in event can be detected by an I/V-converter that converts the current, that starts to flow when cantilever and electrode come into contact, into a voltage. The I/V-converter is needed since the current that is flowing is intentionally kept at a low level to protect the cantilever from overheating and melting by a large resistor placed between the voltage source and cantilever.

Supply of the voltage over the electrode and cantilever is done by a 12-bit Data Acquisition box from National Instruments. The maximum voltage range of the analog output is 0-5 V [46]. These low voltage levels would required extremely small gaps between cantilever and electrode since a gap of 2.4 µm would required more than 7 volts for a 500 µm cantilever.

Variables	Accuracy
Length, width	0.25 [µm]
Gap	0.1[nm]
Curvature	10[nm]
Slope of electrode	10 [nm]
Voltage	0.04 [V]

Table 6-1: Measurement accuracy of different variables.

To increase the voltage, the output is amplified by a 20x Voltage Amplifier. The increase of the voltage can be done by 0.2 mV at a time, which after amplification becomes 4 mV. The supplied voltage is regulated by Labview System Design Software. With this software a program is made which allows for the direct input of a voltage, or a step-wise increase of the voltage from a predetermined level.

Measurement of the dimensions of the cantilever's dimensions are done by placing the stage underneath a White Light Interferometer, WLI, manufactured by Bruker. This Bruker CounterGT-1 3D Optical Microscope has a vertical resolution smaller than 0.1 nm, and a lateral resolution of 0.25 µm [47]. This microscope is also used to oversee the positioning of the cantilever over the electrode. The tip of the cantilever is moved next to the cantilever after which a height measurement is made. This measurement is needed to guarantee the clearance between cantilever and electrode. After this measurement the cantilever is placed over the electrode, being certain that the base of the chip doesn't make contact with the electrode. As mentioned in Section 5-1-2, this contact would result in the absence of charge building up on the electrode and cantilever surfaces. When the cantilever is considered correctly placed over the electrode the height of the z-stage is increased to decrease the gap between cantilever and electrode.

Measurement error and accuracy

With the accuracies of the different measurement tools established, it is now possible to calculate the maximum calculated error due to measurement uncertainties. Using the values from Table 6-1 in Equation 5-5 gives a maximum error due to the independent variables of 0.62%. Using the same measurement accuracies and Figure 5-7 yields a total maximum error for the dependent variables of 4.73%. The total error due to measurment inaccuracies is 5.55%. (Note: These calculations have been performed on the smallest commercially available cantilever with a length of 90 µm and a width of 15 µm. Longer cantilevers show smaller errors since the influence of the measurement accuracy becomes smaller.)

6-1-2 Reference cantilevers

The first cantilevers used in these experiments are force calibration probes manufactured by Bruker. These three rectangular cantilevers are made of silicon. Special processing methods are used to ensure that the cantilevers have uniform rectangular cross-sections [48]. The nominal probe characteristics are given in Table 6-2 and close-up images made in a SEM are shown in Figures 6-1a and 6-1b. A detailed list of the calibrated values for the cantilever stiffness can be found in Appendix B. The aim of the experiments performed with these cantilevers is to determine the stiffness and compare with to the calibrated values. This comparison will show whether the model can be used with further calibration attempts.

	Length (µm)	Width (µm)	Thickness (µm)	Frequency (kHz)	Spring Constant (N/m)
Cantilever A	97	29	2	293	10.4
Cantilever B	197	29	2	71	1.30
Cantilever C	400	29	2	18	0.157

Table 6-2: Nominal reference cantilever characteristics.

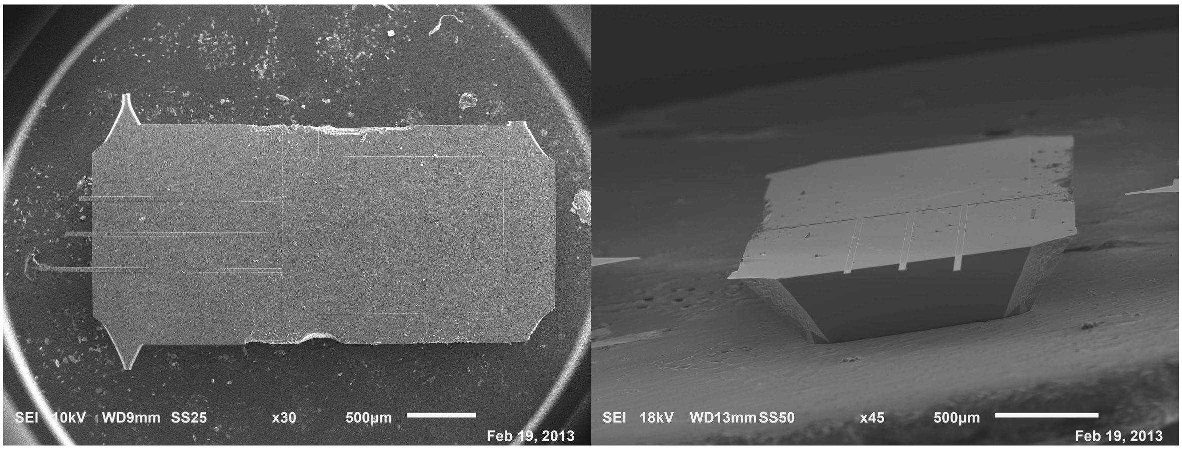

(a) Topview of reference probe. **(b)** Sideview of reference probe.

Figure 6-1: Close-up of Bruker calibration probe made with a Scanning Electron Microscope. (a)Top view of calibration probe showing three reference cantilevers. (b) A sideview of the same calibration probe.

6-1-3 Commercial AFM probes

After the determination of the stiffness of the reference cantilevers, a number of commercially available AFM probes will be calibrated. These probes, supplied by Nanoworld, are of the type CONTR-10 and NCLR-10. The first set of cantilevers is an aluminum coated SPM-sensor made of silicon with a stiffness of approximately 0.2 N/m according to manufacturers specifications. The second set are similarly coated with a stiffness approximately 48 N/m. More detailed information can again be found in Appendix C.

	Length (µm)	Width (µm)	Thickness (µm)	Frequency (kHz)	Spring Constant (N/m)
CONTR-10	448	46	2	0.17	13
NCLR-10	226	36	7.1	4.9	192

Table 6-3: Nominal commercial AFM probe characteristics

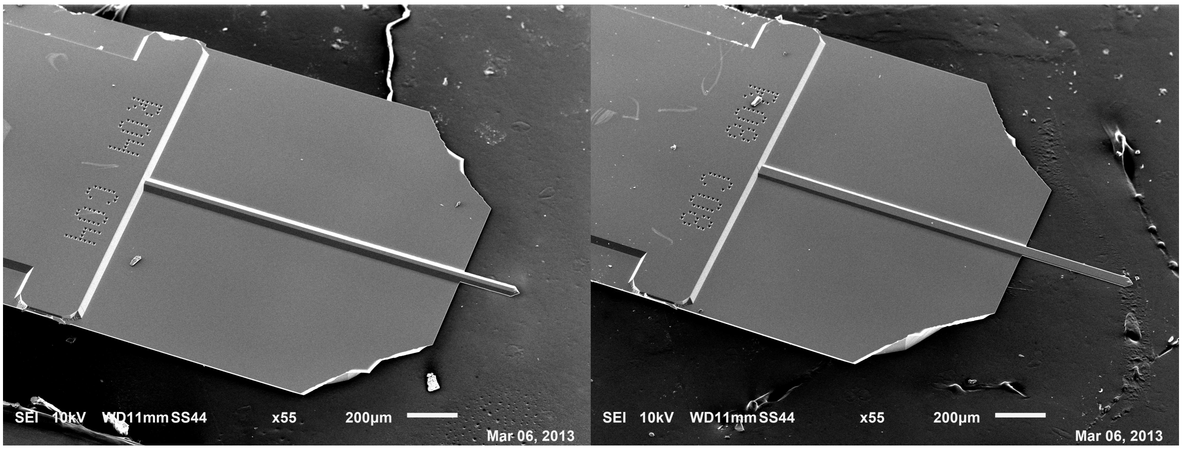

(a) CONTR-10 probe. **(b)** NCLR-10 probes.

Figure 6-2: Close-up view of Nanoworld AFM probes made with a Scanning Electron Microscope. (a) An overview of one of the CONTR-10 probes. (b)An overview of one of the NCLR-10 probes.

6-2 Experimentation

Every experiment starts with inserting one of the reference probes into the experimental set-up. This probe is removed by plastic tweezers from its container and placed on the chip holder of the x-y stage. The whole calibration system is then placed under the WLI, which makes it possible to view its position with relation to the electrode. While using the microscope, the cantilever is positioned over the electrode without the chip coming into contact with the electrode. Care must be taken that the cantilever and electrode are not at the same height, which will cause damage to the cantilever when making contact. The WLI is used to make a scan of the electrode with the cantilever positioned over it. This scan makes a three dimensional surface measurement, with information about the height of every point. An image of one of these scans can be seen in Figure 6-3. The data from this measurement is used to determine the values for the length L, width b, curvature ρ and electrode angle α. The offset between the cantilever's bas in relation to the edge of the electrode can also be determined by this measurement. However, as mentioned in Section 5-1-2, this value can be neglected for offsets lower than 10 μm. Since the force calibration probe is fitted with three cantilevers, the positioning needs to be done in a different way. As already shown, shorter and thus stiffer cantilevers have a higher pull-in voltage than comparable longer cantilevers. Increasing the voltage with all three cantilevers positioned over the electrode will result in the pull-in of the weakest cantilever first. Since electrical contact between both terminals is made, no additional charge will build up and the other two cantilevers will not deflect. The cantilever with the highest stiffness needs to be placed over the electrode first. After pull-in is achieved for this cantilever, the chip is moved sideways so that the second cantilever is also positioned over the electrode. With it's lower pull-in voltage, this cantilever will be pulled-in first which makes it possible to record the pull-in voltage. This process is then repeated for the third cantilever.

The same data is used to measure the length, width and curvature of the cantilever. Since the data will not supply the curvature value, a fit of the curvature equation has to be made

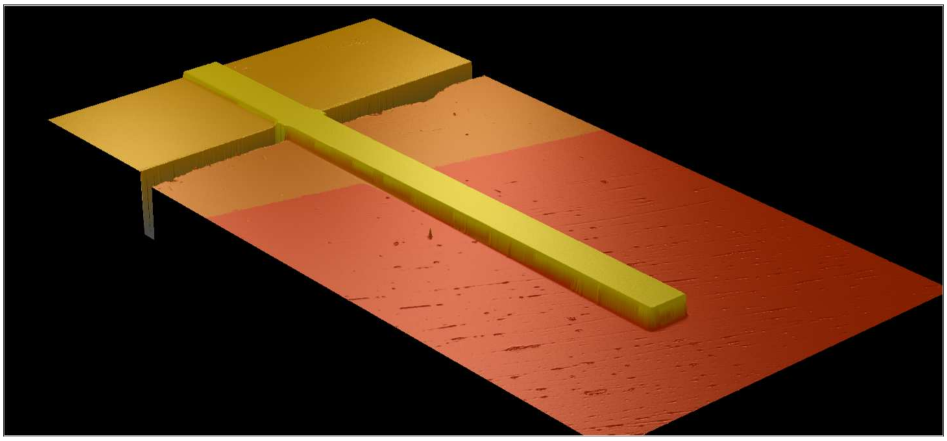

Figure 6-3: White Light Interferometry image of a long reference cantilever suspended over an electrode.

with the data of the cantilever. In Figure 6-4a a plot of the measurement data is shown. This measurement data imported into Matlab Equation (4-2) is used to fit a curve over this data. The value found for ρ will be used later to calculate the stiffness.

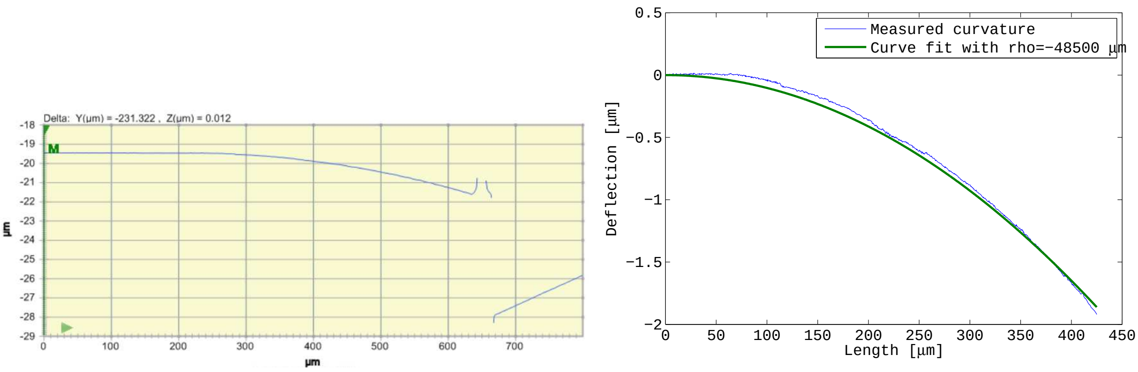

(a) Measurment data from the WLI. **(b)** Measured data vs. curve fitted solution.

Figure 6-4: Estimating the curvature of the cantilever with use of measurement data and curve fitting algorithm of Matlab. (a) Measurement data from White Light Interferometer showing the deflection of the cantilever with its due to its curvature. In the lower right of this figure the electrode can be seen. Note the gradient of the electrode compared to the cantilever. (b) A curve fit done in Matlab to find the curvature value. In this case the curvature is $48.500\,\mu\mathrm{m}$.

With the values for the length $[L]$, width $[b]$, curvature $[\rho]$ and gradient of the electrode $[\alpha]$ acquired, the pull-in voltages are determined. As mentioned earlier, the potential can be raised with increments of as small as $4\,\mathrm{mV}$ at a time. This potential increase is first performed with increments of $20\,\mathrm{V}$, to get an indication of the height of the pull-in voltage. When pull-in occurs, the potential is lowered one increment and the increment size is set to $0.4\,\mathrm{V}$. During preliminary testing of the experimental set-up it was found that the I/V-converter necessary for the detection of the moment of pull-in did not function properly. Without this converter it was necessary to detect the pull-in moment visually using the WLI. The increase of electrostatic force causes the cantilever to bend towards the electrode. This can be seen on the monitor of the WLI by the movement of the interference pattern along the length of the cantilever. When the pull-in occurs the cantilever tip is pulled instantly against the electrode, causing the cantilever to move out of focus. Because the cantilever tip is no longer in focus the interference pattern disappears at the tip indicating that pull-in had occurred. When pull-in occurred the voltage is reduced to zero and the electrode is lowered to increase the gap. The distance the electrode is lowered depends on the stiffness of the cantilever. As explained, stiff cantilevers need higher voltages for pull-in to occur. Since the potential difference is limited to 100 V the gap can't get too large. Hence, the gap was increased by 0.1 µm at a time for stiff cantilevers, and by 1 µm for more compliant cantilevers. When the gap is has been increased the voltage is again increased until pull-in. This procedure is repeated three times to get three pull-in voltages.

Chapter 7

Results and observations

This chapter will present the results of the measurements performed as was discussed in Chapter 6. The subject of these measurements was a set of reference cantilevers with three different stiffness levels and two commercial AFM probes. After the results are displayed, observations made during the experiments will be discussed.

7-1 Results

Reference cantilevers

Each force calibration probe with three cantilevers had three different stiffness values, the highest approximately 7 [N/m], the middle approximately 1 [N/m] and the weakest approximately 0.1 [N/m]. The cantilever's dimensions were measured with a Scanning Electron Microscope and displayed in Table 7-1. Along with these measurements the three Pull-in voltages are displayed, corresponding to a increasing gap. The gap increase per measurement is displayed underneath the Pull-in voltages. The resulting calculated stiffness k_{calc}, using the Fourth-order model, is then displayed. The calibrated stiffness k_{ref}, as supplied by the reference cantilever manufacturer, is displayed underneath. This reference stiffness has a reported uncertainty approaching 5% [48]. The comparison between the reference values and the calculated values is shown in Figures 7-1a, 7-1b and 7-1c. The values with their uncertainties displayed overlap each other for most of the cantilevers. This indicates that the calculated stiffness is close to the reference stiffness.

Nanoworld CONTR-10

The CONTR-10 cantilever supplied by Nanoworld is a contact mode AFM probe with a stiffness of approximately 0.16 [N/m]. The manufacturer reports an inaccuracy of 10% for this type of cantilever. The reference stiffness values are calculated using the Beam Estimation method discussed in Chapter 3. The width, length and thickness are measured with optical

	1 - Short	1 - Medium	1 - Long	2 - Short	2 - Medium	2 - Long	3 - Short	3 - Medium	3 - Long	4 - Short	4 - Medium	4 - Long	5 - Short	5 - Medium	5 - Long
Length [µm]	88.9	190.3	388.2	89.8	188.3	389	89.89	189.3	389.2	90.8	191.24	388.7	88.8	190.2	0
Width [µm]	31.4	31.4	32.8	31.8	31.4	31.8	30.9	31.4	29.4	32.35	32.8	32.3	32.3	34.7	0
Height [µm]	1.8	1.8	1.8	1.8	1.8	1.8	1.8	1.8	1.8	1.8	1.8	1.8	1.8	1.8	0
V_{pi1} [V]	67.25	44.38	49.66	0	69.99	62.95	61.58	70.38	48.88	0	60.41	38.51	53.37	63.14	0
V_{pi2} [V]	71.55	59.43	55.32	0	78.40	69.01	71.94	79.18	54.55	0	75.95	53.08	74.09	79.37	0
V_{pi3} [V]	75.26	76.64	61.39	0	87.20	74.87	82.70	88.17	60.21	0	94.04	78.20	97.75	96.77	0
Δg [µm]	0.1	1	1	0	0.5	1	0.25	0.5	1	0	1	1	0.5	1	0
k_{calc} [N/m]	6.83	0.914	0.094	0	0.833	0.090	7.10	0.946	0.095	0	0.795	0.097	6.91	0.841	0
k_{ref} [N/m]	7.57	0.976	0.114	0	0.927	0.11	7.33	0.948	0.105	0	0.884	0.105	7.79	0.892	0

Table 7-1: The results of determining the pull-in voltage of the reference cantilever. (Zero values mean that the cantilever broke off during testing and no further data is available.)

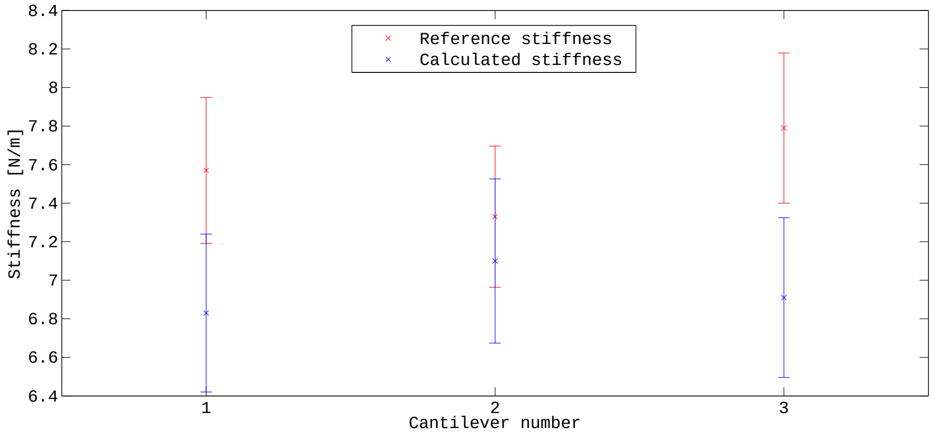

(a) Calculated stiffness versus reference stiffness (Long).

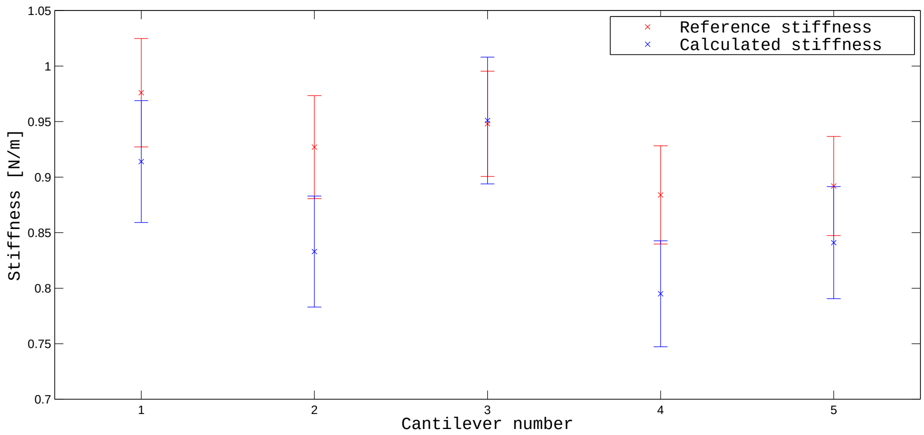

(b) Calculated stiffness versus reference stiffness (Medium).

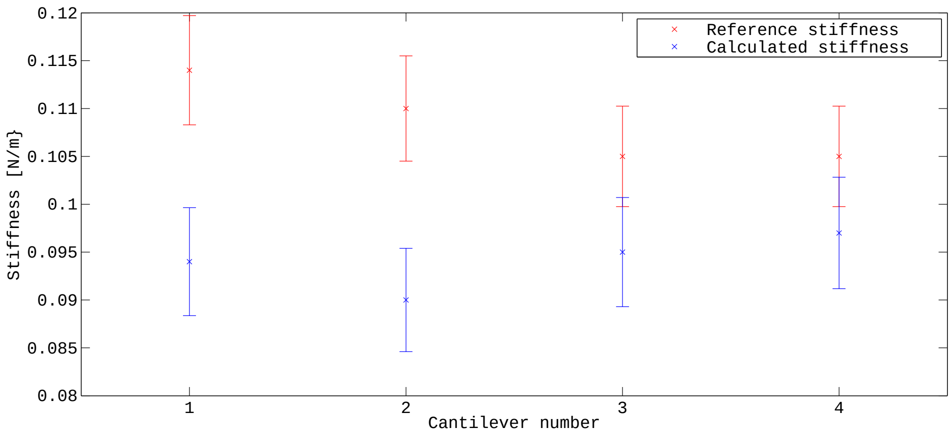

(c) Calculated stiffness versus reference stiffness (Short).

Figure 7-1: (a,b,c) The calculated values with their uncertainties plotted versus the reference values for the three types of cantilevers measurements [49]. Figure 7-2 shows the difference between the manufacturers stated stiffness and the calculated stiffness. Since the cantilever have a triangular tip, it was necessary to use the model which takes this tip into account. The dimensions and pull-in voltage as well as the change in gap are displayed in Table 7-1.

	Probe 1	Probe 2	Probe 3
Length [µm]	448	448	448
Width [µm]	46	46	46
Height [µm]	1.9	2.0	2.0
V_{pi1} [V]	30.20	44.67	37.92
V_{pi2} [V]	34.12	49.86	42.81
V_{pi3} [V]	39.39	55.52	47.11
Δg [µm]	1	1	1
k_{calc} [N/m]	0.14	0.15	0.14
k_{ref} [N/m]	0.17	0.16	0.16

Table 7-2: Results of pull-in experiments of three CONTR-10 cantilevers.

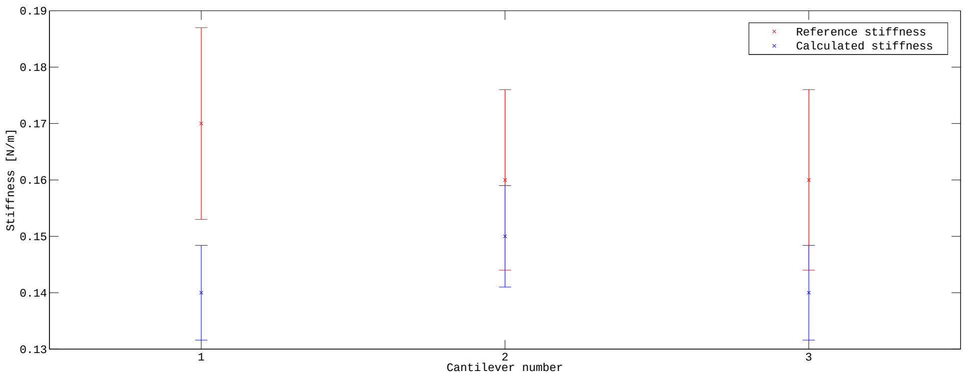

Figure 7-2: Comparison of stiffness supplied by the manufacturer and calculated stiffness of CONTR-10 cantilevers.

Nanoworld NCLR-10

The NCLR-10 cantilever also supplied by Nanoworld is a tapping mode AFM probe with a stiffness of approximately 47 [N/m]. The manufacturer reports an inaccuracy of 20% for this type of cantilever. The stiffness values are calculated using the Beam Estimation discussed in Chapter 3. The width, length and thickness are measured with optical measurements [49]. Figure 7-3 shows the difference between the manufacturers stated stiffness, the reference stiffness, and the calculated stiffness.The dimensions and pull-in voltage as well as the change in gap are displayed in Table 7-1.

	Probe 5	Probe 6	Probe 7
Length [µm]	226	226	226
Width [µm]	36	36	36
Height [µm]	7	7	7
V_{pi1} [V]	69.71	71.79	37.92
V_{pi2} [V]	76.78	78.41	42.81
V_{pi3} [V]	80.62	85.54	47.11
Δg [µm]	0.1	0.1	0.1
k_{calc} [N/m]	36.5	39.2	51.9
k_{ref} [N/m]	47	46	59

Table 7-3: Results of pull-in experiments of three NCLR-10 cantilevers.

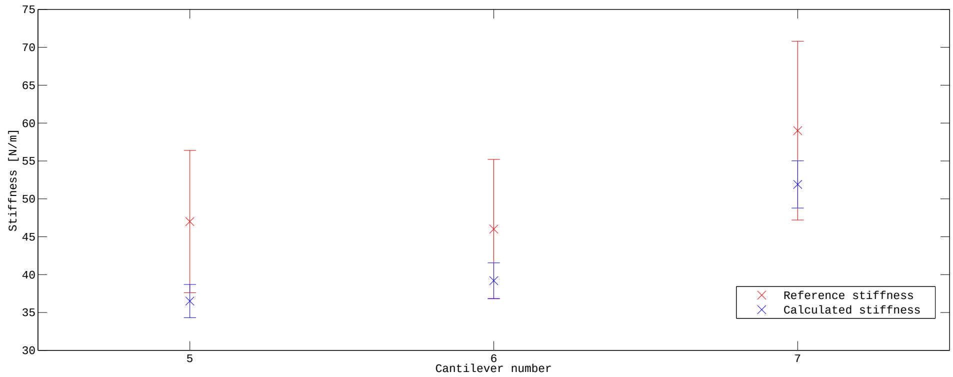

Figure 7-3: Comparison of stiffness supplied by the manufacturer and calculated stiffness of NCLR-10 cantilevers.

7-2 Observations

The results of the experiments performed on the three different AFM probes show that the calculated stiffness values are close to the reference values. These reference values are supplied by the manufacture with an certain inaccuracy. Looking at the results of the reference cantilevers shown in Figures 7-1a, 7-1b and 7-1c, it is clear that the calculated values are close to the reference values. In most cases the calculated value lies within the uncertainty boundaries. Calculating the mean error for the different cantilever lengths shows that the mean error is below 11%. It is also evident that all the calculated stiffness values lie below the reference values. The results of the Nanoworld AFM probes, shown in Figures 7-2 and 7-3, indicate that the calculated values are again lower than the reference values. The mean error of these measurements for the CONTR-10 cantilevers is 13.7% and 16.3% for the NCLR-10 cantilevers.

During the experiments the following observations were made:

- **Geometry -** The data sheet supplied with the reference cantilevers only gave nominal values for the width, length and thickness of the cantilever. This made it necessary to measure the true dimensions under the Scanning Electron Microscope. This measurement showed that although the probes were manufactured on the same wafer, the dimensions varied between cantilevers.

  The data sheet supplied with both the CONTR-10 and NCLR-10 cantilevers, gave the width, length and thickness of these cantilevers. Additional measurement with the SEM showed these values to be incorrect. The width of the NCLR-10 cantilevers was off by almost 33% in some cases. This measurement error contributes to the high inaccuracy of the these cantilevers. The dimensions obtained from the measurements done in the SEM were used in the calculations.

- **Stiction -** Stiction is a term for the unintentional adhesion of compliant microstructure surfaces when restoring forces are unable to overcome interracial forces such as capillary, electrostatic, van der Waals, Casimir forces and other kinds of "chemical" forces [50]. The stiction problem can be divided into two categories: release-related stiction and in-use stiction [51]. The stiction occurring here can be referred to as in-use stiction. When the pull-in voltage has been reached, the cantilever moves down towards the electrode and is pulled against its surface. This result can be seen in Figure 7-4. Even though the electrostatic force disappears after contact between electrode and cantilever, the momentum of the cantilever is high enough to deform and conform to the surface of the electrode. After the removal of the potential over the cantilever and electrode, the restorative elastic force of the beam is not high enough to counteract the stiction forces. Two approaches were used to release the cantilever from the electrode. The first was to lower the electrode away from the cantilever. Bending the cantilever downward increased the elastic force counteracting the stiction which caused the cantilever to pull free. This approach was not able to release the compliant cantilevers though. A compliant cantilever has lower restorative force to pull itself free from the electrode. For these cantilevers it was necessary to move the cantilever away from the electrode in a lateral direction. This combination of movement along the electrode surface and the restorative forces was sufficient to pull the cantilever free.

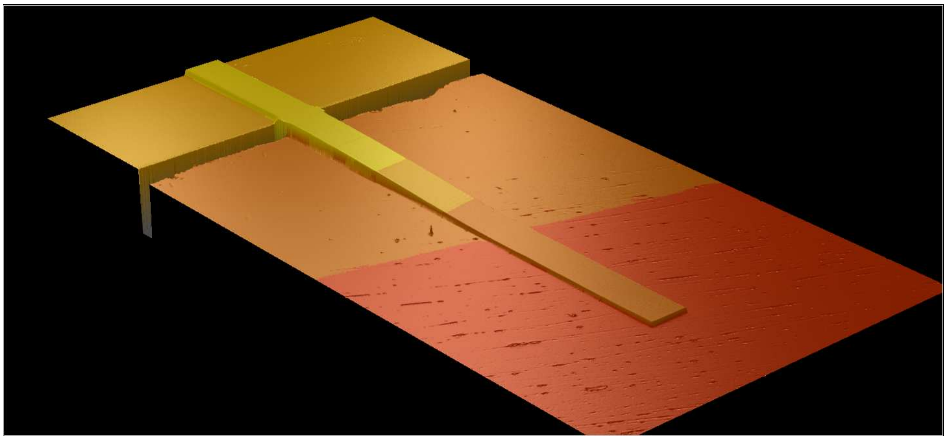

Figure 7-4: White Light Interferometry image of a long reference cantilever attached to the electrode surface after the pull-in voltage has been reached.

- **Vibrations near pull-in -** When increasing the voltage over the cantilever and electrode it was observed that the cantilever started to oscillate when the pull-in voltage was approached. This oscillation is attributed to the fact that the structure has almost zero stiffness around the pull-in point. The interaction of the elastic bending forces and the electrostatic forces cause the beam to deflect greatly by a minimal input. As it is only possible to increase the voltage with steps of 0.04 V at a time, this step could cause to oscillation to pass through the pull-in point. This lead to a pull-in voltage that is lower than the true pull-in voltage. In some cases pull-in occurred due to the movement of the White Light Interferometer used to observe the phenomenon. This shows that even though the cantilever hasn't reached the pull-in point yet, a small disturbance can deflect the cantilever through the pull-in point. It was discovered that by continually increasing the voltage, the cantilever was not given enough time to start to vibrate. Although the steps were kept the same this vibration was no longer present. The downside of this method was that the steps needed to be increased at a fast pace. As pull-in happens extremely fast the voltage increase was often stopped too late resulting at voltage level that was too high.

- **Tilting of electrode -** One of the shortcomings of the experimental set-up was the fact that the electrode was tilted along the length axis of the cantilever. One side of the electrode is thus positioned closer to the cantilever than the other. This height difference creates unequal forces along the width of the cantilever causing a torque around the length axis. This torque interferes with stiffness calculation as the force acting on the cantilever is no longer only an end load but a combination of torque and end load.

Chapter 8

Design and fabrication

From the experimental results it can be concluded that the model describing the pull-in behavior complies with the objective set at the start of this thesis since the accuracy is between 10-15%. The results and observations of the previous chapter are used to design an experimental set-up. This set-up has aspects that duplicate the conditions of a AFM probe faces when it is still connected to the production wafer. The requirements of this set-up will be presented. With these requirements a number of concepts are developed from which the best concept will be chosen. This concept will be modeled in Comsol Multiphysics to evaluate if the behavior can still be approximated by the model.

8-1 Requirements

As shown in Section 1-1-1, a production wafer may contain anywhere from a hundred to more than a thousand AFM probes. The goal is to calibrate each of these cantilevers without removing them from the wafer. This can be accomplished in two ways: either the probes are calibrated by a system moving from probe to probe, or a system is designed in such a way that all the probes can be calibrated without movement. Being able to calibrate every probe with the use of one stationary structure is less complex then having to position a calibration system at every probe. It also reduces the handling time of the wafer which limits the amount of contamination. The requirements of the calibration set-up are:

- Stationary structure onto which the wafer, containing the probes, is placed.
- Equipment able to measure the geometry of the cantilever, either simultaneously or one-by-one.
- Electrode(s) to create the potential voltage between cantilever and electrode.
- Means to create a gap increase between pull-in measurements.
- Structures that prevent stiction.

The following measurement equipment can be used to measure the variables used in the calculation of the stiffness:

1 Dimensions of the cantilever

Using a measurement microscope like a White light Interferometer, shown in Figure 8-1a, gives values for the length and width of the cantilever. Automated measurement systems allow the placement of the cantilever underneath the microscope and with the use of image recognition software the geometry is measured. By scanning the surface with an focused laser

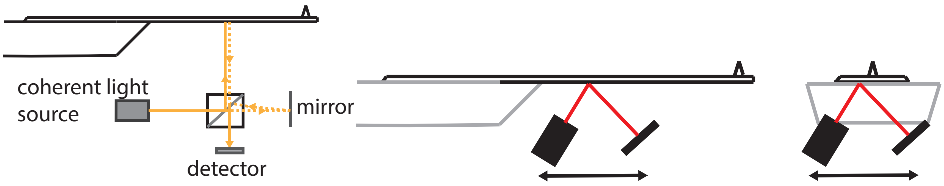

(a) White light interferometer.

(b) Optical laser beam.

Figure 8-1: To measure the dimensions, the following equipment can be used: (a) A white light interferometer measures the interference between two reflected light paths. (b) The focused optical beam only reflects on a photo detector when it is aimed at the cantilever. When no reflection is measured the end of the cantilever is found.

beam, Figure 8-1b, the reflection of the beam is measured on a position detector. When the beam reaches the end of the cantilever, the light is no longer reflected signaling the end of the measurement. With a measurement along the length and perpendicular to the length, the length and with can be determined respectively.

2 Gap

With the thickness of the cantilever unknown, it is difficult to measure the gap between the cantilever and electrode from above. However, if the differential gap method is used instead, only knowledge of the changed distance between electrode and cantilever is needed. Having the electrode placed on an actuator capable of moving it in a vertical direction, it is possible to change the gap as shown in Figure 8-2a.

The second possibility is first placing the production wafer on one test structure and measuring the pull-in voltage shown in Figure 8-2b. Moving it to a test structure with a different electrode height will give the second pull-in voltage. With knowledge of the surface topology, the difference in height can be recorded in advance.

A third option is to use electrodes that have different heights, Figure 8-2c. Using the lowest electrodes first will give a high pull-in voltage, then using higher electrodes will give another, lower, pull-in voltage. The difference in height between the electrodes is now used as the relative change of the gap. The offset in height between electrodes can be measured beforehand. The model will, in this case, need to take into account that the electrodes underneath the cantilever have a different surface area.

(a) Actuator moving electrode.

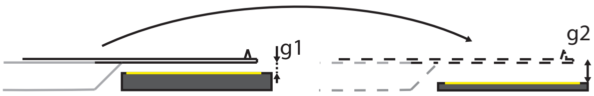

(b) Placing wafer at different structures.

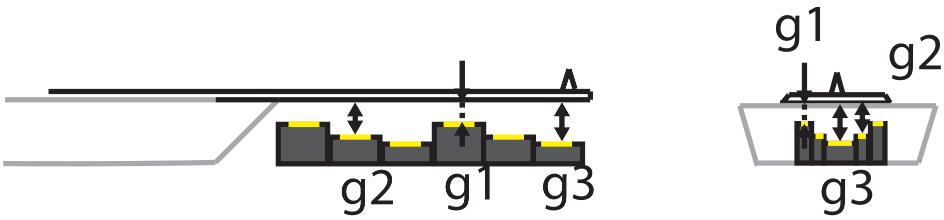

(c) Stepped electrodes.

Figure 8-2: To use the differential gap method it is necessary to know the relative height between gaps. This can be done by: (a) Moving the electrode with the use of an actuator. Feedback from the actuator shows the increase in gap. (b) Having different test structures. The wafer is moved to the first structure with gap $g1$ and a pull-in measurement is done. It is then moved to structure two with gap $g2$ to get the second pull-in voltage. (c) Using different electrodes placed together creates different gaps. By charging the electrodes separately three pull-in voltages are measured. (note: the yellow lines represent the electrode surfaces.)

3 Radius of curvature

The optical beam deflection method (Figure 8-1b) and the White Light Interferometer (Figure 8-1a) can both be used to measure the cantilever's curvature. Traversing the optical beam along the length of the cantilever will cause the beam to deflect since the angle of incidence changes with the curvature of the cantilever. Comparing the change of the reflection angle with the translational movement of the laser beam will give information about the cantilever's curvature. The White Light Interferometer uses the interference pattern, caused by objects being located at different heights, to determine the change of height of the cantilever. A data set of the height of every point in the viewing field of the microscope is recorded. Using image recognition software, the curvature of the cantilever can be found by fitting a suitable curve of the measured data.

4 Pull-in detection

An I/V-converter converts the current that starts flowing after contact into a voltage, Figure 8-3a. Another way is to keep watching for the changing interference pattern with a WLI. A third option is to measure the change of capacitance due to cantilever moving closer to the electrode. A sudden increase of the rate of change of the capacitance will signal the pull-in moment, Figure 8-3b.

5 Prevention of stiction

The stiction causing the cantilevers to stick to the electrodes either needs to be avoided or the stiction forces need to be kept as low as possible. The observations made in the previous

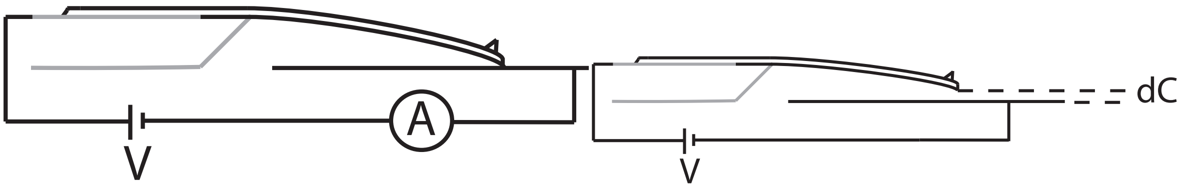

(a) Measure flowing current. **(b)** Measure change in capacitance.

Figure 8-3: Detection of the pull in moment can be done by: (a) Measure the current that starts to flow after pull-in. As this current is very low it needs to be converted by an I/V-converter. (b) Since the cantilever and electrode are essentially a capacitor the movement creates a change in the capacitance between them. The pull-in moment is characterized by a sudden increase in change of capacitance.

chapter stated that for compliant cantilevers a relative large movement was necessary to release the cantilever from the electrode surface. These movements are not possible with a stationary structure which means that the reduction of stiction needs to be performed differently. By reducing the area the cantilever comes into contact with, when the pull-in voltage is reached, the stiction force will be diminished. Creating small structures that prohibit the movement of the cantilever to the electrode with a small surface area would keep the cantilever in place until the bias voltage is removed. After removal the bending energy stored in the cantilever is sufficient to release the cantilever from these structures.

6 Alignment

All the AFM chips need to be aligned over the test locations simultaneously. The AFM chips and thus the cantilevers must be aligned in such a way that they are located over the electrodes. This can be done by making use of the shape of the chip or of the alignment groves made in the chip. By using the same anisotropic etchant used in the manufacture of the AFM chip an inverse of the AFM chips geometry can be made. This will allow the chips to position themselves and keep the cantilever positioned above the electrode.

8-2 Final design

From the requirements and the available measurement systems a suitable combination is made for the final design. This final design will be used to fabricate a new experimental set-up that copies the conditions of in-wafer calibration.

8-2-1 Measurements

To measure the variables needed to establish the cantilever's stiffness, a number of different measuring devices can be used. Five out of the six variables can be measured using a White Light Interferometer. The strength of this type of microscope is the fact that topological data is measured and presented as three dimensional data. From this data, using image recognition software, the dimensions, curvature and height differences can be easily measured. The orientation of the cantilever, with respect to the electrode, is also measured.

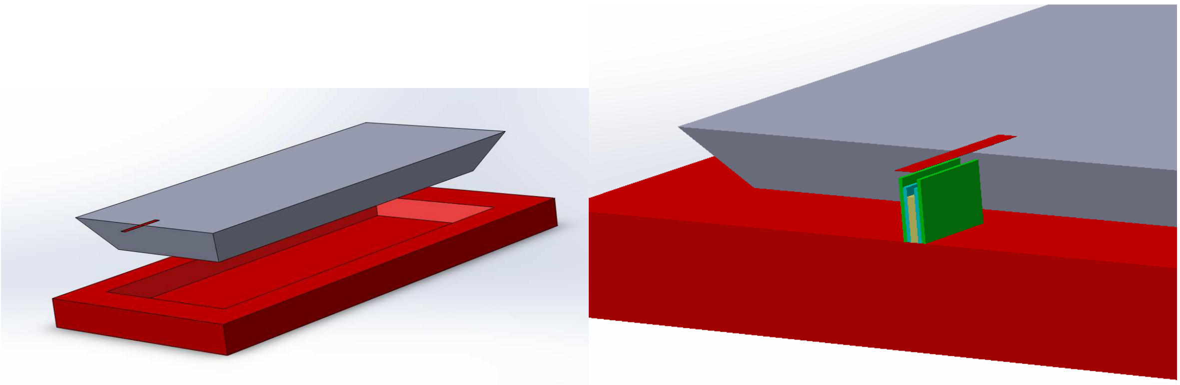

(a) Structure limiting the movement of the AFM chip.

(b) Positioning the cantilever over the electrodes.

Figure 8-4: The alignment of the AFM probe over the electrodes is done in the following way: (a) The structure onto which the production wafer is placed has recesses that conform to the shape of the AFM chip. (b) The cantilevers are aligned over the electrode due to the shape of the recess. The structures underneath the cantilevers represent the stepped electrodes. Similar colors denote the same height.

8-2-2 Electrodes

The electrodes with different heights, from now on referred to as the stepped electrodes, looks the most advantageous. The stepped electrodes are multiple electrodes that can be charged independently from each other and have different heights. The difference in heights makes it possible to use the differential gap method without the need of moving the wafer. With these electrodes fixed to the testing structure it is obvious that the area of the individual electrodes is smaller then when a single electrode is used. These electrodes can be oriented in two ways along the cantilever: either lengthwise or perpendicular. So far the electrode was modeled as an infinite plate. The width of the cantilever was necessary in Equation (4-13) to determine the width of the electrode area that is covered by the cantilever. Using an electrode with a smaller width than the cantilever means that the width of the electrode is needed instead of the cantilever's. The effect of dividing the electrode in multiple electrodes on the pull-in voltage has been investigated with the use of COMSOL Multiphysics. The results of one of these computations is shown in Figure 8-5a and Figure 8-5b The results of these computations show that the model computed in COMSOL Multiphysics has a mean error of 3,55% compared to the Fourth-order model. It has not been established what causes this error but the error is low enough to investigate the use this type of electrode.

Lengthwise stepped electrodes

The lengthwise stepped electrodes, shown on the right of Figure 8-2c, are a number of electrodes placed parallel to the cantilever. Along the center-line of the cantilever the distance to the first electrode is the largest. Moving outward to the sides, the electrodes increase with different step heights which decreases the gap. The lowest electrode is twice the width of the electrodes to either side, to keep the surface area equal between cantilever heights.

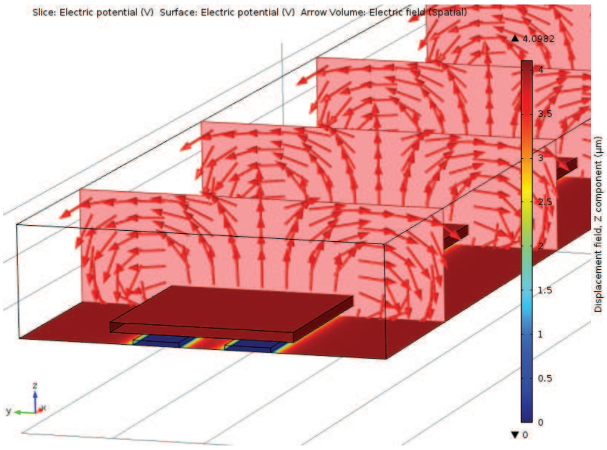

(a) Electric potential and electric field.

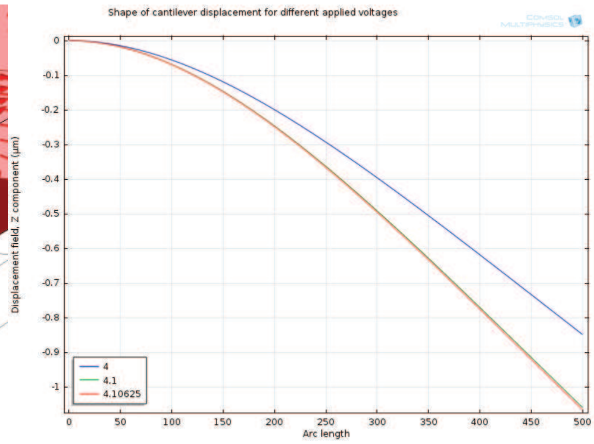

(b) Voltage plot against deflection

Figure 8-5: Comsol pull-in computations of stepped electrode. (a) The electric potential is given by the colors, the arrows indicate the direction of the electric field lines. (b) A plot of voltages against deflection. The highest voltages that can be calculated, before the model loses, equilibrium is the pull-in voltage.

Perpendicular stepped electrode

The perpendicular stepped electrodes, shown on the left of Figure 8-2c, are electrodes placed along the width of the cantilever. A pattern of three electrodes with different gaps is continued along the length of the cantilever. This arrangement necessitates a change in Fourth-order model. The distances of the electrodes, with respect to the base of the cantilever, need to be measured and used as the boundaries of the integrals in Equation (4-13).

Both electrode designs have an added advantage. When pull-in occurs, the area of the electrode that comes into contact with the cantilever is much smaller than with one large electrode. The smaller area will decrease the amount of stiction, which will cause the cantilever to detach more easily and allow it to return to its rest position. A disadvantage is the increase in voltage levels needed to cause pull-in as the electrode area has become smaller. The added change in the Fourth-order model for the perpendicular stepped electrode requires accurate measurement of the electrodes with respect to the base of the cantilever.

8-2-3 Alignment

The alignment of the AFM chips in the production will be accomplished by creating structures that force the AFM chips into place. These structures are the opposite of the underside of the AFM chip which automatically aligns the cantilevers over the electrodes. This has already been shown in Figure 8-4a.

8-3 Fabrication

Before fabrication of the wafer testing structure can begin, it is necessary to evaluate the measurement uncertainties caused by the use of the stepped electrodes. Hence an interim set-up has been created that can, if successful, be scaled up to support an entire wafer. The design of this interim set-up will need to prove:

- The effectiveness of the alignment of the cantilevers over the electrodes.
- The best orientation of the stepped electrode.
- Errors caused in the calculation of the stiffness due to the stepped electrode.

The design of the set-up is limited to fabrication capabilities present at the Delft Institute of Microsystems and Nanoelectronics (Dimes). It is assumed that the reader of this thesis has sufficient knowledge of microfabrication techniques. The details of these techniques will not be discussed further as they are readily available in literature on this subject. The fabrication steps take place at the front- and backside of the wafer. The fabrication steps per side will be discussed further. The fabrication steps are identical for both the lengthwise and perpendicular stepped electrode.

8-3-1 Frontside

Starting with a 6-inch wafer the frontside is coated with a layer of silicon oxide, SiO_2 , to electrically insulate the silicon. This insulation is needed to prevent electrical contact between the wafer and the AFM chip as the structure on the wafer is used to align the cantilever. The SiO_2 is coated by a positive resist material which is exposed by a light-source. After developing the resist, the wafer is etched to remove the unwanted material. The wafer is then sputter coated with a 200 nm layer of aluminum. The same process of applying a resist, exposure and developing is used to pattern the aluminum. Wet etching of the wafer removes the aluminum not coated by the resist. This layer is needed to create the first electrode. This will simplify the electrical contact to this electrode later on. The result of the deposition and etching of the first two layers is shown in Figures 8-6a and 8-6b. The first two layers use the same lithographic mask to pattern the resist. The resist covers most of the material except the hole that will be used to align the AFM chip

The wafer frontside is then coated by a 1 µm layer of Plasma Enhance Chemical Vapour Deposition, PECVD SiO_2. The exposure and developing of a resist result in protected areas of this step. Dry etching of the PECVD SiO_2 uncovered areas creates the first step that will support an second array of electrode structures. Figure 8-7a and 8-7b show the overall structure and a close-up of the area that's to be used as an electrode. A rectangular area is left open to allow for a connection with the now buried layer of aluminum.

Repeating the same process for another layer of PECVD SiO_2 creates the second step necessary for the third height level. The PECVD SiO_2 that was deposited in the previous step, is covered by a second layer to protect it from a second round of dry etching. This ensures that the geometry of the first pattern is not affected by the etchant. A similar rectangular windows is made to facilitate the connection with the aluminum.

Another sputter coated 200 nm layer of aluminum is applied. After application of the resist, exposure and developing result in the patterned electrodes after wet etching of the aluminum. These two patterned electrodes in combination with the buried layer of aluminum serve will be used to find three pull-in voltages for the three different gaps that are created. The final shape and size of the electrodes can be seen in Figures 8-9a and 8-9b.

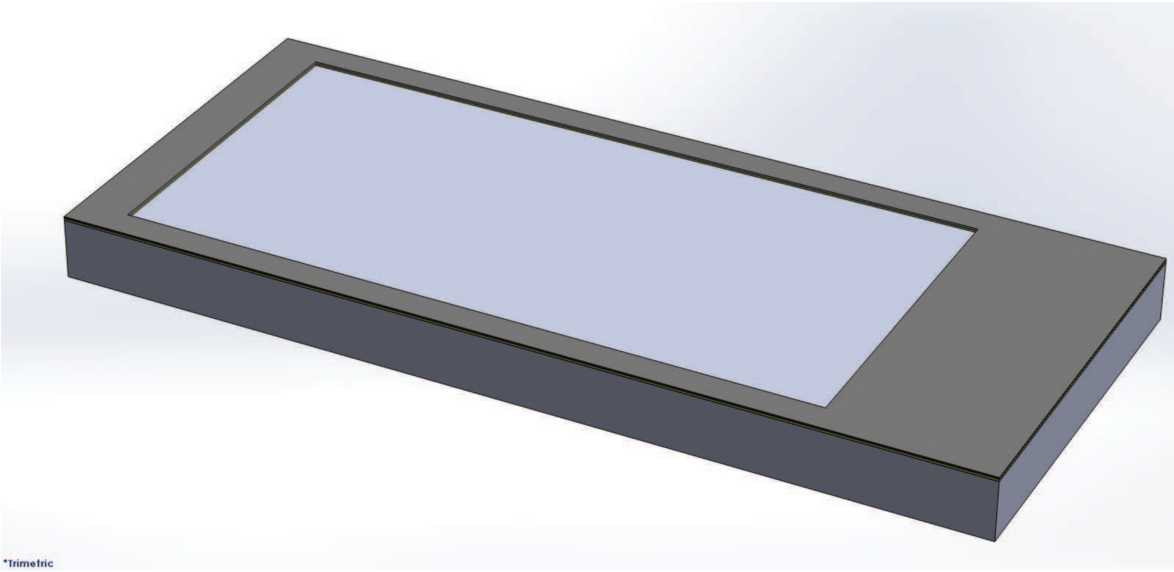

(a) Patterned layers of siliconoxide and aluminum.

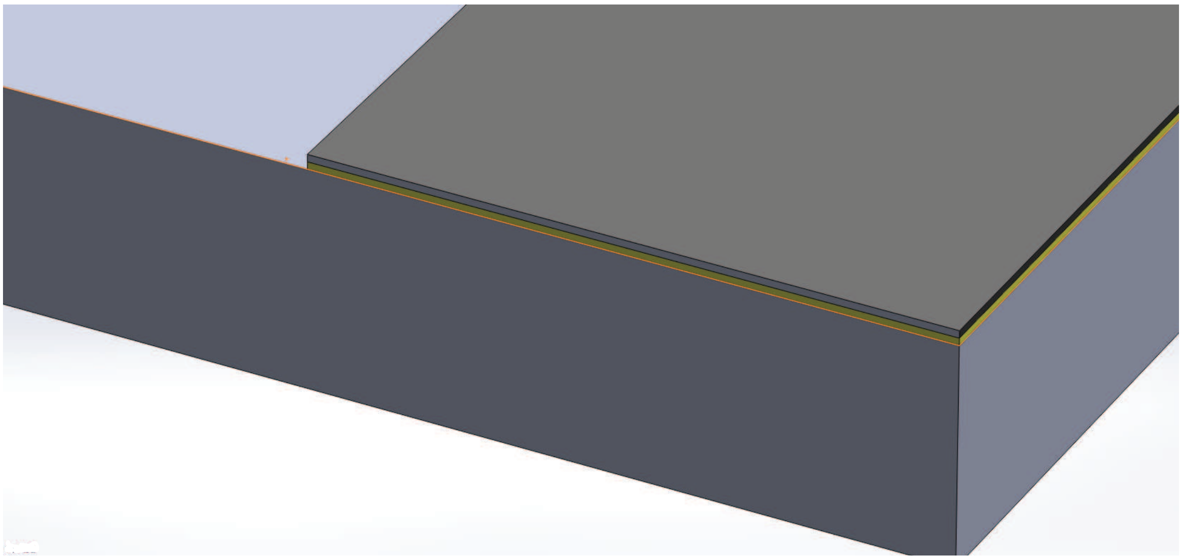

(b) Cross-section of first two layers.

Figure 8-6: The result of the etching of the first two deposited layers. (a) An overview of the silicon-oxide and aluminum layer. (b) A close-up the same layers show that the patterns used are identical.

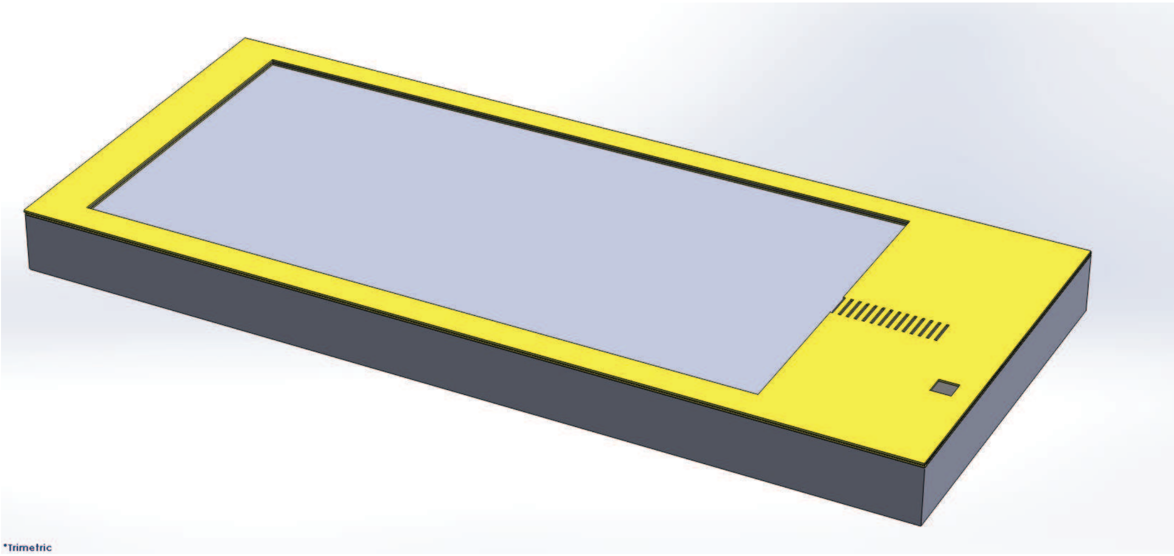

(a) Overview of PECVD oxide layer 1.

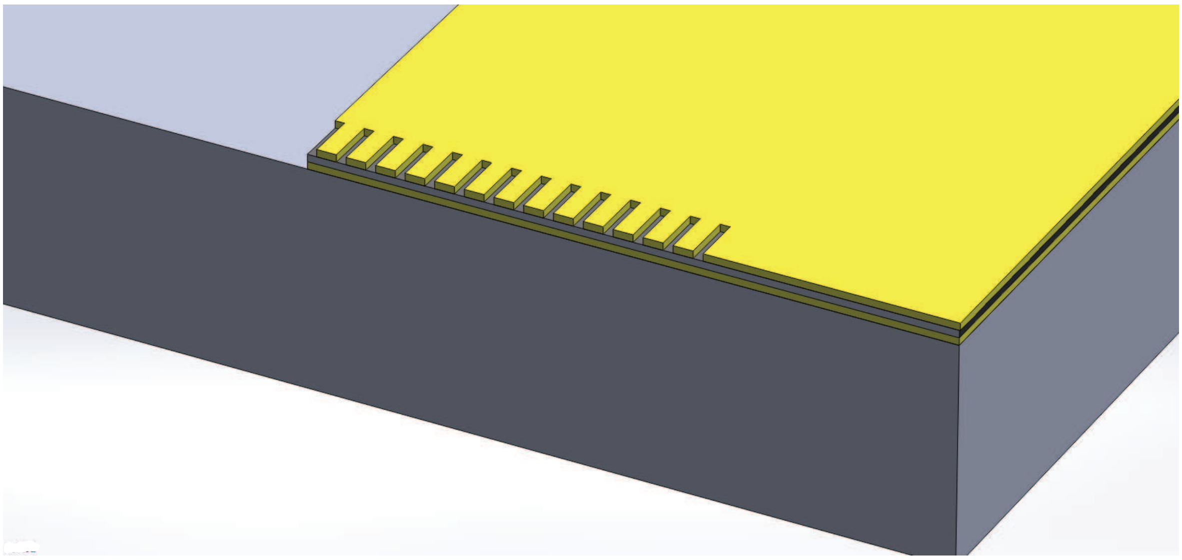

(b) Close-up of the PECVD oxide layer.

Figure 8-7: The patterned layer of PECVD oxide. (a) The overview of this layer show the hole for the AFM chip and the areas left open to connect the aluminum layer buried underneath. (b) A close-up of the layer shows that the layer is etched all the way through to the aluminum.

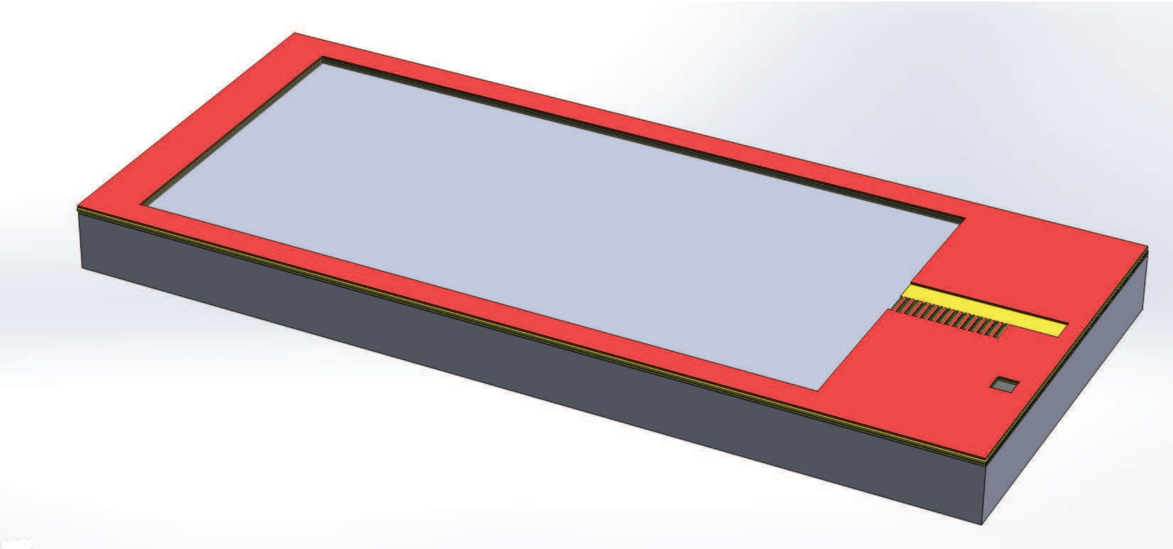

(a) Overview of PECVD oxide layer 2.

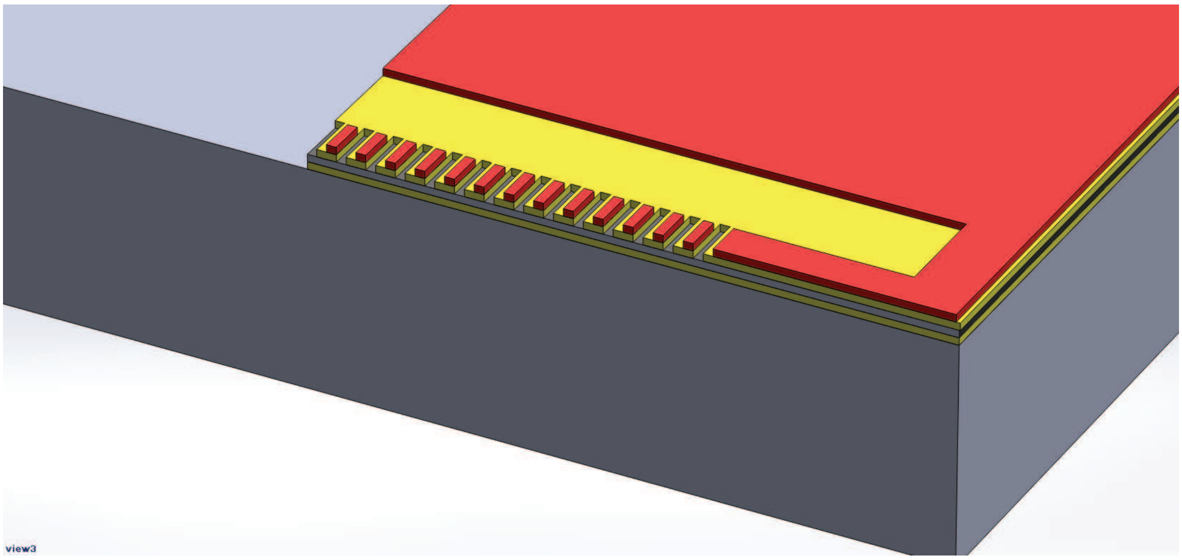

(b) Close-up of the second PECVD oxide layer.

Figure 8-8: The second layer of PECVD oxide is deposited on top of the first. (a) The areas not coated by the second PECVD layer are the second level of electrodes. The second PECVD layer will be the third level of electrodes. (b) Close-up of the three levels to be used as electrodes.

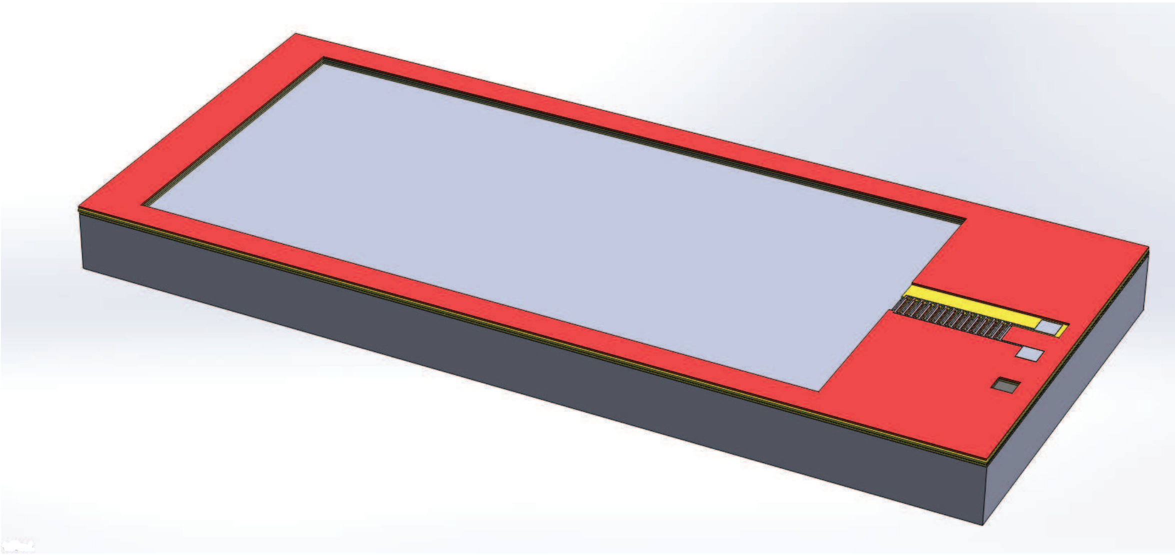

(a) Overview of patterned aluminum layer.

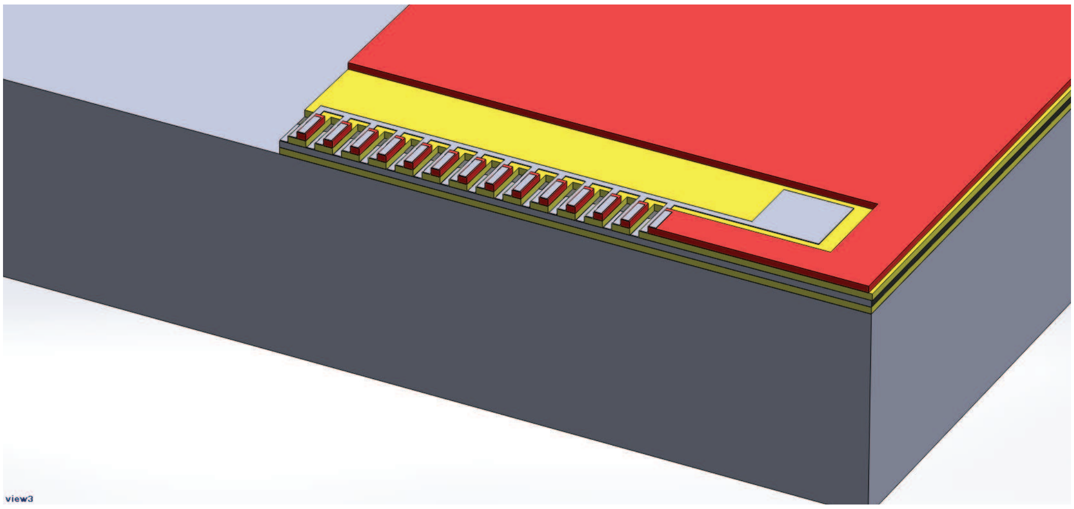

(b) Close-up of the three electrodes.

Figure 8-9: After the patterning and etching of the aluminum all the electrodes have been formed. (a) The three square areas are used to connect the electrodes to a bias voltage. (b) Close-up of the three created electrode levels.

8-3-2 Backside

The backside of the wafer is coated with a layer of PECVD oxide with a thickness of 1.4 µm. This layer is used to protect areas of the wafer from the Deep Reactive Ion Etching, DRIE. Patterning, coating and developing of the resist opens areas that are to be removed by the dry etching that follows next. Then DRIE is used to create a hole through the wafer that is to function as the chip holder. The applied layer of PECVD SiO_2 is removed by dry etching. The resulting structure is the finished set-up. The hole in the structure is used to align the cantilever over the electrodes, Figure 8-10b. After alignment the pull-in voltages can be determined.

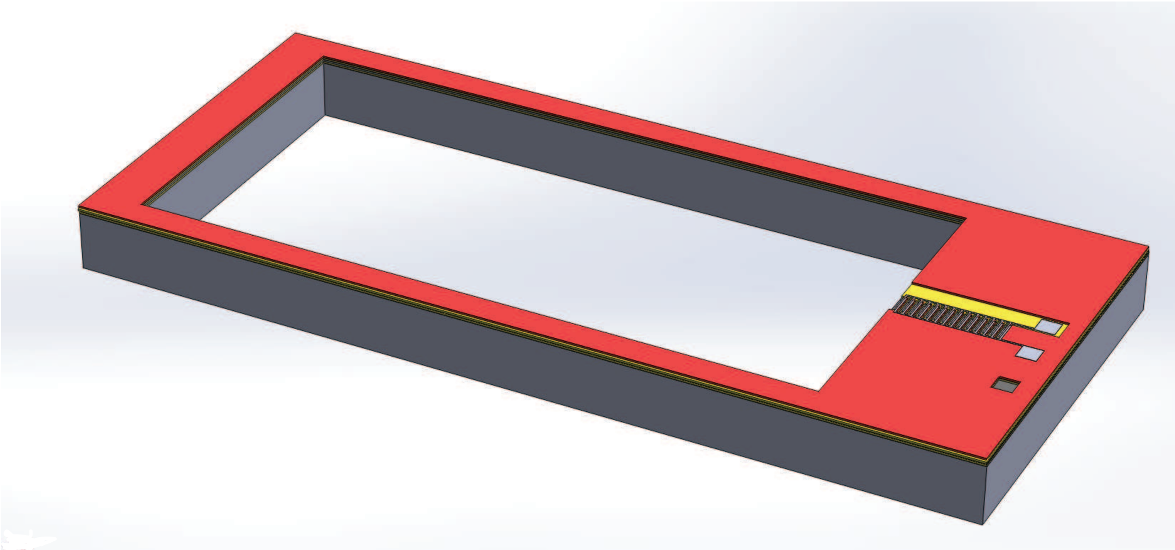

(a) Finished test structure.

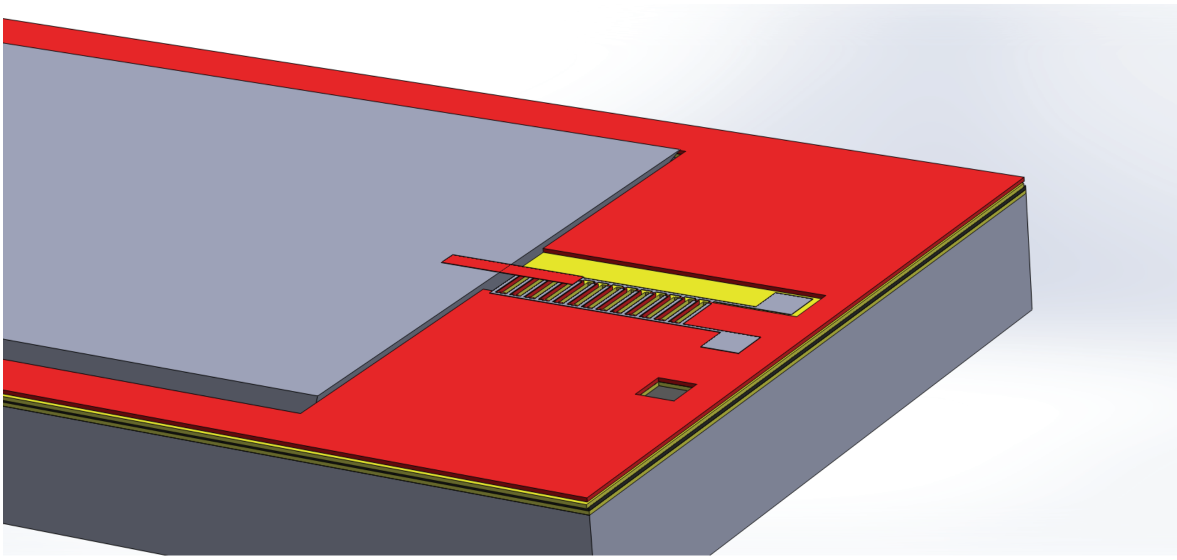

(b) AFM chip placed in the test structure.

Figure 8-10: After the DRIE etch the structure is finished. (a) The hole made in the structure is used to align the AFM chip above the electrodes. (b) AFM chip placed in the test structure. It is shown how the cantilever is positioned above the perpendicular electrodes.

Conclusion Part 2 - Experimentation and conceptual design

This part of the thesis dealt with the experiments performed on AFM probes and reference cantilevers. The measurment inaccuracies of the equipment used with the existing experimental set-up allowed the calculation of the total inaccuracy of the calculated stiffness. With this inaccuracy known, a number of experiments has been performed. The results of this experiments showed that the Fourth-order model has an inaccuracy of approximately 13% compared to values supplied by the manufacturers of the cantilevers. There were larger inaccuracies present in a number of experiments. These have been attributed to the lacking of or wrongful information supplied by the manufacturer. Having determined that the Electrostatic Pull-in Instability method can be used for calibration purposes, a conceptual design of a new test set-up has been designed. The aim of this design was focused on calibrating cantilevers still connected to production wafers. Due to breakdown of manufacturing equipment this set-up has not been manufactured.

Chapter 9

Conclusions

This chapter will present the conclusions of this master thesis. These conclusions will be given in chronological order, from the first chapter until the last.

Cantilever bending

The AFM probe consist of a chip onto which a cantilever is fixed. This cantilever with micrometer dimension has a scanning tip at its end that is used to scan surfaces. This tip has a radius in the nanometer range. The following items about the bending of this cantilever were discussed:

- The chip carrying the cantilever has standardized dimensions. These dimensions allow the chip to be used in any brand of AFM. Alignment groves underneath the chip allow for accurate repositioning of the cantilever tip.
- The geometry of the cantilever can be rectangular or triangular.
- The beam can be loaded in three different ways. Either by a force, moment, torque or a combination thereof acting at the end of the beam. These loads cause a deflection of the beam. The amount of deflection is given by the stiffness.
- The cantilever can be modeled as a beam or a plate. The chosen model has an impact on the calculation of its stiffness. Since the cantilever is a combination of two materials it is not possible to estimate a value for the combined Young's modulus and Poisson's ratio. This will introduce an error in the stiffness calculation.

Conclusions

Based on this discussion, the following can be concluded:

- Although the loads acting on the end of the cantilever can cause different rotations and displacements, only the case where a vertical load is applied at the end of the cantilever is considered. The forces interacting with the cantilever are best approximated by this type of loading.
- Modeling the cantilever as a plate shows the best approximation of the stiffness. Calculations done in Finite Element software show that when the cantilever is approximated as a plate the deflection is similar to calculations using plate theory.

State of the art

The cantilever's stiffness is currently estimated by a number of different calibration techniques. These techniques use different physical properties of the cantilever to calculate its stiffness. These techniques have advantages and disadvantages. The disadvantages of these techniques led to the introduction of a new calibration technique using a different physical property. The following items have been discussed:

- The calibration techniques can be divided into three groups: Dimensional, Static and Dynamic calibration. The range of inaccuracies is between 0.4-30%. Some techniques only require the dimensions of the cantilever while others use the cantilever during calibration. Using the cantilever during calibration can lead to contamination of or damage to the cantilever.
- The most accurate calibration techniques require expensive machinery and are time consuming. The fast techniques show moderate inaccuracies, but precise knowledge of material properties is needed.
- The new calibration technique, using the Electrostatic Pull-in Instability of the cantilever, applies a bias voltage between the cantilever and an electrode. At a certain voltage, the Pull-in Voltage, the system becomes unstable. This instability voltage is a function of the stiffness and the gap between cantilever and electrode.
- The interaction between the bending energy of the cantilever and the electrostatic energy is non-linear.
- The lumped model is not sufficient to describe the bending of the beam. A 2-dimensional model describing this behavior is a fourth-order differential which has no exact solution.

Conclusions

Based on the study into the current calibration techniques and the pull-in instability, the following can be concluded:

- The inaccuracy of calibration techniques lies between 0.4-30%. The most used technique, because of its ease of use, is Thermal tune. This technique has an inaccuracy of 20%.
- Since the gap between cantilever and electrode is hard to measure, a new method to solve the pull-in voltage is suggested. This differential gap method requires information on the change of the gap between experiments. This makes the calculation much easier.
- The fourth-order differential describing the behavior of a beam can't be solved analytically, necessitating a different approach to the problem.

Modeling the cantilever beam

Since the fourth-order differential model can't be solved analytically the behavior of the beam and plate is modeled differently. This chapter introduced the different models developed to study this interaction. The models have varying levels of complexity. Some include fringing fields, curvature of the beam and the complex shape functions, where others model the beam as straight with a square law shape function. The following observations were made:

- Fringing fields are present whenever an object is electrically charged. These fields increase the attractive force between an oppositely charged object.
- The manufacturing process can leave residual stress inside the cantilever. These stresses cause bending of the cantilever, which changes the size of the gap along the length of the cantilever.
- Solving the problem with the potential energy equations gives a solution that can be solved numerically. This equation requires a shape function describing the movement of point along the cantilever towards the electrode.
- The triangular tip present at certain cantilevers has an influence on the electrostatic force.

Conclusions

Based on the results of the different models the following can be concluded:

- A comparison was made between the model describing the cantilever behavior and experimental results. The experimental results were obtained from a experimental set-up where all the dimensions were closely monitored. This comparison showed that the full-order and fourth-order model had a mean error lower than 5% compared with the experimental results.
- Another comparison between the different models and a Finite Element analysis showed that taking fringing fields into account would lead to low values of the pull-in voltage. The full-order and fourth-order model showed a mean error of less then 0.5% with this FE analysis, making them the best models.
- The full-order model is computationally expensive and can't be used in the differential approach. The fourth-order model can be used in this approach and requires less computations. This model will be used for further experiments.

Error budgeting

The model describing its behavior is only as accurate as the values that are used in the calculation. To study the effect of inaccuracies of different variables an error sensitivity analysis has been performed. Observations made during this analysis were:

- The model is described by independent and dependent variables. The dependent variables influence each other making the resulting error larger than its summation.

- The orientation and offset of the electrode, compared to the AFM chip, introduces two new sources of calculation errors. The model is adapted to include these errors in the calculation of the stiffness inaccuracy.

Conclusions

Based on these observations and calculations the following is concluded:

- Measurement inaccuracies in the estimation of the gap and electrode angle have a large impact on the calculated stiffness. The error in the stiffness will be greater than 20% for measurement errors of 10% or more.
- The impact on the stiffness due to inaccuracies in the length and curvature is smaller but too large to neglect.
- The offset between electrode and AFM chip can be neglected if the distance is kept below 10 µm. For smaller distances the resulting error is smaller than 0.07% which can be neglected.

Experimental set-up

The equipment used during the experimentation had its own measurement inaccuracies. These inaccuracies were listed and the total inaccuracy of the calculated stiffness was estimated. Three different types of AFM probes were introduced. The first was a probe carrying three reference probes used for AFM cantilever calibration. The second and third were regular AFM probes used for surface scanning. The experimental procedure was discussed and the results of measurements made during this procedure were displayed.

Conclusions

From the calculations and experimentation done in this chapter it can be concluded that:

- The inaccuracy of the calculated stiffness due to the inaccuracies of the available equipment was 5.55%. Although this value is relatively small, the models accuracy has not yet been determined.
- The measurements done on the curvature of the cantilevers showed that some cantilevers were bent with a radius of 40 mm. The change of the gap at the tip was almost 2 µm making it clear that this curving can't be neglected as the electrostatic force scales with the third power of the change of the gap.

Results

To find the accuracy of the model compared to the real world, a number of experiments with different AFM probes has been performed. Between these probes there were four distinct stiffness levels: Stiff (approximately 47 [N/m]), Medium (approximately 7 [N/m]), Compliant (approximately 1 [N/m] and Very Compliant (approximately 0.1 [N/m]). Observations made during these experiments showed:

- The reported geometry of the manufacture could be up to 33% inaccurate. This level of inaccuracy would lead to large calculation errors if this geometry is accepted as true.
- The cantilever of the more compliant AFM probes tended to stick to the electrode surface. Removal of the bias voltage was not enough to restore the cantilever to its resting position. For the most compliant cantilevers it was necessary to move the cantilever along the electrode surface to break the attractive forces.
- The electrode had a slight rotation along the length axis of the cantilever. This causes part of the electrode to be closer to the cantilever. This angle could not be implemented in the model, which led to another source of measurement error. An added side effect was a torque acting on the cantilever, which meant that the cantilever was no longer only loaded in the height direction.
- Vibrations occurring around the pull-in point caused the cantilever to snap towards the electrode too early. This vibration, caused by the stiffness of the cantilever reaching a low value, was caused by the stepwise application of the voltage.

Conclusions

Based on these observations the following conclusions can be made:

- The model describing the electrode behavior displayed a mean error of around 13% for the Medium to Very Compliant cantilevers. This mean error is within the objectives laid out at the beginning of this thesis, making the Electrostatic Pull-in Instability method usable as a calibration method.
- For the stiffest electrode the mean error reached 16.3%. This value is higher than given in the objective, which would indicate that EPI could not be used for stiffer cantilevers. However, the difference in mean error could be attributed to the Beam Estimation equation used in the evaluation of the cantilever's reference stiffness. As has been shown the dimensions given by the manufacture could be underestimated by almost 33% leading to incorrect values of the stiffness.
- Cantilevers sticking to electrodes are hard to remove as the elastic energy is not sufficient to counteract the stiction. The stiction either needs to be prevented or a different method of counteracting the stiction needs to be investigated.
- The vibration near the pull-in point adds another error in the stiffness calculation. The oscillation causes the cantilever to move past the pull-in point at lower voltage levels. Using these voltages levels will result in a lower stiffness. By continuously increasing the voltage this vibration could be removed. However, this will lead to higher pull-in voltages, as the moment to stop the voltage increase is difficult to determine.

Design and fabrication

A new design has been proposed for a test structure that is able to copy the conditions of AFM probes connected to the production wafers. With these conditions as a guideline, a choice has been made of measurement equipment and possible solutions for change of the gap between the cantilever and electrode. This choice led to the final design proposal of the new test set-up.

From this design it can be concluded:

- A white light interferometer system is able to measure most of the required variables. These variables are the length L, width w, curvature ρ and differential gap Δg.
- The pull-in voltage will be measured by an I/V-converter as this gives the exact moment the cantilever hits the electrode.
- Stepped electrodes can be used to act as an electrode at different height levels.
- By structuring a surface the AFM chip can be aligned with the electrodes.

General conclusions

The results presented in this thesis have shown that current calibration techniques have disadvantages that make it difficult to accurately measure the cantilever's stiffness. The Electrostatic Pull-in Instability method proposed has fewer of these disadvantages making it a better method. Looking at the equations describing the pull-in phenomenon is was determined that the non-linear nature is difficult to describe. Analytical solutions have been presented which ease the calculations and give a good approximation of this behavior. From these analytical solutions the best performing one was selected to be used as a model to describe the behavior. It was determined that this model would be able to calculate the stiffness with an inaccuracy of 5% compared to finite element calculations. Comparative analysis between the model and AFM probes showed that the calculated stiffness had an inaccuracy of approximately 13% compared to the values stated by the manufacturer. This inaccuracy was below the limit stated in the objective making the Electrostatic Pull-in instability method a viable calibration technique. With the EPI method as a guideline a concept of a test set-up has been made that will copy the conditions of AFM probes attached to their production wafers. If succesfull this set-up could be scaled up to be used for in wafer calibration purposes.

Chapter 10

Recommendations

The following recommendations should be considered if further research is to be done in the use of EPI as a calibration technique. Recommendations for the model describing the pull-in behavior:

- The metal layer, deposited to increase reflectivity, changes the Poisson's ration and Young's modulus. This necessitated the use of the Bernoulli beam theory instead of the plate theory. The impact of this layer on the Poisson's ration and Young's modulus should be investigated to see if the plate theory could be used instead.
- The model, as it stands now, is not able to take rotations along the cantilever's length-axis into account. To complete the model this inclusion should be considered.
- The fourth-order model was chosen as it is better usable with the differential gap method. If a new solution is found to solve the measurement of the gap, an investigation of the inaccuracy of the full-order model should be considered.

Recommendations for the new experiment:

- The shape of the AFM chip's base has been assumed to be without any tolerances in its dimensions. As the thickness of wafers can vary, this will lead to changes of the ground plane of the AFM chip. These chances could lead to the chip not fitting in the proposed structure. This structure should be adapted to account for these tolerances.
- The used White Light Interferometer was only able to scan an area of 15x15cm. This is not large enough to scan a whole wafer and a design should be considered that is able to scan a whole wafer.
- Calculations on the use of the stepped electrode showed a difference between the calculated pull-in voltage and the pull-in voltage from the finite element model. The origin of this difference has not been investigated yet.

- The use of the buried aluminum layer will have field lines passing through the PECVD oxide on top of it. The effect of this electric field needs to be calculated, as the added layers change the dielectric constant at those locations.

Appendix A

Derivation of Fourth-order model

This derivation is a copy of the one given in [41] with a minor correction of the end result:

By using the Taylor's series expansion, one can expand the term $\frac{1}{(G-w)}$ in the total potential energy about the initial equilibrium position, i.e. $w = 0$, as

$$\frac{1}{G-w} = \frac{1}{G} + \frac{w}{G^2} + \frac{w^2}{G^3} + \frac{w^3}{G^4} + \frac{w^4}{G^5} + \Lambda \tag{A-1}$$

Truncating the remaining terms Λ of the electrical potential energy yields the total potential energy of the fourth-order model as

$$\int_0^L \frac{EI}{2}\left(\frac{d^2w}{dx^2}\right)dx - \int_0^L \frac{\varepsilon_r\varepsilon_0 bV^2}{2}\cdot\left(\frac{1}{G} + \frac{w}{G^2} + \frac{w^2}{G^3} + \frac{w^3}{G^4} + \frac{w^4}{G^5}\right)dx \tag{A-2}$$

By the use of the assumed mode method this equation becomes

$$U = \int_0^L \frac{EI}{2}(\eta\phi'')^2 dx - \int_0^L \frac{\varepsilon_r\varepsilon_0 bV^2}{2}\cdot\left(\frac{1}{G} + \frac{\eta\phi}{G^2} + \frac{(\eta\phi)^2}{G^3} + \frac{(\eta\phi)^3}{G^4} + \frac{(\eta\phi)^4}{G^5}\right)dx \tag{A-3}$$

At a transition from a stable to an unstable equilibrium state, the first-order and second-order derivatives of the total potential energy with respect to η both equal zero, i.e.

$$\frac{dU}{d\eta} = EI\eta\int_0^L (\phi'')^2 dx - \frac{\varepsilon_r\varepsilon_0 bV^2}{2}\left(\int_0^L \frac{\phi}{G^2}dx + 2\eta\int_0^L \frac{\phi^2}{G^3}dx + 3\eta^2\int_0^L \frac{\phi^3}{G^4}dx + 4\eta^3\int_0^L \frac{\phi^4}{G^5}dx\right) = 0 \tag{A-4}$$

$$\frac{d^2U}{d\eta^2} = EI\int_0^L (\phi'')^2 dx - \frac{\varepsilon_r\varepsilon_0 bV^2}{2}\left(2\int_0^L \frac{\phi^2}{G^3}dx + 6\eta\int_0^L \frac{\phi^3}{G^4}dx + 12\eta^2\int_0^L \frac{\phi^4}{G^5}dx\right) = 0 \tag{A-5}$$

Rearranging Equations (A-4) and (A-5) as

$$EI\eta \int_0^L (\phi'')^2 dx = \frac{\varepsilon_r \varepsilon_0 b V^2}{2} \left(\int_0^L \frac{\phi}{G^2} dx + 2\eta \int_0^L \frac{\phi^2}{G^3} dx + 3\eta^2 \int_0^L \frac{\phi^3}{G^4} dx + 4\eta^3 \int_0^L \frac{\phi^4}{G^5} dx \right) \tag{A-6}$$

$$EI \int_0^L (\phi'')^2 dx = \frac{\varepsilon_r \varepsilon_0 b V^2}{2} \left(2 \int_0^L \frac{\phi^2}{G^3} dx + 6\eta \int_0^L \frac{\phi^3}{G^4} dx + 12\eta^2 \int_0^L \frac{\phi^4}{G^5} dx \right) \tag{A-7}$$

Dividing Equation (A-6) by Equation (A-7) gives

$$\eta = \frac{\int_0^L \frac{\phi}{G^2} dx + 2\eta \int_0^L \frac{\phi^2}{G^3} dx + 3\eta^2 \int_0^L \frac{\phi^3}{G^4} dx + 4\eta^3 \int_0^L \frac{\phi^4}{G^5} dx}{2 \int_0^L \frac{\phi^2}{G^3} dx + 6\eta \int_0^L \frac{\phi^3}{G^4} dx + 12\eta^2 \int_0^L \frac{\phi^4}{G^5} dx} \tag{A-8}$$

Then one can rearrange Equation (A-8) as

$$\left(8 \int_0^L \frac{\phi^4}{G^5} dx \right) \eta^3 + \left(3 \int_0^L \frac{\phi^3}{G^4} dx \right) \eta^2 - \int_0^L \frac{\phi}{G^2} dx = 0 \tag{A-9}$$

Rewriting Equation (A-9) as

$$\eta^3 + a_1 \eta^2 + a_2 = 0 \tag{A-10}$$

where the constants a_1 and a_2 are

$$a_1 = \frac{3 \int_0^L \frac{\phi^3}{G^4} dx}{8 \int_0^L \frac{\phi^4}{G^5} dx}, \; a_2 = \frac{- \int_0^L \frac{\phi}{G^2} dx}{8 \int_0^L \frac{\phi^4}{G^5} dx} \tag{A-11}$$

Equation (A-10) is a cubic equation of η and can be solved by the Cardan solution. The real number solution of Equation (A-10) gives rise to the coefficient η_{in} at pull-in as

$$\eta_{in} = S + T - \frac{a_1}{3} \tag{A-12}$$

where

$$S = \sqrt[3]{R + \sqrt{Q^3 + R^2}} \qquad T = \sqrt[3]{R - \sqrt{Q^3 + R^2}} \tag{A-13}$$

$$Q = \frac{-{a_1}^2}{9} \qquad R = \frac{-27a_2 - 2{a_1}^3}{54} \tag{A-14}$$

Substituting Equation (A-12) into Equation (A-7) and solving for V gives the closed-form solution for the pull-in voltage V_{in} of the fourth-order model as

$$V_{in} = \left(\frac{EI}{\varepsilon_r \varepsilon_0 b} \cdot \frac{\int_0^L (\phi'')^2 dx}{\int_0^L \frac{\phi^2}{G^3} dx + 3(S + T - a_1/3) \int_0^L \frac{\phi^3}{G^4} dx + 6(S + T - a_1/3)^2 \int_0^L \frac{\phi^4}{G^5} dx} \right)^{1/2} \tag{A-15}$$

Appendix B

Reference cantilever data sheet

Probe	Lever	Frequency(kHz)	Spring constant [N/m]
1	Long	14.71	0.114
	Medium	60.02	0.976
	Short	249.82	7.57
2	Long	14.79	0.110
	Medium	60.48	0.927
	Short	249.61	7.82
3	Long	14.63	0.105
	Medium	59.74	0.948
	Short	247.10	7.33
4	Long	14.51	0.105
	Medium	59.32	0.884
	Short	245.59	8.18
5	Long	14.61	0.107
	Medium	59.65	0.892
	Short	247.48	7.79

Table B-1: Table with parameters of the individual cantilevers. Supplied by Bruker

Appendix C

Cantilever data of NCLR-10 and CONTR-10

Type:			Unit No.:		
NCLR-10			68080F12L841		
Probe No.	T[µm]	W[µm]	L[µm]	C[N/m]	f[kHz]
1	7,00	36	226	4.6E+1	188
2	7,00	36	226	4.7E+1	189
3	7,20	36	226	5.0E+1	193
4	7,20	36	226	5.0E+1	193
5	7,10	36	226	4.7E+1	190
6	7,00	36	226	4.6E+1	188
7	7,50	37	226	5.9E+1	202
8	7,30	37	226	5.4E+1	197
9	7,00	36	226	4.6E+1	188
10	7,10	36	226	4.7E+1	189

Table C-1: Table displaying the dimensional data of the NCLR-10 probes. Its stiffness and resonance frequency are displayed as well.

Type:			Unit No.:		
NCLR-10			75343F10L890		
Probe No.	T[µm]	W[µm]	L[µm]	C[N/m]	f[kHz]
1	2,00	46	448	1.6E-1	13
2	2,00	46	448	1.6E-1	16
3	2,00	46	448	1.6E-1	13
4	1.90	46	448	1.6E-1	13
5	2.00	46	448	1.6E-1	13
6	2,00	46	448	1.7E-1	13
7	2,00	46	448	1.7E-1	14
8	2,00	46	448	1.7E-1	13
9	2,00	47	448	1.8E-1	14
10	2,10	47	448	2.1E-1	14

Table C-2: Table displaying the dimensional data of the CONTR-10 probes. Its stiffness and resonance frequency are displayed as well.

Bibliography

[1] P. Russell, "AFM Probe Manufacturing," 2008.

[2] C. Clifford and M. Seah, "The determination of atomic force microscope cantilever spring constants via dimensional methods for nanomechanical analysis," *Nanotechnology*, vol. 1666, 2005.

[3] H. de Vries, "Dictionary of Nanotechnology."

[4] H. Sadeghian, C. K. Yang, J. F. L. Goosen, A. Bossche, P. J. French, and F. V. Keulen, "Method for the Calibration of Atomic Force Microscope Cantilevers Spring Constant : Application of Electrostatic Pull-in." 2011.

[5] L. M. Pluimers, *Feasibility study for AFM probe calibration using the probe's Electrostatic Pull-in Instability*. PhD thesis, Technical University Delft, 2013.

[6] Merriam-Webster, "Encyclopaedia Britannica," 2013.

[7] G. B. M. Lutwycehe, C. Andreoli, "5 x 5 2D AFM cantilever arrays a first step towards a Terabit storage device," *Sensors and Actuators*, vol. 73, no. 1, pp. 89–94, 1999.

[8] NanoWorld, "Nanosensors - Alignment Chip."

[9] C. a. Clifford and M. P. Seah, "The determination of atomic force microscope cantilever spring constants via dimensional methods for nanomechanical analysis," *Nanotechnology*, vol. 16, pp. 1666–1680, Sept. 2005.

[10] R. H. Poelma, H. Sadeghian, S. P. M. Noijen, J. J. M. Zaal, and G. Q. Zhang, "A numerical experimental approach for characterizing the elastic properties of thin films: application of nanocantilevers," *Journal of Micromechanics and Microengineering*, vol. 21, p. 065003, June 2011.

[11] W. D. Pilkey, *Analysis and Design of Elastic Beams*. John Wiley & Sons, 2002.

[12] R. Hibbeler, *Mechanics of Materials*. Pearson Prentice Hall, 2005.

[13] J. M. Neumeister and W. a. Ducker, “Lateral, normal, and longitudinal spring constants of atomic force microscopy cantilevers,” *Review of Scientific Instruments*, vol. 65, no. 8, p. 2527, 1994.

[14] D.-A. Mendels, M. Lowe, A. Cuenat, M. G. Cain, E. Vallejo, D. Ellis, and F. Mendels, “Dynamic properties of AFM cantilevers and the calibration of their spring constants,” *Journal of Micromechanics and Microengineering*, vol. 16, pp. 1720–1733, Aug. 2006.

[15] R. S. Gates and M. G. Reitsma, “Precise atomic force microscope cantilever spring constant calibration using a reference cantilever array.,” *The Review of scientific instruments*, vol. 78, p. 086101, Aug. 2007.

[16] C. Clifford and M. Seah, “Improved methods and uncertainty analysis in the calibration of the spring constant of an atomic force microscope cantilever using static experimental methods,” *Measurement Science and Technology*, vol. 125501, 2009.

[17] P. J. P. J. Cumpson, P. Zhdan, and J. Hedley, “Calibration of AFM cantilever stiffness: a microfabricated array of reflective springs.,” *Ultramicroscopy*, vol. 100, pp. 241–51, Aug. 2004.

[18] S. Rana, P. M. Ortiz, A. J. Harris, J. S. Burdess, and C. J. McNeil, “An electrostatically actuated cantilever device capable of accurately calibrating the cantilever on-chip for AFM-like applications,” *Journal of Micromechanics and Microengineering*, vol. 19, p. 045012, Apr. 2009.

[19] E. Bonaccurso, F. Schönfeld, and H.-J. Butt, “Electrostatic forces acting on tip and cantilever in atomic force microscopy,” *Physical Review B*, vol. 74, p. 085413, Aug. 2006.

[20] M.-S. Kim, J.-H. Choi, Y.-K. Park, and J.-H. Kim, “Atomic force microscope cantilever calibration device for quantified force metrology at micro- or nano-scale regime: the nano force calibrator (NFC),” *Metrologia*, vol. 43, pp. 389–395, Oct. 2006.

[21] J. R. Pratt, J. a. Kramar, D. B. Newell, and D. T. Smith, “Review of SI traceable force metrology for instrumented indentation and atomic force microscopy,” *Measurement Science and Technology*, vol. 16, pp. 2129–2137, Nov. 2005.

[22] J. P. Cleveland, S. Manne, D. Bocek, and P. K. Hansma, “A nondestructive method for determining the spring constant of cantilevers for scanning force microscopy,” *Review of Scientific Instruments*, vol. 64, no. 2, p. 403, 1993.

[23] J. E. Sader, I. Larson, P. Mulvaney, and L. R. White, “Method for the calibration of atomic force microscope cantilevers,” *Review of Scientific Instruments*, vol. 66, no. 7, p. 3789, 1995.

[24] F. Serry, “Improving the accuracy of AFM force measurements: The thermal tune solution to the cantilever spring constant problem,” *Application Notes. Veeco Instrument Inc.: Santa ...*, pp. 1–4, 2005.

[25] J. L. Hutter and J. Bechhoefer, “Calibration of Atomic Force Microscope Tips,” *Review of Scientific Instruments*, vol. 64, no. 7, p. 1868, 1993.

[26] J. L. Hutter and J. Bechhoefer, "Calibration of atomic-force microscope tips," *Review of Scientific Instruments*, vol. 64, no. 7, p. 1868, 1993.

[27] H. Sadeghian, G. Rezazadeh, and P. M. Osterberg, "Application of the Generalized Differential Quadrature Method to the Study of Pull-In Phenomena of MEMS Switches," *Journal of Microelectromechanical Systems*, vol. 16, pp. 1334–1340, Dec. 2007.

[28] J. Abdi, a. Koochi, a. S. Kazemi, and M. Abadyan, "Modeling the effects of size dependence and dispersion forces on the pull-in instability of electrostatic cantilever NEMS using modified couple stress theory," *Smart Materials and Structures*, vol. 20, p. 055011, May 2011.

[29] X. Liang and S. Shen, "Effect of electrostatic force on a piezoelectric nanobeam," *Smart Materials and Structures*, vol. 21, p. 015001, Jan. 2012.

[30] Y. J. Hu, J. Yang, and S. Kitipornchai, "Pull-in analysis of electrostatically actuated curved micro-beams with large deformation," *Smart Materials and Structures*, vol. 19, p. 065030, June 2010.

[31] S. Pamidighantam, R. Puers, K. Baert, and H. a. C. Tilmans, "Pull-in voltage analysis of electrostatically actuated beam structures with fixed$ndash$fixed and fixed$ndash$free end conditions," *Journal of Micromechanics and Microengineering*, vol. 12, pp. 458–464, July 2002.

[32] V. Leus and D. Elata, "Fringing Field effect in electrostatic actuators," Tech. Rep. May, Israel Institute of Technology, Faculty of Machinical Engineering, 2004.

[33] L. C. Wei, A. B. Mohammad, and N. Mohd, "Analytical Modeling For Determination Of Pull-In Voltage For An Electrostatic Actuated MEMS Cantilever Beam," *ICSE2002*, pp. 233–238, 2002.

[34] W. Soedel, *Vibrations of Shells and Plates, Second Edition.* New York: Dekker, 1993.

[35] S. M. C. Abdulla, H. Yagubizade, and G. J. M. Krijnen, "Analysis of resonance frequency and pull-in voltages of curled micro-bimorph cantilevers," *Journal of Micromechanics and Microengineering*, vol. 22, p. 035014, Mar. 2012.

[36] K. E. Petersen, "Dynamic micromechanics on silicon techniques and devices," *Transactions on electron devices*, vol. 02, no. 10, 1978.

[37] R. Legtenberg, J. Gilbert, S. Senturia, and M. Elwenspoek, "Electrostatic curved electrode actuators," *Journal of Microelectromechanical Systems*, vol. 6, no. 3, pp. 257–265, 1997.

[38] B. C. Lee and E. S. Kim, "Analysis of partly corrugated rectangular diaphragms using the Rayleigh-Ritz method," *Journal of Microelectromechanical Systems*, vol. 9, pp. 399–406, Sept. 2000.

[39] H. Sadeghian, G. Rezazadeh, and E. A. Sani, "Some Design Considerations on the Electrostatically Actuated Fixed-Fixed End Type MEMS Switches," *Journal of Physics: Conference Series*, vol. 34, pp. 174–179, Apr. 2006.

[40] J. Chen, S. Kang, and J. Zou, "Reduced-order modeling of weakly nonlinear MEMS devices with Taylor-series expansion and Arnoldi approach," *...Systems, Journal of*, vol. 13, no. 3, pp. 441–451, 2004.

[41] Y.-C. Hu, "Closed form solutions for the pull-in voltage of micro curled beams subjected to electrostatic loads," *Journal of Micromechanics and Microengineering*, vol. 16, pp. 648–655, Mar. 2006.

[42] R. K. Gupta, "Electostatic Pull-in Test Structure Design for in-situ Mechanical Property Measurements of Microelectromechanicsl Systems (MEMS)," *PhD. Thesis*, 1998.

[43] G. Rezazadeh and H. Sedghian, "The influence of stress gradient on the pull-in phenomena of microelctromechanical switches," *Journal of Physics: Converence Series*, vol. 34, 2006.

[44] M. K. Yeh, N. H. Tai, and B. Y. Chen, "Influence of Poisson's ratio variation on lateral spring constant of atomic force microscopy cantilevers.," *Ultramicroscopy2*, vol. 108, no. 10, pp. 1025–1029, 8.

[45] J. R. Taylor, *An Introduction to Error Analysis, The study of uncertainties in physical measurements*. University Science Books, 1997.

[46] N. Instrument, "USB-6008 -12 Bit DAQ data sheet," 2010.

[47] Bruker, "Data Sheet GT-1," 2012.

[48] Bruker, "CLFC Force Calibration Cantilevers - Support Note 013-000-000," 2013.

[49] G. NanoAndMore, "E-mail communication with Nanoworld," tech. rep., 2013.

[50] Y. Zhao, "Anti-stiction in MEMS and NEMS," *Acta Mechanica Sinica (English Version)*, vol. 19, no. 1, 2003.

[51] B. Kim and T. Chung, "A new organic modifier for anti-stiction," *...Systems, Journal of*, vol. 10, no. 1, pp. 33–40, 2001.